REPUBLIC OF IRAQ

MINISTRY OF HIGHER EDUCATION AND SCIENTIFIC RESEARCH

AL-FURAT AL-AWSAT TECHNICAL UNIVERSITY

ENGINEERING TECHNICAL COLLEGE NAJAF

COOLING PERFORMANCE ENHANCEMENT OF PV SYSTEMS USING A MULTI-FLOW CHANNEL

MOHAMMED ABD AL SALAM MAJEED

B. TECH.

IN MECHANICAL ENGINEERING TECHNIQUES OF POWER

2024

COOLING PERFORMANCE ENHANCEMENT OF PV SYSTEMS USING A MULTI-FLOW CHANNEL

A THESIS

SUBMITTED TO THE DEPARTMENT OF MECHANICAL ENGINEERING TECHNIQUES OF POWER
IN PARTIAL FULFILLMENT OF THE REQUIREMENTS FOR
MASTER OF THERMAL TECHNOLOGIES DEGREE IN MECHANICAL ENGINEERING TECHNIQUES OF POWER (M.TECH.)

BY

MOHAMMED ABD AL SALAM MAJEED

(B. Tec. Mechanical Eng.)
2006

Supervised by

Assist. Prof. Dr. Salah M. Salih

February / 2024

بِسْمِ اللَّهِ الرَّحْمَٰنِ الرَّحِيمِ

﴿ وَمَا تَوْفِيقِي إِلَّا بِاللَّهِ ۚ عَلَيْهِ تَوَكَّلْتُ وَإِلَيْهِ أُنِيبُ ﴾

صدق الله ألعلي العظيم

سورة هود، الآية (88)

DECLARATION

I hereby declare that the work in this thesis is my own and has not been submitted to other organizations or for acquiring any other degree.

Signature:

Name: Mohammed Abd Al Salam Majeed

Date: / / 2024

ACKNOWLEDGMENT

Praise be to Allah for all His blessings, and thanks be to Allah for His success in completing this work of ours. I extend my sincere thanks and appreciation to my supervisor, **Assist. prof. Dr. Salah M. Salih**, for his continuous support and guidance in the completion of this work.

I express my special thanks to the head of the Department of Mechanical Power Technologies Engineering and the professors working at the Technical College / Najaf for their help. With my sincere thanks and gratitude to every member of my family, especially my dear father and patient mother, my wife, and all my brothers for their support and standing with me all the way.

Mohammed Abd Al Salam Majeed

/ / 2024

Supervisors Certification

I certify that the thesis entitled " **Cooling Performance Enhancement of PV Systems Using a Multi-Flow Channel**" submitted by Mohammed Abd Al Salam Majeed has been prepared under our supervision at the Department of Mechanical Engineering Techniques of Power, College of Technical Engineering-Najaf, AL-Furat Al-Awsat Technical University, as partial fulfillment of the requirements for the degree of Master of Technologies in Thermal Engineering.

Signature:

Name: Assist. Prof. Dr. Salah M. Salih

(Supervisor)

Date: / / 2024

In view of the available recommendation, we forward this thesis for debate by the examining committee.

Signature:

Name: Assist. Prof. Dr. Adel A. Eidan

Head Mechanical Eng. Tech. of power Dept.

Committee Certification

We certify that we have read the thesis entitled " **Cooling Performance Enhancement of PV Systems Using a Multi-Flow Channel** " submitted by Mohammed Abd Al Salam Majeed, and as an examining committee, examined the student's thesis in its contents. And that, in our opinion, it is adequate as a thesis for the degree of Master of Technologies in Thermal Engineering.

Signature:

Name: Assist. Prof. Dr. Salah M. Salih

(Supervisor)

Date: / / 2024

Signature:

Name: Assist. Prof. Dr. Ahmed Razzaq Hasan

Member

Date: / / 2024

Signature:

Name: Dr. Wisam Jasim Kadhim

Member

Date: / / 2024

Signature:

Name: Prof. Dr. Qahtan A. Abed

(Chairman)

Date: / / 2024

Approval of the Engineering Technical College- Najaf

Signature:

Name: Assist. Prof. Dr. Hassanain Ghani Hameed

Dean of Engineering Technical College- Najaf

Date: / / 2024

Linguistic Certification

This is to certify that this thesis entitled "**Cooling Performance Enhancement of PV Systems Using a Multi-Flow Channel**" was reviewed linguistically. Its language was amended to meet the style of the English language.

Signature:

Name: Assist. Prof. Dr. Khalid Jaber Ouclah

Date:

Abstract

Enhancement of the cooling performance of photovoltaic/thermal (PV/T) collector using transverse fins, with multi-flow channel is investigated numerically and experimentally. The study aims to improve the electrical efficiency of PV/T systems with turbulent generation to increase exchange between absorbent panel, and airflow with less pressure drop. The effect of different mass flow rates (MFR) of (0.04, 0.05, 0.06, 0.07, and 0.08) kg/s, and various solar flux of (600, 800, and 1000)W/m^2, on PV panel temperature, and PV/T system performance are studied.

The experiments were conducted under an indoor test condition in the laboratory using three tungsten halogen lamps (3000W) as a solar simulator. For the PV/T air system using the multi-flow channel with a project area of (0.524) m^2. Width (W) (0.61 m), height (H) (0.061 m), the aspect ratio (W/H) is set at (10) to achieve a fully turbulent flow in the PV/T collector.

The numerical study is also conducted using the commercially available COMSOL Multiphysics 5.5 program to solve the three-dimensional governing equations for continuity, momentum, energy, and turbulent model equations (κ-ε). The current simulations are carried out under the same boundary conditions to achieve the accuracy of the experimental data with an average error estimated to be (1.576%).

Which indicated results numerical, experimental that the air temperature is inversely proportional to the air MFR, and the overall efficiency is highly dependent on the air MFR, and solar flux intensity.

In addition, the experiment result shows that the higher value, at air MFR (0.04-0.08)kg/s, solar flux (600 W/m^2) for electrical, thermal, and overall efficiency are (16.62-17.03)%, (53.49-65.57)%, and (70.11-82.6)%, respectively. At the same MFR, and solar flux (1000W/m^2), (15.5-16.26)%, (63.34-74.14)%, and (78.84-90.4)%, respectively. Furthermore, percentage increase in output power (28.44%) by (15.93W).

The increased mass flow rate led to a reduction in the PV temperature, and improved electrical performance. The percentage of the decrease in the PV temperature at the mass flow rate (0.08 kg/s) is (28.94%), and the maximum PV temperature reduction is about (19.53°C). The best net electrical power added to the production of the PV module is (7.37W), recorded at (MFR) of (0.05 kg/s), and solar flux (1000 W/m^2).

TABLE OF CONTENTS

NOMENCLATURE

Symbol	Definition	Unit
A	Area	m^2
Am	Area of the (PV)module	m^2
Ac	Area of the Photovoltaic Cell	m^2
T*b*	Backplate temperature	°C
T*pv*	Solar cell temperature	°C
T*amb*	Ambient temperature	°C
T*i*	Inlet temperature	°C
T*o*ut	Outlet temperature	°C
$\bar{T}f$	meam air temperature	°C
Re	Reynolds number	---
K	Thermal conductivity	W/m.K
CP	Specific heat of the air	J/kg K
G	Solar flux	W/m^2
Pmax	Maximum power	W
FF	Fill factor of the PV module	---
PF	Packing factor of the PV module	---
I	Current of the PV module	A
V	Voltage of the PV module	V
u	Velocity component at x-axis	m/s
v	Velocity component at y-axis	m/s
w	Velocity component at z-axis	m/s
Nc	Number of the cells	---
h	Heat transfer coefficient	W/m^2 K
H	Height of the collector	m
W	Width of the collector	m
L	Length of the collector	m
$\dot{m}$	Mass flow rate	kg/s
U	Overall heat loss coefficient	W/m^2. K
Ub	Collector back loss coefficient	W/m^2 K
Ut	Collector top loss coefficient	W/m^2 K
Q*u*	Useful energy	W
D_h	Hydrodynamic channel diameter	m
g	Glass	---
r	Radiation	---
s	Sky	---
w	Wind	---
v	Velocity	m/s
C_μ, $C_{1\varepsilon}$, $C_{2\varepsilon}$	Constant in turbulence model	---
U, V, W	Total velocity vectors	m/s
ΔP	Pressure drops through collector	Pa
x, y, z	Cartesian coordinates	m

Greek Symbols

Symbol	Definition	Unit
ε	Dissipation rate of turbulent kinetic	---
σ	Stefan-Boltzmann constant	W/ $m^2.K^4$
τ	Transmission coefficient	---
α	Absorption coefficient	---
μ	Dynamic viscosity	$N.s/m^2$
∅	Any of the variables to be solved	---
η	Efficiency	%
ρ	Density of air	Kg/m^3
Γ_e	Effective diffusion coefficient $=\frac{\upsilon_e}{\sigma_e}$	$N.s/m^2$
σ_k, σ_ε	Turbulent Prandtl number for κ, ε	---
τα	Effective transmittance-absorbance	---
υ	Kinematic viscosity	m^2/s
υ_e	Effective kinematics viscosity	m^2/s
υ_t	Eddy or turbulent viscosity	m^2/s
κ	Kinetic energy of turbulent	---
ηth	Thermal efficiency	%
ηpv	Electrical efficiency	%
ηov	Overall efficiency	%
ηr	Reference efficiency	%

Subscripts

Symbol	Title
PV	Photovoltaic Cell
PV/ T	Photovoltaic/Thermal Collector
ASHRAE	American Society of Heating, Refrigeration and Air Conditioning Engineers.
CFD	Computation fluid dynamics
κ-ε	Three-equations turbulence model
MFR	Mass flow rate
Isc	Short circuit current of the PV module
Voc	Open circuit voltage of the PV module
ARC	Ethylene-vinyl acetate
EVA	Anti-reflective coating
RANS	Reynolds Averaged Navier Stokes

Chapter One

Introduction

CHAPTER ONE

INTRODUCTION

1.1 General Concept

Promising forecasts reflect the impressive technical gains achieved due to the use of renewable energy sources, which would provide immeasurable environmental benefits because of the reduction of harmful emissions compared to fossil fuels. Sustainable energy applications have been highlighted and developed through their inexhaustible sources. Solar Energy is one of the Middle East's greatest and most abundant sources especially in Iraq. The incoming solar radiation can be collected and used in various forms, including electricity generation, solar heaters, building heating, etc. [1]–[5].

Figure (1.1) shows a summary of the estimated solar energy available for power generation and other energy applications in Iraq. It represents a long-term average of daily/annual direct natural radiation totals [6]

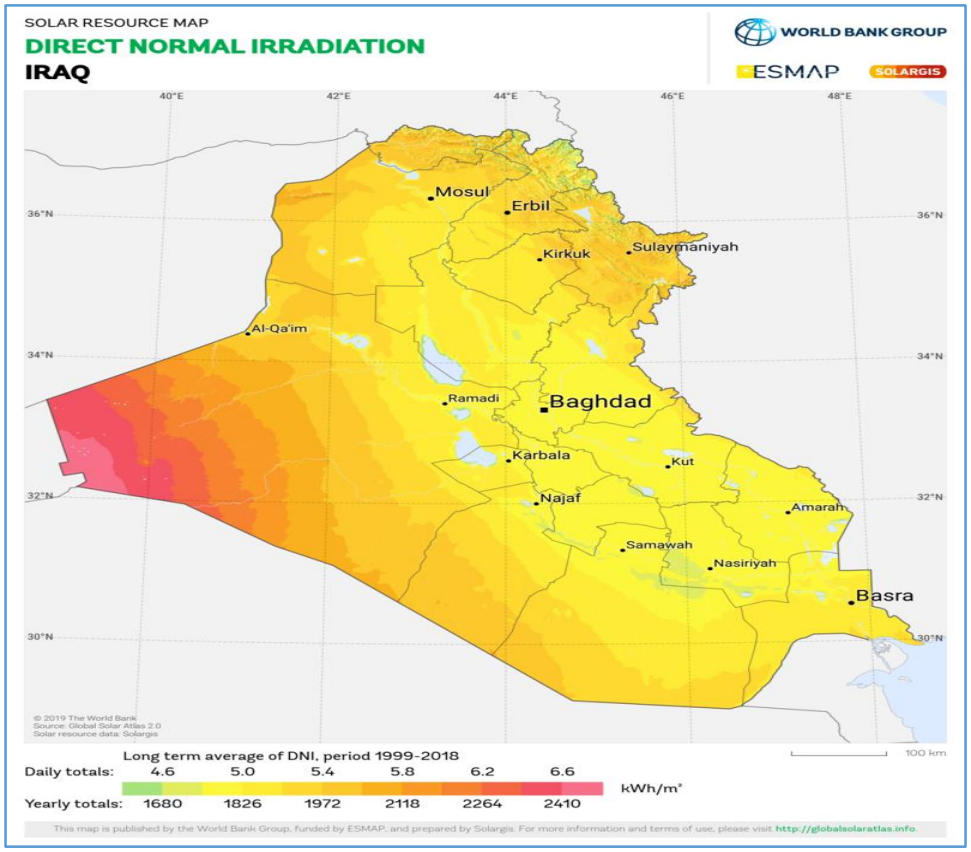

Figure (1.1) Shows a summary of the solar energy available in Iraq [6].

1.2 Solar Radiation

The flux of radiation energy is an important source in many solar applications. Such as The most effective one is direct solar radiation which falls in the form of a beam directly on the surface of the earth without passing through obstacles and it is called beam radiation. However, reflected on the surface after passing through barriers such as clouds, it is partially polarized and diffused which is called diffuse radiation. Moreover, there is reflected radiation due to falling on objects [1], as shown in Figure (1.2). and influenced by the atmospheric layer, which reduces their total intensity. The three types of radiation have long-wave, which increases their thermal energy [7].

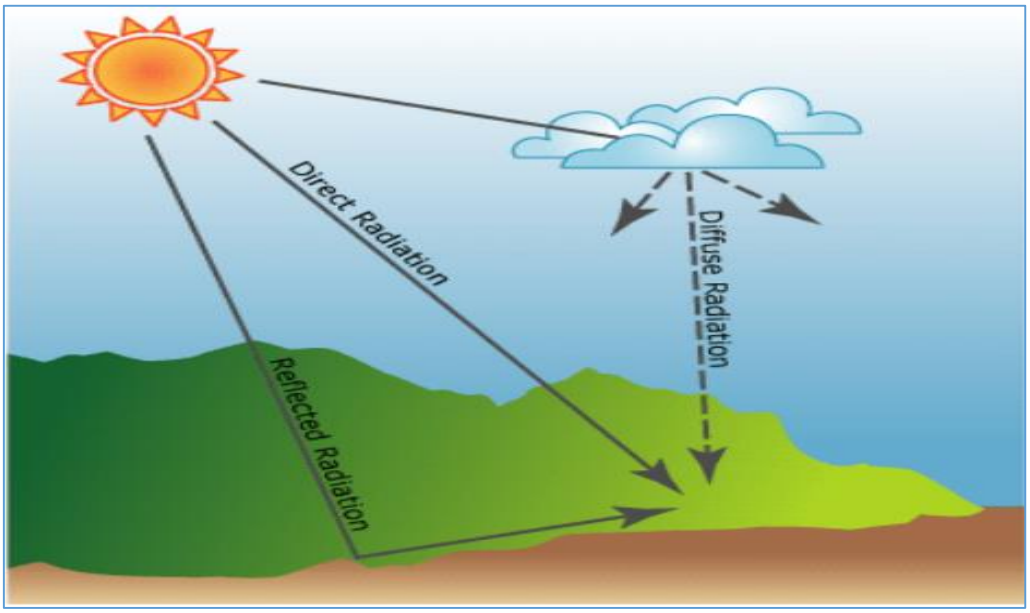

Figure (1.2) Scheme shows types of solar radiation[8].

1.3 Photovoltaic (PV) Panel

PV cells are solid modules that absorb solar radiation (light, heat) falling on the area unit. Electricity is generated by converting light into electrical energy due to the loss and gain of electrons, thus generating an electromotive force without needing a heat engine. Among its advantages:

1. Less maintenance, as it have no moving parts.
2. The required power control from the lowest power to the large stations.
3. Adding cells or panels to increase the productive capacity very easy.

4. Environmentally friendly, and sustainably sourced [1].

The (PV) cell is made of a semiconductor silicon material consisting of two layers, the first (silicon + phosphorus) and the second (silicon + boron). An assembled unit consists of six layers: glass on top, silicon layers, anti-reflective coating (ARC), ethylene-vinyl acetate (EVA), Tedlar back, and metal back sheet [9]. PV Cells are the best applications of renewable source, as they are used in many uncomplicated fields [1],[10], as shown in Figure (1.3).

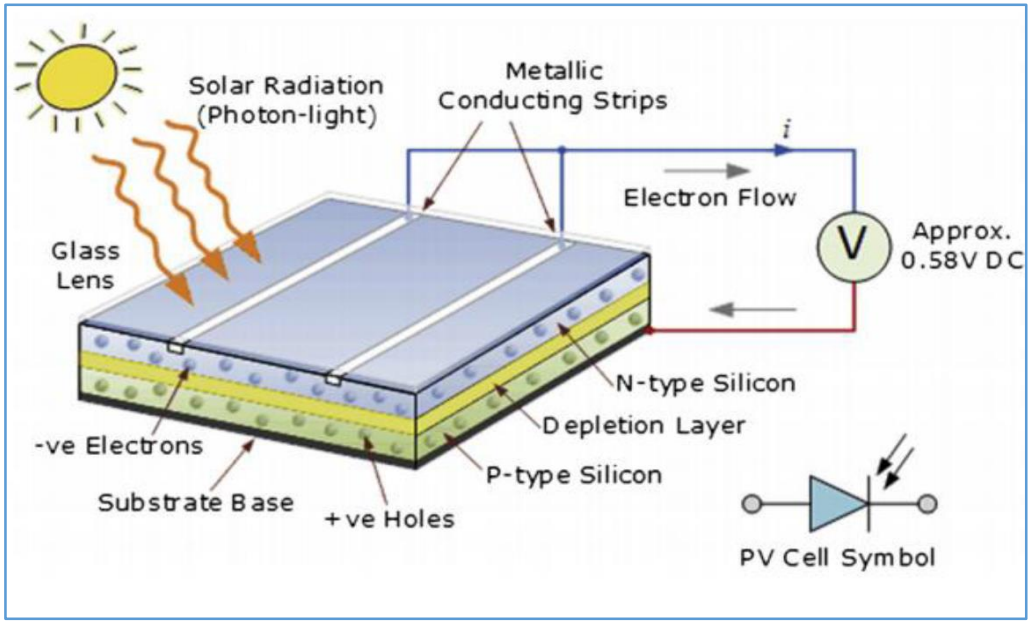

Figure (1.3) Schematic showing the working principle of a PV module [11]

1.3.1. Types of (PV) Technology

The silicon photovoltaic cell is classified as follows:

i. Monocrystalline (PV) cells:- This type contains crystalline capillary particles with a high efficiency of (14-15) %, which may reach higher than other types. However, it is relatively expensive due to the complexity of the manufacturing procedures, which rises the starting cost. It is also taken into account that the electrical efficiency is greatly affected by temperature and the intensity of solar radiation, which causes a decrease in efficiency by (0.4-0.5) % when the temperature rises by one degree Celsius above the standard test temperature, compared to thin-membrane cells [1].

ii. Polycrystalline (PV) cells:- These are manufactured by combining monocrystalline silicon by pouring the silicon into alloys after melting and

then cutting it into slices. One of the advantages of this type is lower production cost, as the manufacturing process is easier and less complicated than the first type. However but it is less efficient, estimated at (13-15) % with the same temperature effect coefficient [1].

iii. Amorphous (PV) cells:- Also called thin-film cells, silicon cells are arranged in thin homogeneous layers that can absorb light more effectively than crystalline silicon. Hence its cells are visible and thin [1].

The standard test conditions for the efficiency of (PV) cells are temperature (25 °C) and solar radiation (1000 W/m^2), which gives the cells the greatest efficiency and the highest possible electrical capacity. However because of the low conversion efficiency, which does not exceed (9%-20%) according to the specifications of the cell, more than (80%) of the capacity is not invested into electricity still, most of it is converted into thermal energy. Heat leads to a rise in the temperature of the cell, and thus the electrical efficiency of the cell decreases, which negatively affects performance of PV cell [9], [12]. Decreasing the temperature by one degree Celsius increases the electrical efficiency of PV cell by (2%) per (0.01 kg/sec) coolant flow rate [12].

Improving the efficiency of the (PV) cell is important and vital for saving power and money, and the efficiency can reach (28%). The efficiency relation with cell temperature is an inverse proportion. A small part of the radiant is transformed into electricity, and the larger part is transformed into unwanted heat energy. It is necessary to make accurate calculations to determine the purpose of using (PV) cells and the energy produced under natural climatic conditions and with different loads. Figure (1.4) shows a graphical diagram of different radiation intensities and the relation between the power produced and the cell temperature [1][7].

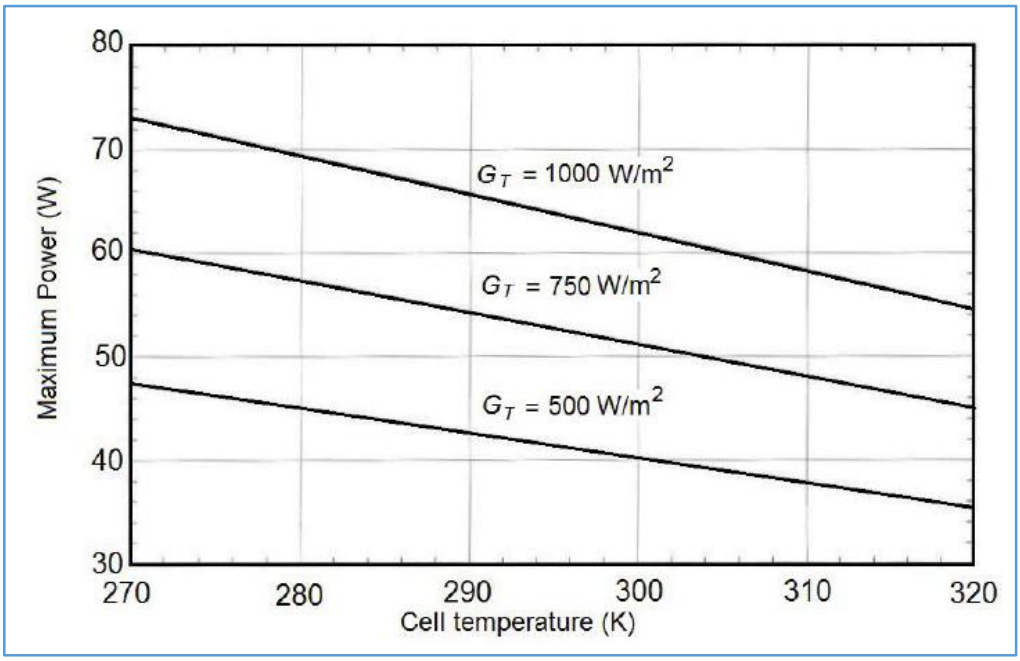

Figure (1.4) Illustrates relationship between the power produced by the cell and the temperature [7].

1.3.2. Characteristics of (PV) Cells

The figure (1.5) shows the characteristics focus PV cell on connecting it to variable loads to find the amount of voltage difference (V) and current (I) when the cell is connected in parallel with the variable load [13].

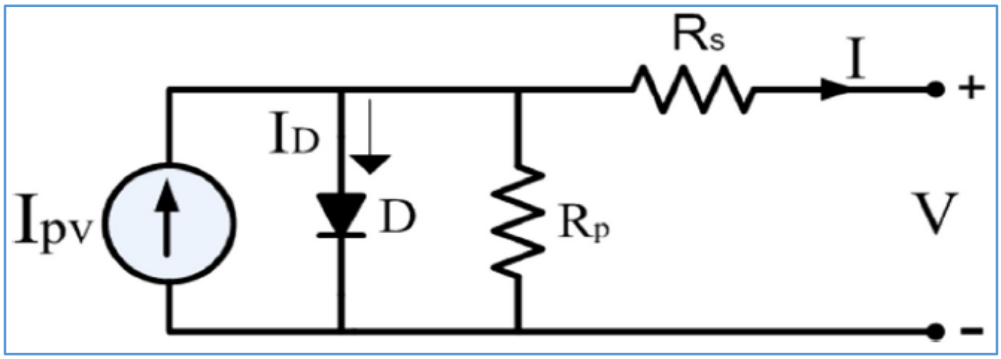

Figure (1.5) Equivalent circuit of the solar cell [14]

The (I-V) curve shows that the current starts from the highest value continues, and decreases gradually when the voltage rises to record levels. The greatest current and voltage values are at a very high solar radiation intensity, as in Figure (1.6). Reading the short-circuit current (Isc) appears at the intersection of the curve with the y-axis (voltage = zero). For the same procedure, at the intersection of the x-axis, they obtained the cell open-circuit voltage (Voc). They also extracted the energy produced from Joule's law

(voltage × current). at the point where the maximum power is produced is known as the maximum voltage (Vmpp) and the maximum current of the circuit (Impp) [6]. Through the maximum point of the (I-V) curve, the electrical efficiency of the cell (PV) can be calculated, so it is considered the most important point of the curve. Theoretically, the cell power (PV) is the maximum power produced by the cell under standard conditions, and when compared with the actual capacity, is called the fill factor (FF) [15]. Usually, the filling factor is less than one, and the closer it gets to one, the better the performance.

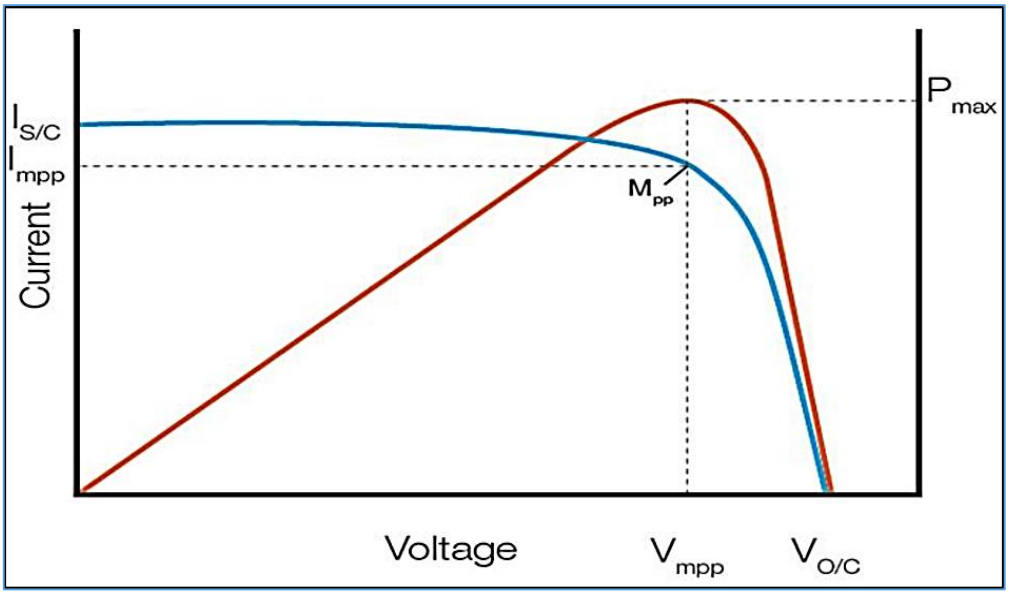

Figure (1.6) I-V and P-V Curves [16].

The cell current (PV) and the open circuit voltage gradually increase with solar radiation. While the short circuit current is proportional with solar radiation [7]. The performance of the cell is affected by the temperature. It is determined by drawing a curve (I-V) for each temperature at different radiation values; then, it is clear that the maximum power output is decreases with the increase in temperature. The experimental results showed that the maximum production decreases by about (20%) when the temperature rises (50°C) higher than the standard test temperature (25°C) [15]. Increasing the short circuit current by (0.05%) for each increase by (1 °C), while the open circuit voltage (Voc) decreases by (-0.5%), as seen in Figure (1.7).

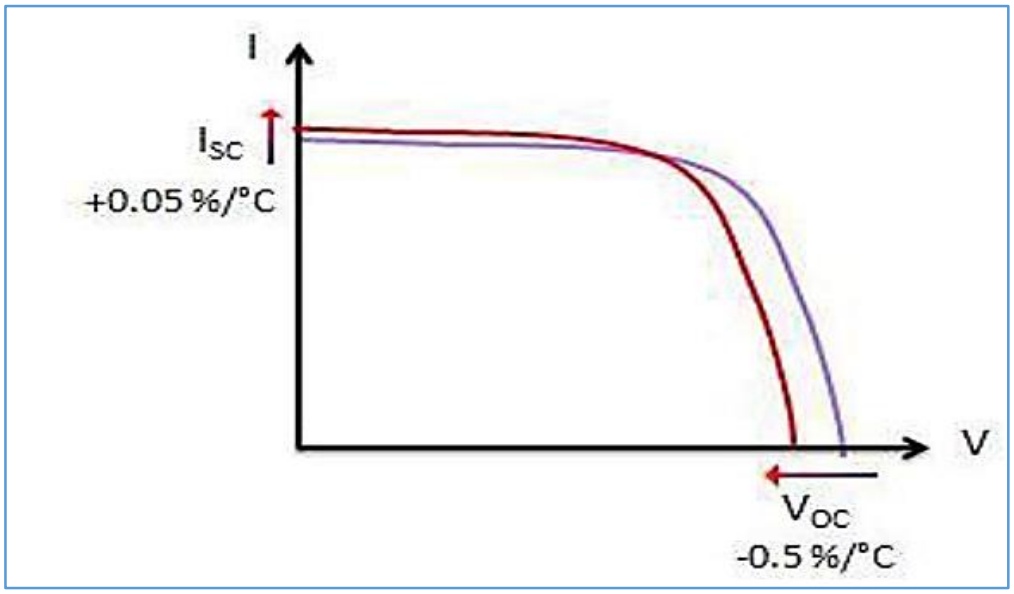

Figure (1.7) I-V Curve with the effect of temperature on the (PV) voltage [1].

From the curve (1.7), the shunt resistance and the series resistance can be determined to know the losses in the cell (PV) that reduce the efficiency. Success, the best performance, and the highest efficiency, the shunt resistance should be at the highest level and the series resistance at its minimum [17].

1.4 Solar Energy Applications

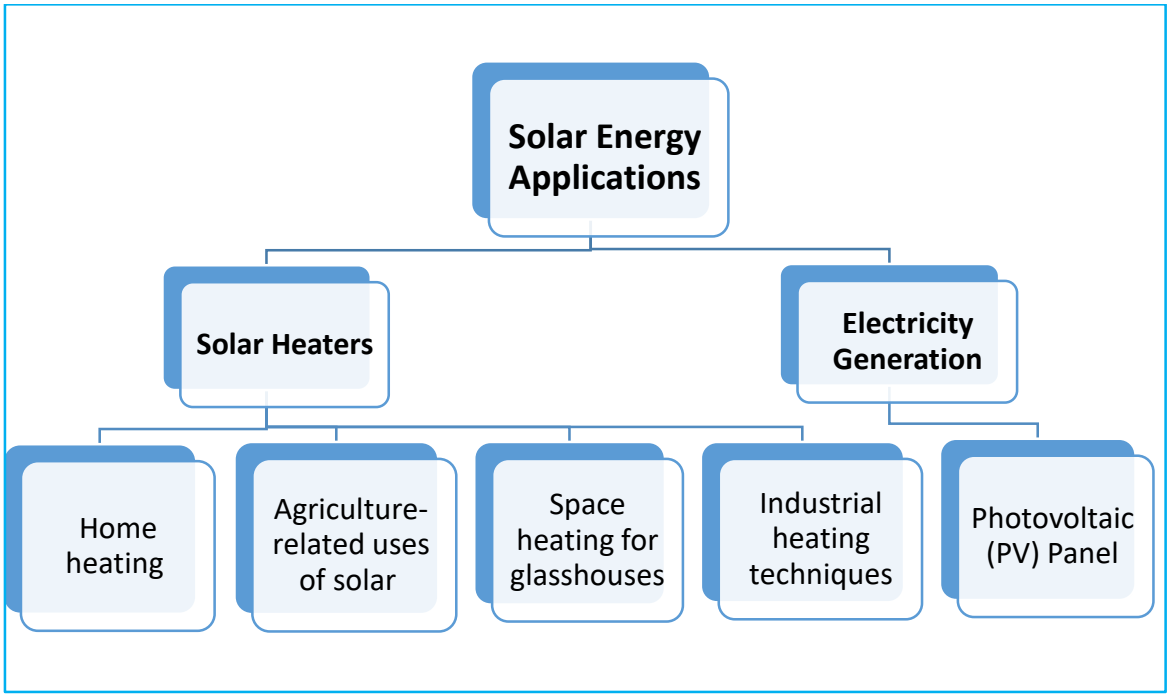

Figure (1.8) Illustration diagram solar energy applications [1] [18].

1.5 Study Motivation

Temperature is the main problem that restricts performance and reduces module efficiency (PV). High temperature leads to lower cell productivity, and lower conversion efficiency. as the percentage of solar radiation converted into electrical energy is from (13-15)%, and the rest turns into unwanted heat, increasing the cell temperature and reducing efficiency. Efforts were devoted to address these risks to reach obtain the optimal efficiency of the PV cells, at standard test conditions (25 °C), and solar radiation (1000 W/m^2) by heat transfer and disposal techniques.

1.6 The Scope of the Present Study

This study will focus on the following investigations to enhance electrical and thermal performance by reducing PV temperature and increasing electrical efficiency:

i. Numerical approach

Simulate and develop 3D numerical model using Comsol, to investigate the differences between three different flow channels: Rectangular, triangle, transverse fins with mult-flow. Then, the suggested models will be validated against previous studies

ii. Experimental approach

Design and perform PV/T experiments to test the adopted cooling technigues, and measure PV/T important parameters.

1.7 Objectives of Thesis

The objectives of this thesis are:

1. Three different models of PV/T air systems are analyzed numerically, with rectangular, triangular, and transverse fin channels. Then an optimal model is selected, according to the minimum PV temperature of the solar panel.

2. Fabricating cooling PV/T system to minimize the cells' operating temperature for Iraqi weather conditions.
3. Investigating the effect of air MFR, on outlet temperature, solar panel temperatures, thermal and electrical efficiencies.
4. Evaluating different rates of solar flux on the PV cells temperature, the outlet air temperature, thermal and electrical performances.
5. Studying the electrical performance of the solar panel by using a PV analyzer.
6. Associating theoretical and experimental results build a CFD model for the system for further investigations to the compatibility between them.

Chapter Two

Literature Review

CHAPTER TWO

LITERATURE REVIEW

2.1 Introduction

This chapter focuses on previous studies that led to improving the performance of solar cells by reducing temperatures and increasing solar radiation absorption energy. The researchers devoted efforts to designing PV/T systems with different shapes and heat transfer media (air, water, and nanofluids) that would increase the surface area exposed to cooling, with low speed of the coolant, as well as create turbulent flow, etc.

2.2 Experimental and Theoretical Approach

The research revolves around reviewing the different methods of cooling (PV) modules to reach the desired objective and the required results to derive scientific evidence from them, they are classified according to the following methods:

2.2.1 PV/T Cooling Systems using Air

Maysam Gholampour, Mehran Ameri, (2015) [19], created of hybrid transpiration (PV/T) air model see Figure (2.1) that produces thermal and electricity simultaneously, using computerized fluid dynamics (CFD) technology. Good agreement was obtained between the measured and simulated values, with the greatest relative root mean square percent deviation (RMSE) (9.13%) and the lowest correlation coefficient (R-squared) (0.92).

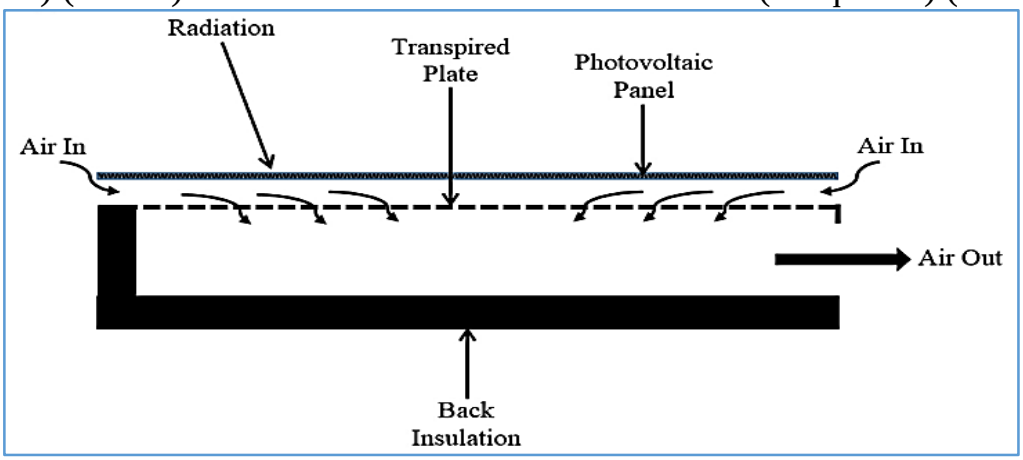

Figure (2.1) The PV/T flat transpired collector [19].

Amin M. Elsafi, P. Ganadhidasan, (2015) [20], studied the comparison between compound parabolic concentration (CPC) and a flat double-pass (PV-T) system. The model was developed and verified experimentally; the study deal with the structure of fins as shown in Figure (2.2), the effect of their chemical composition and shape on performance with the without-fins model. The results showed that the thermal gain for one year (1%) for a (PV/T) with fins compared with (PV/T) without fins, and (3%) annual electrical gain for (PV/T) with fins increased, compared with for (PV/T) without fins.

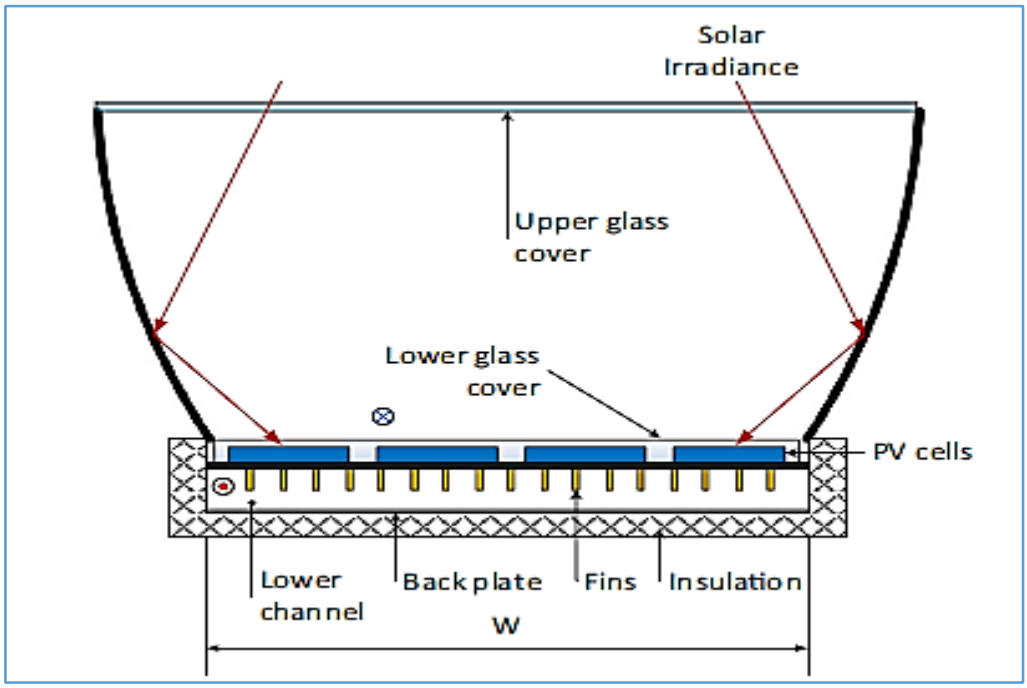

Figure (2.2) Diagram front view of finned double-pass (CPC)(PV/T) collector [20].

Jin-hee Kim et al. (2016) [21], focused on a heat recovery technology from (PV/T) collectors by a Heat-Recovery Ventilator (HRV). Furthermore, through a system (PV/T) that utilizes air as a heat transfer medium, a device (HRV) vacuums the air carrying heat of the system inside to heat buildings simultaneously, compensated with cold air due to the pressure difference during this procedure. Showed that experimental results of the (PV/T) system

with HRV at a (1 kW) the thermal performance, and electrical performance were analyzed, compared to the (PV/T) system without the (HRV) device.

Sonveer Singh et al. (2016) [22], analyzed the thermal performance of a double-channel semitransparent photovoltaic system (DCSPV/T) as shown in Figure (2.3), the surface heat transfers by air at two channels were upper and lower (DCSPV/T). Showed that the results, thermal gain (TG), electrical gain (EG), total energy gain (OEG), and total thermal gain (OTG) for (DCSPV/T) module compared with a single-channel semitransparent photovoltaic system (SCSPV/T), results were recorded (34.57%, 71.51%, 5.78%, 35.41%), respectively.

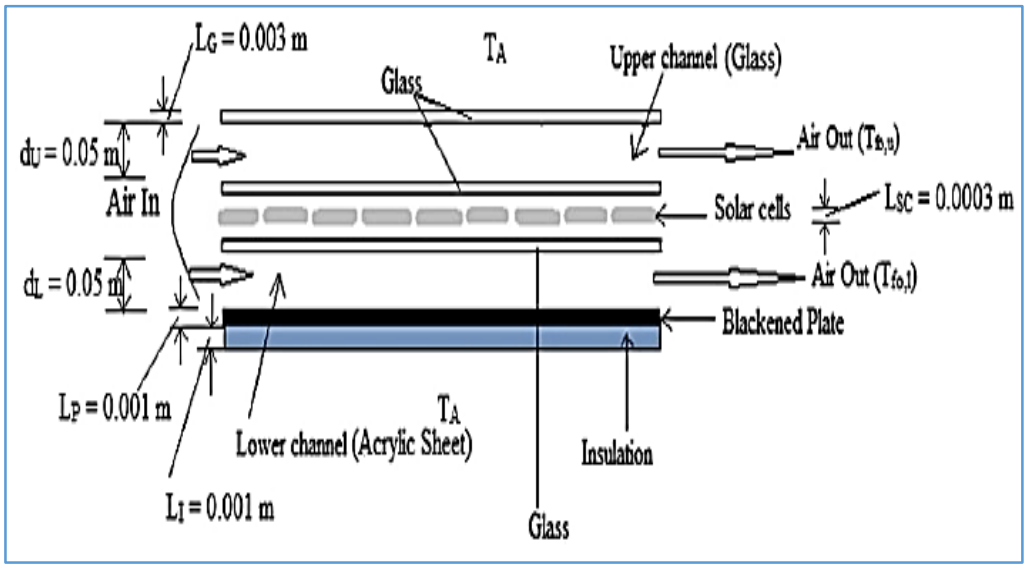

Figure (2.3) Side view (DCSPV/T) module [22].

Mohamed El Amine Slimani et al. (2016) [23], studied the comparison of four solar system mechanisms: (PV-1) panel, hybrid solar air (PV/T-2), glazed hybrid solar collector (PV/T-3), and double path glazed hybrid solar collector (PV/T-4). Numerical results showed a overall energy efficiency rate for (PV-1), (PV/T-2), (PV/T-3), and (PV/T-4), their values (29.63%, 51.02%, 69.47%, 74%), respectively. As shown in Figure (2.4).

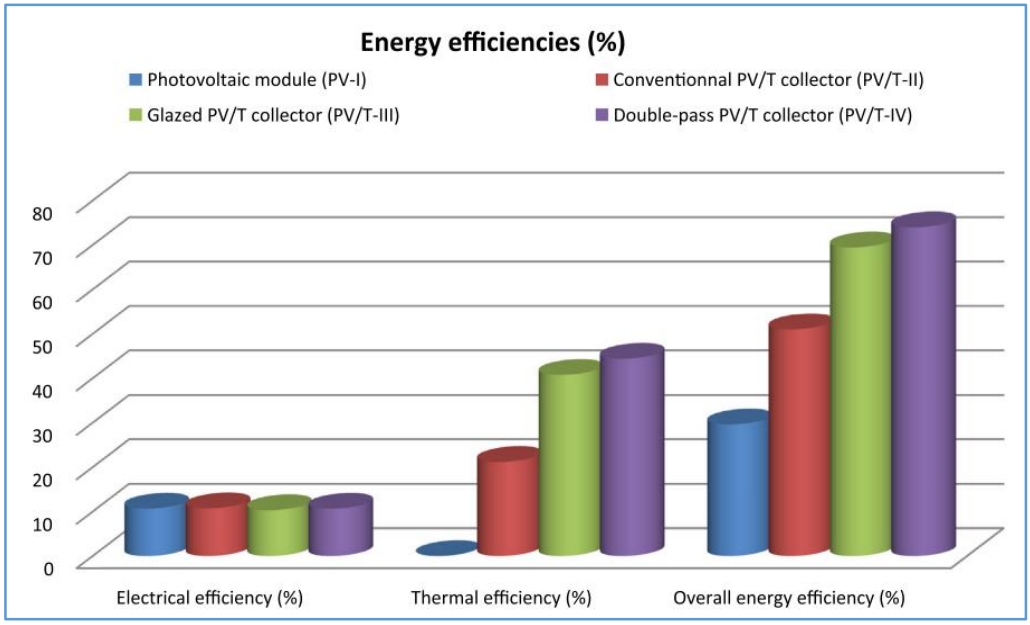

Figure (2.4) Achart showing the comparison among of electrical, thermal, and overall efficiencies for four configurations [23].

Shyam, G. N. Tiwari, (2016) [24], concentrated on the efficiency, air temperature, thermal energy, and exergy for (PV/T) collectors covered semitransparent layer, case (1): the cover at inlet air, case (2): the cover at outlet air. As shown in Figure (2.5). The results confirmed that when the mass flow rate decreased with a small number of collectors connected in the chain, case (1) recorded the best performance, while the higher flow rate and a large number of collectors gave the two states the same performance.

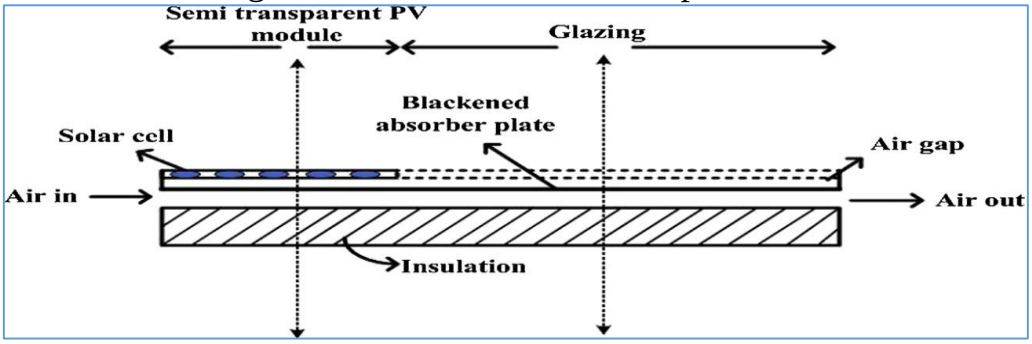

Case (1)

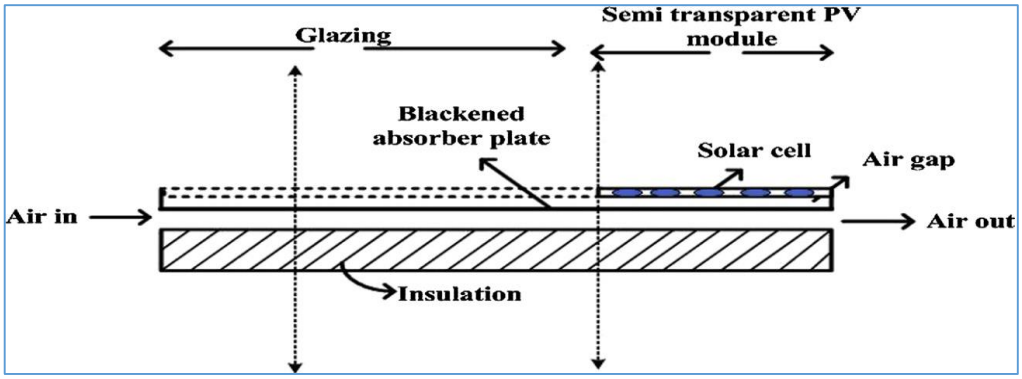

Case (2)

Figure (2.5) Side view of series connected PV-T air collector partially covered by semitransparent PV modules at the inlet of air collector (Case 1), (case 2) [24].

Ahmad fudholi et al. (2017) [25], presented an experimental, theoretical study to analyze the performance of a (PV/T) collector with a ∇-groove, the test was performed under solar flux (385 - 820) W/m², with a mass flow rate of (0.007-0.07) kg/s. Showed that results temperatures decreases when the mass flow rate of air is rising for various solar fluxes because air flows stronger into the accumulator when the mass flow rate of air increases as shown in Figure(2.6). Moreover, for solar fluxes of (300-1000) W/m², thermal efficiency increases when the mass flow rate of air is rising.

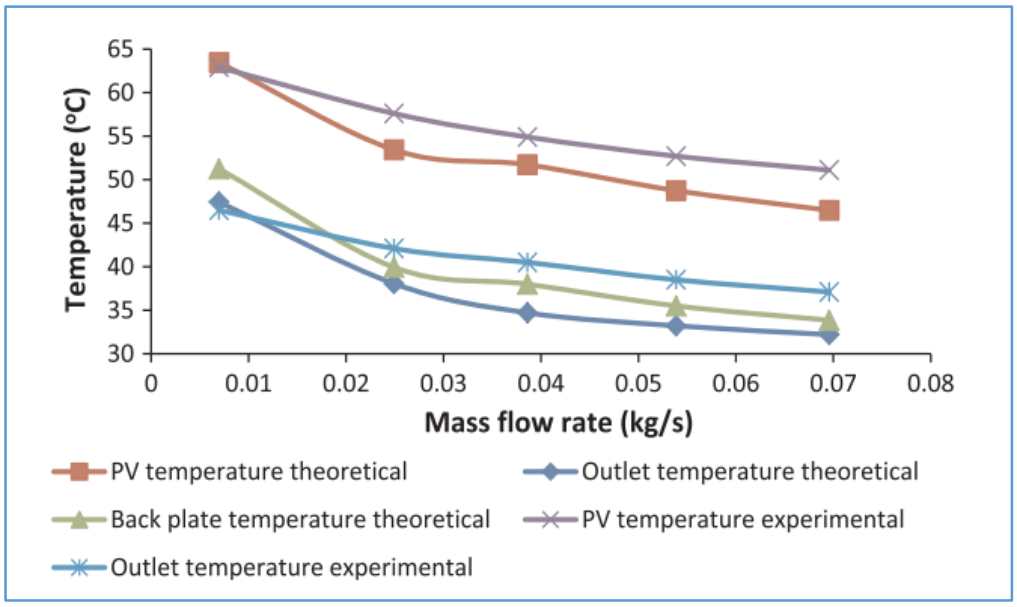

Figure (2.6) The curve shows the theoretical and experimental results PVT collector with a ∇-groove at 820 W/m^2 solar flux. [25].

Ahmad Fudholi et al. 2018 [26], conducted the theoretical and experimental approach to a (PV/T) air collector with a ∇-groove, as shown in

Figure (2.7). The results of percentage error the outlet air temperature for the theoretical (3.75%) and experimental (5.49%) values. Exergy efficiency (PV/T) with a ∇-groove is (13.36%), and (12.89%) for theoretical and experimental studies, respectively. Furthermore, the air collector sustainability number (PV/T) for theoretical and experimental studies is (1.168, 1.148).

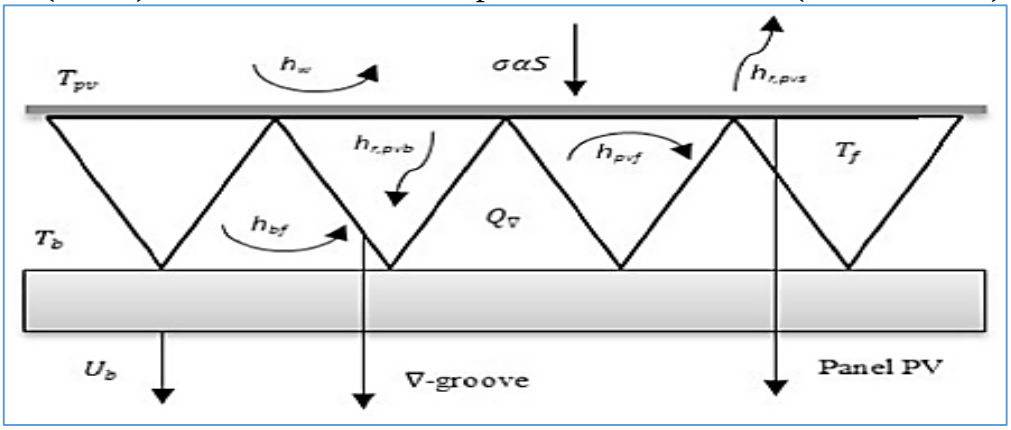

Figure (2.7) Diagram of heat transfer properties in the PV-T air collector with a∇-corrugated absorber [26].

Ahmed Mohsin alsayah et al. (2019) [27], conducted numerical study by using (ANSYS-cfx) program. The study was applied for channel models subjected to forced air current towards the cell (PV/T) base, as shown in Figure (2.8). The study has concluded that the model, of air mesh with fixed aluminum channels installed internally, with dimensions according to a cell base, showed the lowest cost and available in the local market. The study found the best ideal number, position, and inclination angle of horizon, (18), (70 mm) of channel base, and (45-mile angle), respectively.

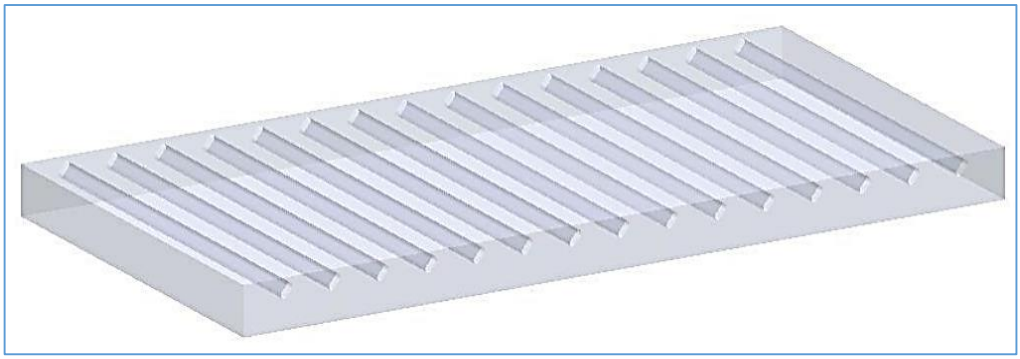

Figure (2.8) Illustration of air guides by the SOLD WORK program [27].

Shuang-Ying wu et al. (2019) [28], analyzed the effect of cooling duct location on the thermal performance of the (PV/T) air system, the first case (1) considers the cooling channel above (PV) plate, and the second (2) is below (PV) plate as shown Figure (2.9). The results were shown at inlet air temperature for the systems (1) case, (2) case, (298.15 K, 295.65 K), respectively. Maximum energy efficiency is obtained from the amount of energy supplied, and the details concentration of the energy quantity hits the wall when calculating the advantages of two cases. Nusselt number amount on PV panels is often equal for both cases. Case (1) is prefer.

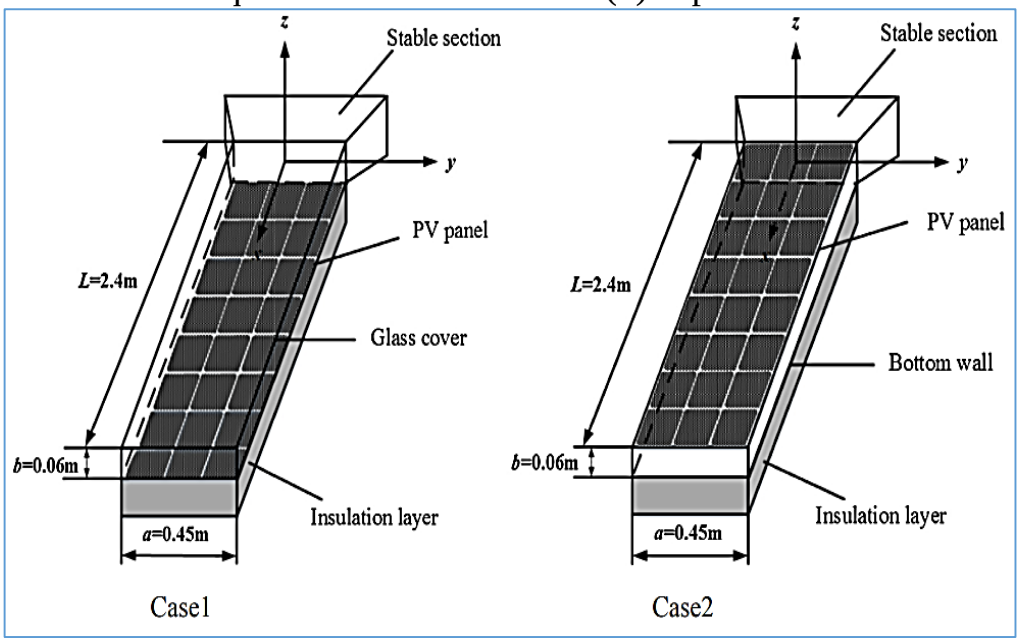

Figure (2.9) Models of air-cooled PV/T systems,[28].

A. Hosseini rad et al. (2019) [29], found innovative analytical and experimental styles to improve the performance of multi-channel photovoltaic-thermal (MCPV/T) systems, as shown in Figure (2.10). At air flow rate (0.005 kg/s) and radiation intensity (926 W/m²), efficiencies were achieved, total electricity, exergy, and energy (9.73%, 10.72%, 47.24%), sequentially. For flow rate (0.011 kg/s), radiant intensity (927 W/m²), and efficiencies (9.35%, 10.40%, 65.10%), respectively. Moreover, the greatest exergy efficiency (13.46%) at a flow rate of (0.024 kg/s). Similarly, the overall energy efficiency

decreases by (70%), with an increase in channel height and the greatest exergy efficiency (13.64%) at channel height (0.011m).

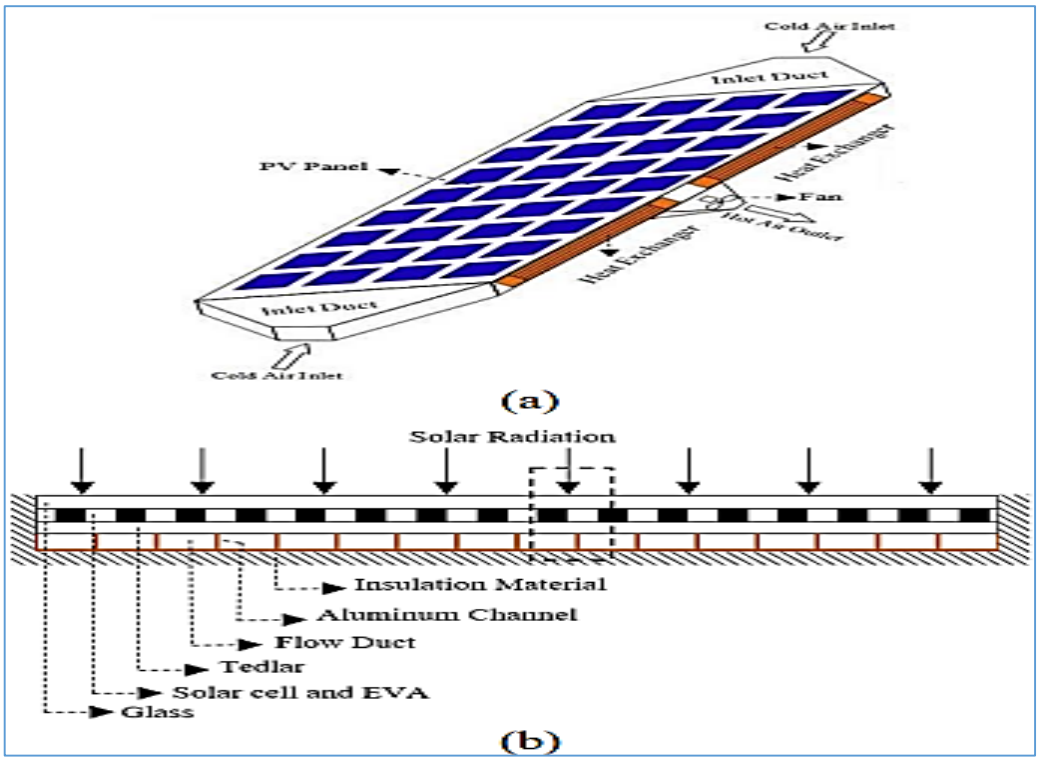

Figure (2.10) A schematic of a designed MCPV/T system. (a): Side view, (b): Cross-section view [29].

Jianjun Hu, Guangqiu Zhaug, (2019) [30], investigated the techniques for improving solar air collector performance, which included of installation of the fins, ribs, and a grille, as shown in Figure (2.11), and the utilization of different forms to regulate airflow, the process of heat transfer between the air and the absorbent plate, replacing the single duct with multiple channels to regulate airflow, placing barriers to generating additional flow, enhancing heat transfer by convection. The main idea is to find a relation between optimization methods, flow regulation, and a discussion of studies on ideal methods and the interconnection of these methods.

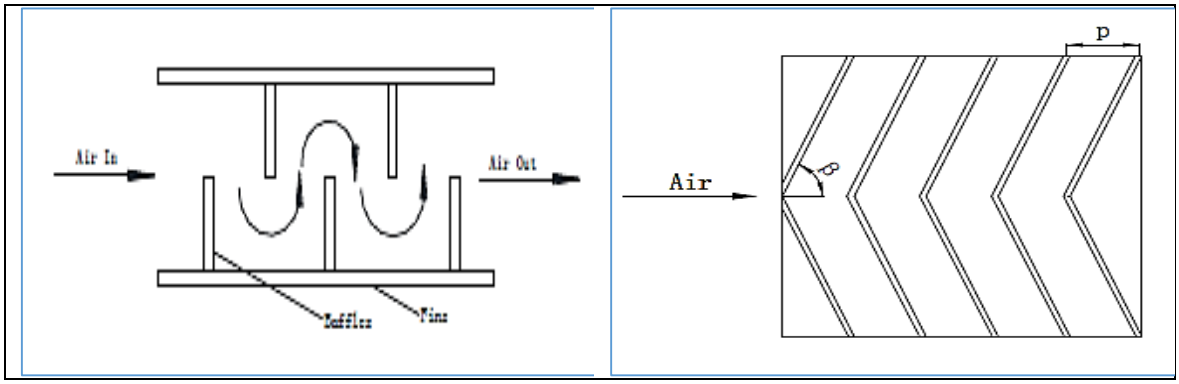

Figure (2.11) Fins with attached baffle, V-shaped without gap rib [30].

Ridwone Hossain et al. (2020) [31], explained a theoretical study that when the temperature of the solar cell increases (1°C), the efficiency of photovoltaic energy conversion decreases by about (0.3%). To reduce these risks by understanding the scientific methodology of the technologies of cooling systems that use different media to dissipate heat.

Yan zhao et al. (2020) [32], studied a numerical modeling and experimental analysis of a novel design of (PV/T) air collector by adding an aluminum structure shaped like a beehive. Experimentally, the system was tested at irradiance (200-600) W/m², with coverage ratios (PV) of 15%, 30%, 45%, 60%, 75%, and 90%. The results of the experimental, numerical analysis of the air collector (PV/T) have shown at instantaneous efficiency of (64%) and coverage percentage (45%). The required thermal efficiency is achieved, and a numerical model has been developed based on the investigation that there is an ideal coverage ratio that can raise the total efficiency under conditions of an experimental, numerical model.

Hwi-ung Choi, Kwang-hwan Choi, (2020) [33], focused on the thermoelectric performance of a novel design (PV/T) collector, as shown in Figure (2.12), consisting of a double air duct with one lane, an irregular transverse rib attached to the bottom of (PV/T) surface. Under air mass flow rates (0.0198 - 0.07698) kg/s, the results recorded of the thermal efficiency of (35.2%-56.72%), and electrical efficiency (14.23%-14.81%).

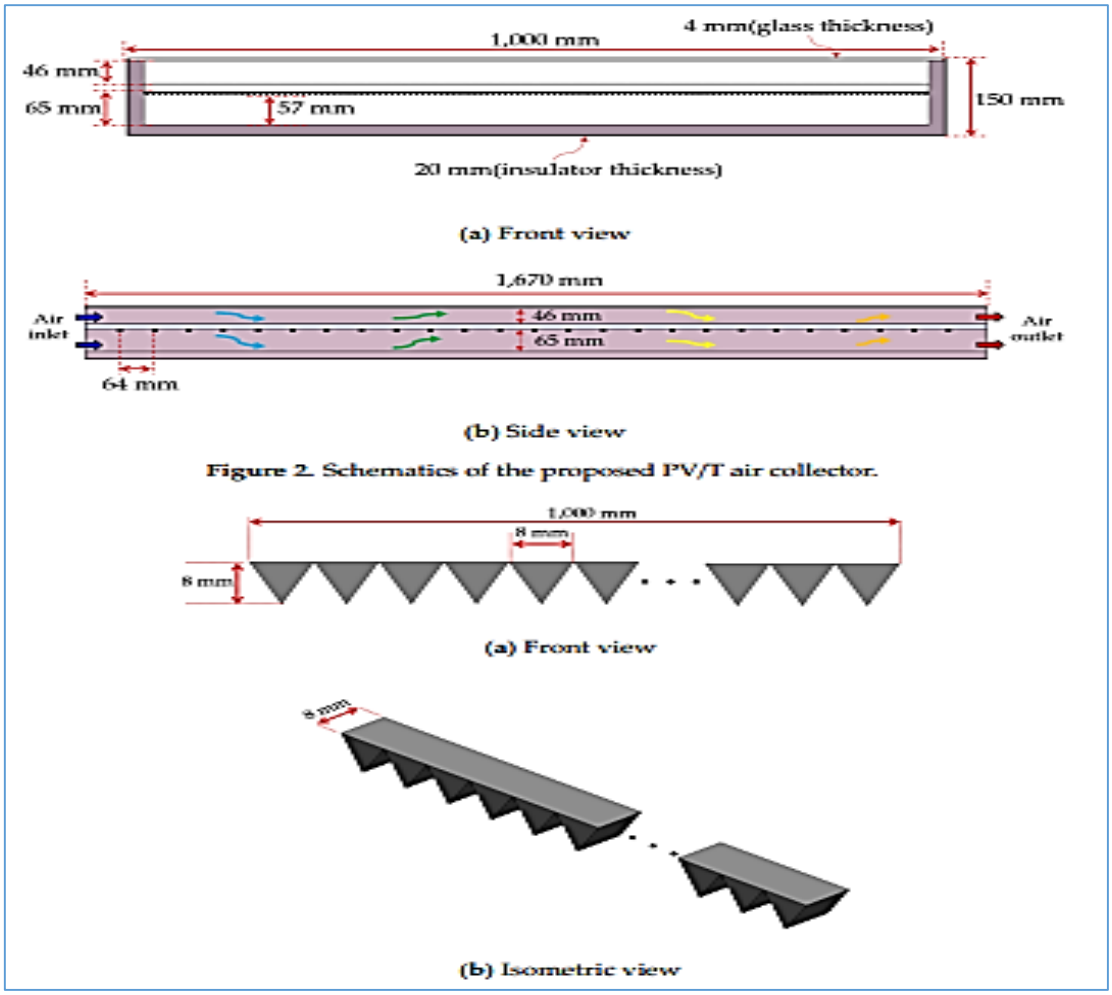

Figure (2.12) Diagrams of the non-uniform cross-section transverse rib installed in the PV-T air collector[33].

Ismail Baklouti, Zied Driss, (2020) [34], focused on the cooling system flow rate and air duct depth to improve the thermal and electrical efficiency of (the PV/T) collector. Study was conducted using (ANSYS Fluent 17.0 and Matlab) programs to analyze airflow characteristics and collector (PV/T) characteristics at different mass flow rates and depths. The results showed that there is good agreement between numerical and experimental comparisons, the effect of increasing the air flow rate and decreasing the channel depth on improving thermal efficiency with a small change in output power.

Table 2.1. The summary of the authors studied PV/T air passed

Author	Module-type	Study-type	ENHANCEMENTS		
			Electric efficiency	Thermal efficiency	Overall Efficiency
Mohamed El Amine Slimani et al, 2016 [23]	PV/-1 PV/T-2 PV/T-3 PV/T-4 air collector.	Experimentally	10.66% 10.73% 10.33% 10.65%	0% 21.19% 40.77% 44.41%	29.63% 51.02% 69.47% 74%
A. Hosseini rad et al, 2019 [29]	MCPV/T air collector	Experimentally	9.35%	39.14%	65.1 %
Yan zhao et al, 2020 [32]	PV/T air- collector with aluminum honeycomb SAC.	Experimentaly,	18.78%	68%	86.78%
Hwi-ung choi, Kwang-hwan choi, 2020 [33]	PV-T air- collector with double duct and rib to bottom (PV/T)	Experimentally	(14.23-14.81)%	(35.2-56.72)%	(49.44 - 71.54)%

2.2.2 PV/T Cooling Systems using Water and Nanofluid.

Ahmed Elnozahy et al. (2014) [35], compared the results of an automatic cooling performance and surface cleaning Experimental (PV) unit on the roof of a building in hot weather with a unit stripped for cooling and cleaning. The results showed a regression in the temperature of the anterior and posterior surfaces by about (45%, and 39%) respectively. The efficiency of the cooling/cleaning unit is (11.7%). the efficiency of the unit without cooling/cleaning (9%). Further,the output power (89.4 W) is the greatest produced by a cooling/cleaning unit versus (68.4 W) for a unit without it.

Kaijun Yang, Chuncheng Zuo, (2014) [36], demonstrated that using a multi-layered micro-channel system of concentrator photovoltaic (CPV) cells extends its life, improves electrical output, and effectively reduces surface temperature. Surface temperature different (CPV) thermal image analysis was recorded by (6.3℃). heat transfer coefficient multi-layer micro-channel is (8235.84 W/m^2.K). and pressure gradient less than (3 kPa). The results confirmed that the hybrid cells (CPV) possess sufficient external capacity due to the low pumping capacity and high electricity production.

Ahmer A. B Baloch et al. (2015) [37], conducted an experimental, numerical analysis and evaluation of a cooled/uncooled (PV) system using convergent channels see Figure (2.13), focusing on the thermal properties based on the convergence angle. The show was the best performance of the average temperature distribution at standard deviation (0.91℃). Temperature readings using convergent cooling (45.1℃) for June month showed, (36.4℃) for December month after it was (71.2℃), (and 48.3℃) for an uncooled system, respectively. The percentage of the output power increased (36.1%) compared to (35.5%) with the uncooled (PV) system.

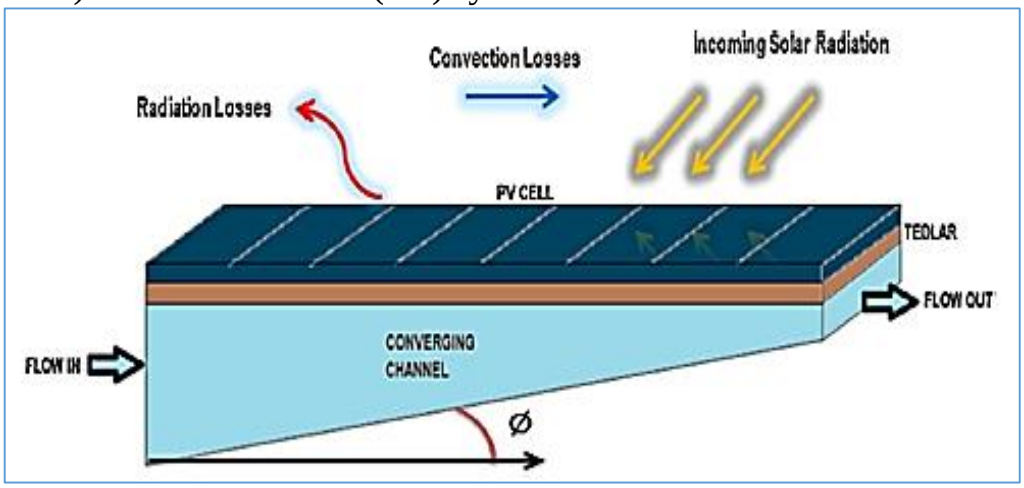

Figure (2.13) Diagram of converging channel with heat transfer modes [37].

Di su et al. (2016) [38], improved the performance of (PV/T) collectors using dual-channel cooling, fluid analysis, and thermal/ electrical efficiency. It was compared with four different liquid collectors see Figure (2.14). Researchers confirmed that the largest amount of heat transfer from the water-water (PV/T) collector, thus as the highest efficiency of electrical and thermal performance provides a sufficient amount of hot water. Furthermore, increased water mass flow rate and higher upper/lower pipe spacing improve overall efficiency.

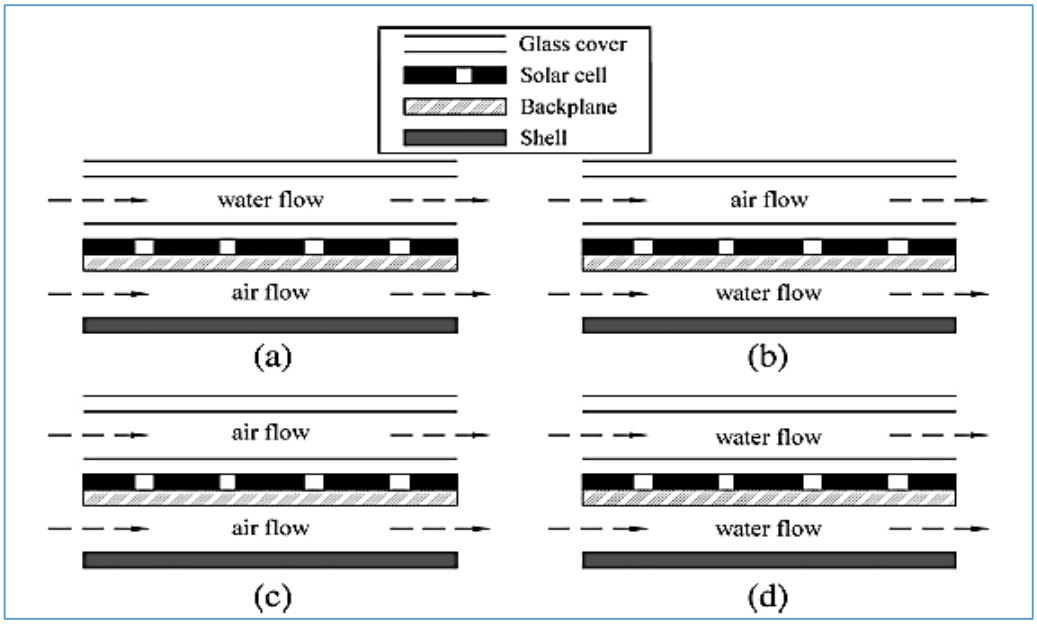

Figure (2.14) Section view of PV/T collector with dual channels for different liquids,[38].

Y. Khanjari et al. (2016) [39], evaluated the effect of nanofluids on the performance of a (PV/T) module, utilizing Ag-water nanofluid and alumina-water nanofluid. Numerical tests were carried out by computational fluid dynamics (CFD). The results showed an increase in the heat transfer coefficient for (Ag-water nanofluid and alumina-water nanofluid) amounts (43% and 12%), respectively. Figure (2.15) shows the differences in the outlet temperature versus the fluid velocity. As the velocity of the fluid increases, the outlet temperature of the decreases.

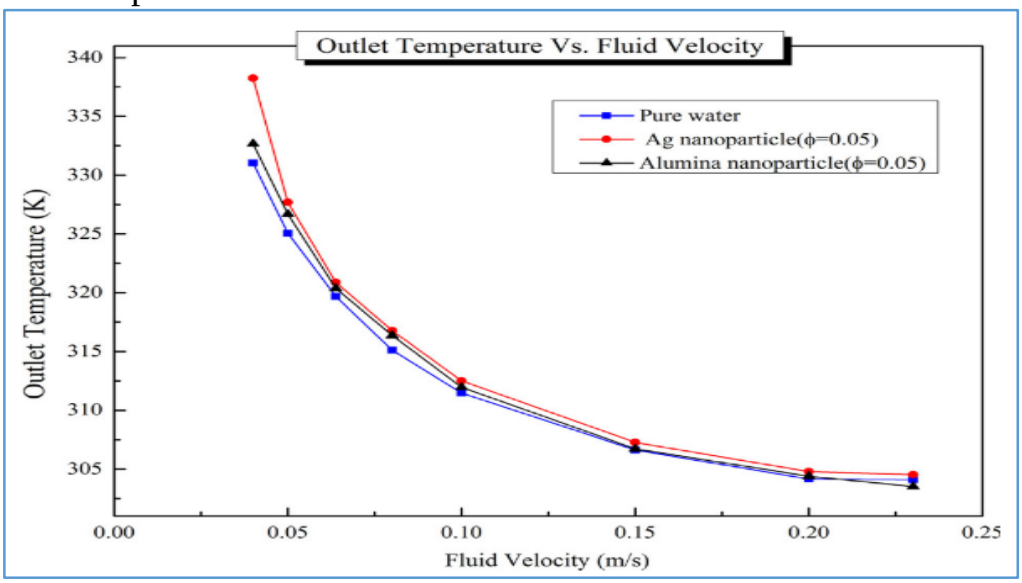

Figure (2.15) shows of outlet temperature versus fluid velocity for alumina-water nanofluid, Ag-water nanofluid, and pure water [39].

Farideh Yazdanifard et al. (2016) [40], simulated the effect of solar radiation, Fill Factor, Reynolds number, collector length, diameter, and the number of tubes on the performance of a water-based (PV/T) system with and without cover glass for laminar and turbulent flow, as seen in Figure (2.16). The results indicated that the energy efficiency of the glazed system is higher than that of unglazed, as long as the collector length, Reynolds number, and fill factor affect the exergy efficiency. Also, they recorded that there was an increase in the factors mentioned above at laminar and turbulent flow and an increase in the mass flow rate in the unglazed system compared with the vitrified one. Furthermore, energy and exergy efficiency will be highest for a laminar and turbulent system.

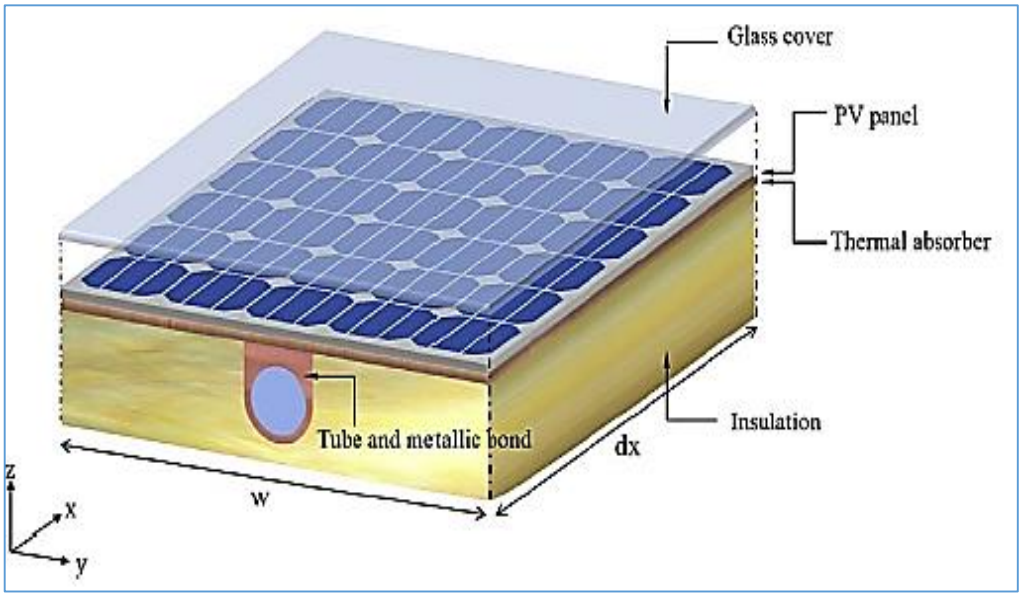

Figure (2.16) Differential components of the (PV/T) [40].

Munzer. S. Y. Ebaid et al. (2017) [41], examined the cooling of (PV) panels utilizing a nano-water cooling medium, a mixture of polyethylene glycol-water (Al_2O_3) at pH (5.7), and a mixture of cetyltrimethylammonium bromide - water (TiO_2) at pH (9.7), for a rectangular aluminum heat exchanger.

The results showed a temperature decrease of (PV) cells for both types compared with water-cooled and non-cooled cells. Further, nano-liquid (Al_2O_3) performs better than (TiO_2) nanofluid, and the higher concentration produces the best cooling.

Farideh Yazdanifard et al. (2017) [42], emphasized the ability of nanofluids to cool (PV/T) collectors and a thorough review of the system properties. The results indicated that the nanoparticles in a laminar system are more efficient compared to the turbulent one, using larger diameter particles leads to an increase in the overall energy efficiency in a turbulent system, while the nanofluids/ water-based fluid shows higher efficiency compared with the nanofluids based on ethylene glycol- water.

H. Fayaz et al. (2018) [43], adopted a three-dimensional model of a (PV-T) panel using a nanofluid multi-walled carbon nanotube (MWCNT-WATER). The results compared to running with water were as follows: improving the electrical efficiency of the (PV/T) panel, with a mass flow rate (of 120 L / h) by about (10.72%), and (10.25%) numerically and empirically, respectively. Thermal energy improvement amount (7.74, 6.89)W per (10 L/h) flow rate. Thermal efficiency (5.62%) numerical, and (5.13%) experimental, as seen in Figure (2.17).

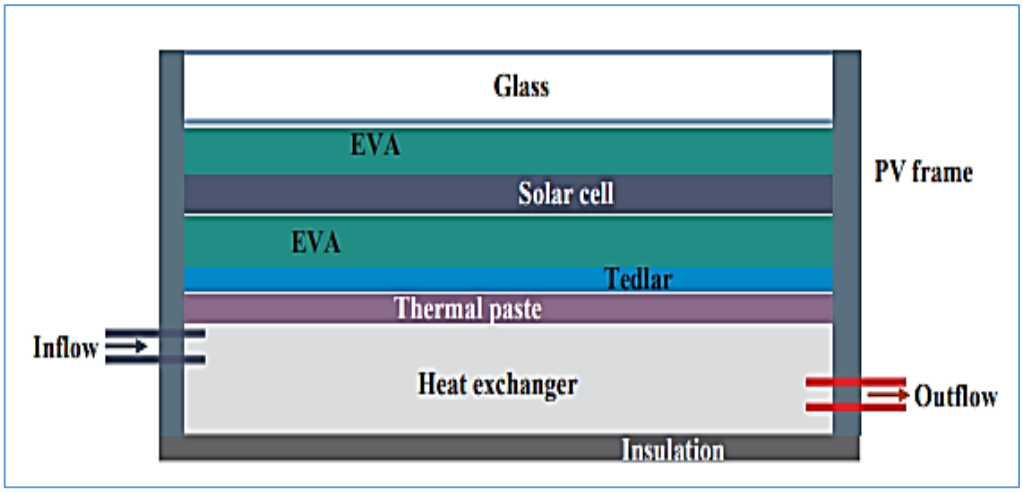

Figure (2.17) Scheme for PV/T,[43].

Ahmed fudholi et al. (2019) [44], studied the effect of the important factors on the performance of (PV/T) systems, using TiO_2/water nanofluid with (0.5 wt% and 1 wt% TiO_2) as coolant (PV-T). The results indicate (1 wt% TiO_2) nanofluid-based (PV/T) collector has an energy efficiency of (85%-89%) compared to (60%-76%) for the water-cooled collector at a mass flow rate of (0.0255 kg/s), at (1% Wt. TiO_2), exergy efficiency is improved by (6.02%) compared with a water-cooled collector, at the same flow rate. Also, new theoretical approach model was developed, compared with theoretical and practical results, for nano-liquid collector (TiO_2/water) (PV/T) to obtain an accurate (97.6%-99.2%) agreement between the theoretical and experimental curriculum.

Joo hee lee et al. (2019) [45], simulated a flat-plate (PV/T) system utilizing nanofluids cooling. Recorded the results the thermal, and electrical efficiencies of the system were using (CuO/water) at an increase of (21.3%), and (0.07%) compared with the water-based systems, respectively. Moreover, electrical efficiency increased slightly, possibly due to an error in the measurements. Thermal efficiency (15.14%) was also recorded for (Al_2O_3/water) systems, and there will be no difference in electrical efficiency between (Al_2O_3/water) and water systems.

Ali radwan et al. (2020) [46], devoted efforts to comparative analysis for the design of a new vacuum photovoltaic collector (VPV/T) with the conventional (PV-T) water-cooled collector. The results indicated that the new collector (VPV-T) has superiority (26.6%) in thermal power without electrical power at (Re=50), solar radiation (1000W/m²), and vacuum pressure (VPV/T) graded (0.01 pa - 10pa) slightly reduces the thermal power gain, therefore, the vacuum pressure increases from (10 Pa - 1.013 E5 Pa)، significantly reducing the thermal power gain with a slight increase in electrical power. Furthermore, overall predictions of exergy efficiency are 40%, and 32% for (VPV/T), and conventional (PV/T), respectively.

Yingbo zhang et al. (2021) [47], studied the numerical potential of a new porous cooling channel, as shown in Figure (2.18), which aims to improve the heat transfer efficiency of (PV/T) cells by Porous holes, compared to traditional cooling channels. The results also showed that a hole with a diameter of (0.006) meters is the best performer to raise the efficiency (PV/T) module by (4.17%), at an average solar irradiance (1000 W/m²), mass flow (0.006 kg/s). Furthermore, a solar irradiance (300-1200) W/m². When the flow rate of the incoming cooling water mass increased (0.002- 0.02) kg/s, the overall efficiency of the system increased from (5.07-18.04) %.

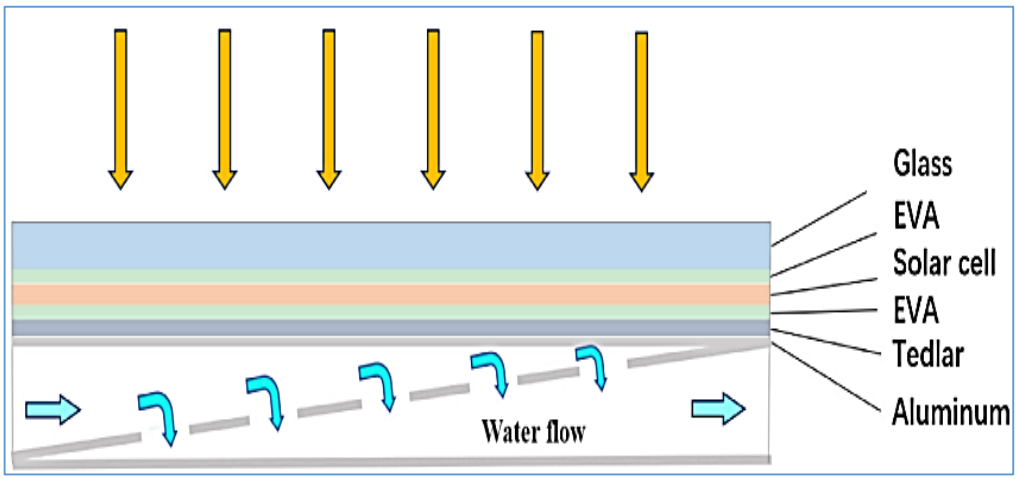

Figure (2.18) Porous layers of the PV/T system,[47].

Yan cao et al. (2021) [48], used the cooling of (PV/T) systems using nanofluids. This approach predicted (200) empirical statements with (13.6%) mean absolute average relative deviation (AARD), (2.548) mean square error (MSE), and regression coefficient (R^2) = (0.9534). Moreover, the (AARD) = 15.21%, and (3% weight, 12.5% nm) for (30 L/h) water - nan silica as a coolant at intense radiation (788.285W/m^2). As an optimum case, it gives the greatest electrical efficiency by (27.7%).

Essam m. abo- zahhad et al. (2022) [49] focused on the technology of hybrid concentrated vacuum photovoltaic systems (VCPV/T) and compared it with the conventional concentrated photovoltaic solar thermal collector (CPV/T). The results showed a percentage increase (VCPV/T) of the greatest temperature in systems was achieved (1%), (1.7%), and (2.16%) at three different concentration ratios (CR) (1,2, and 3), respectively. Overall performance is evident with the results of (VCPV-T) compared to (CPV/T) with (CR) = 3, the greatest predicted thermal, electricity, and exergy (144.5W), (33W) and (17.6W) around 1.00 p.m. for the system (VCPV/T), respectively. It also boosts about (14%) thermal, (10.7%) exergy, and CR=3.

Table. 2.2 The summary of the authors studied PV-T (water, nanofluid) passed

Author	Module-type	Study-type	ENHANCEMENTS		
			Electric efficiency	Thermal efficiency	Overall Efficiency
Di su et al, 2016 [38]	PV/T water collector with dual channels.	Experimentally	Increase 7.8%	64.4%	84%
H. Fayaz et al, 2018 [43]	PV/T nanofluid collector (MWCNT-WATER)	Experimentally	10.72%	79.1%	89.82%
Ahmed fudholi et al. 2019 [44]	PV/T nanofluid collector	Experimentally	11.1%	74.4%	(85-89) %
Yingbo zhang et al. 2021 [47]	PV/T water-collector with a porous layer	Numerically	14.4%	68.8%	83.2%

2.2.3 PV/T Cooling Systems using fluid Combind (Air +Water), (Air + Nanofluid).

Mohd Nazari Abu Bakar et al. (2013) [50], utilized an improved design of the (PV/T) collector, integrating air and water simultaneously. It consists of a twisted copper pipe for the water heating and one pass of air heating, as shown in Figure (2.19). Furthermore, this type of collectors both hot air and water produced, and electricity generated. The results showed that overall efficiency increases compared with the conventional collectors, so simulation procedures indicate that if both fluids operate concurrently, the overall performance is greater.

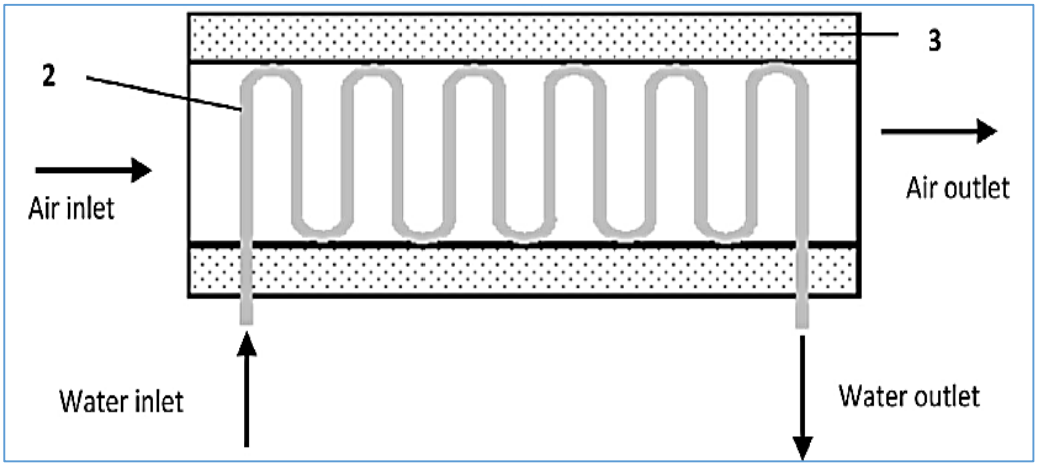

Figure (2.19) Top view cross-section The collector consists of (1) a PV module, (2) twist copper pipe, and (3) an insulation layer [50].

Jie Ji et al. (2014) [51], studied a three-function design of a (PV/T) system based on heating air and water according to weather requirements. The experiments were conducted in different conditions to evaluate the performance. The results of the thermal and electrical efficiency were achieved at the heating condition (46%, 10.2%), respectively. For an air temperature of (20℃) with a flow rate of (0.033 kg/s). Instantaneous thermal efficiency at zero degrees Celsius (37.4%, 44.3%) and air flow rate (0.026, 0.032) kg/s, respectively. In the water-heating process, the thermal efficiency of the

collector was recorded (56.6%) at zero degrees Celsius (36%) compared with other solar collectors.

Hasila jarimi et al. (2015) [52], investigated theoretical and experimental solar (PV) collectors. The tests were conducted as 2D steady-state conditions for three fluid models with the same operating conditions (PV/T) system: air, water, and water-air. As seen in Figure (2.20). Verification is centered between the experimental and simulation results using three methods of error analysis; root means square percentage deviation (RMSPD), mean absolute percentage error (MAPE), and coefficient of determination (R^2). The averages of the three methods were (0.92%), (1.19%), and (0.98%) consecutively. Thus, the study resulted from a good agreement of simulation with the experimental results.

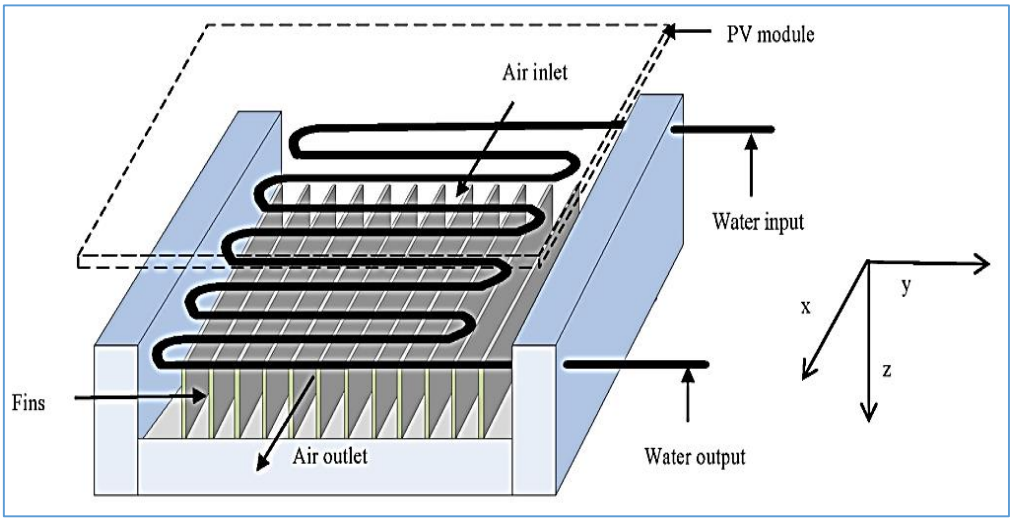

Figure (2.20) The front and top-view cross-section of a combined PV/T solar collector[52].

M.Y. Othman et al. (2015) [53], studied possibility of solar collectors (PV/T) for generate thermal and electrical energy. System components: two (PV) units installed parallel to produce electricity, a copper water pipe, a double flat air collector, and a hot water tank. The experimental calculations were under controlled environmental conditions. At radiation level (800 W/m^2), air flow rate (0.05 kg/s), water flow rate (0.02 kg/s), and output temperature (27.4 ℃). The electrical efficiency, thermal efficiency, and average electrical power

were recorded as 17%, 76%, and 145 W, respectively. It is considered the best experimental result.

Chao Guo et al. (2015) [54], studied numerical simulation and experimentally validation for triple-careers (thermal, electrical, heating) of the (PV/T) system in Figure (2.21). They focused on the water/ air heating based on energy demand differences at steady-state and dynamic models are validated with experimental results. For air heating of the (PV) module, at flow rate was recorded (0.02 kg/m. s). The results are temperature increase and thermal efficiency to obtain balance; for the PV/water-heating module, at wind speed over (5m/s) has been decreasing thermal efficiency.

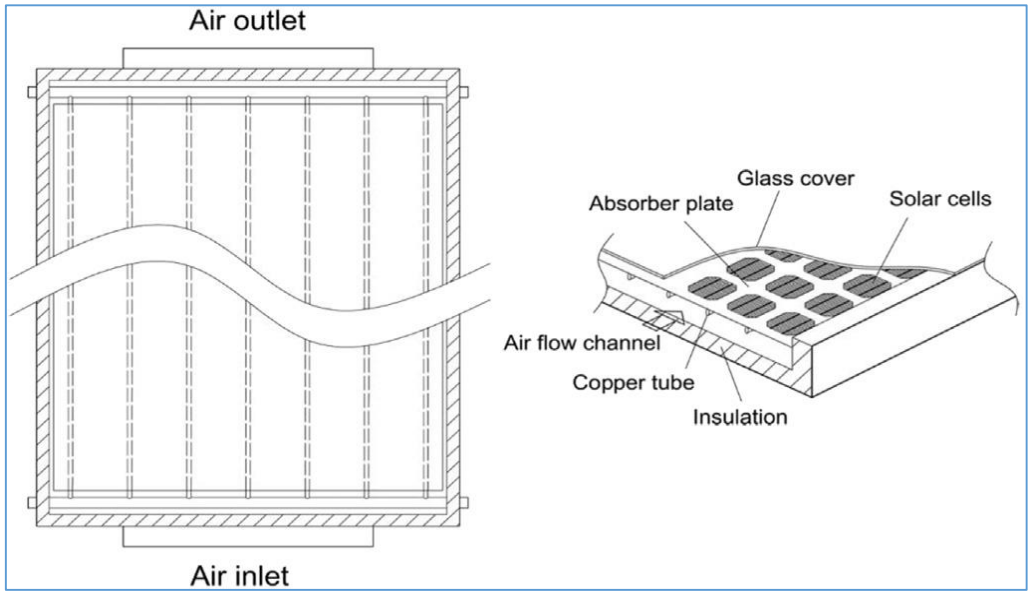

Figure (2.21) Diagram of the three-functional PV/T collector[54].

Kamaruzzaman Sopian et al. (2017) [55], analyzed a mathematical/theoretical approach for the development of a (PV/T) solar collector design with a dual air duct and square section water pipe as in Figure (2.22). The study investigates the performance of the integrated system governed by equations: steady state, one dimension, and energy equilibrium using the linear matrix inverse equation. The simulation results showed the

greatest thermal, electricity, and dual efficiencies (15.3%, 13.26%, and 88.19%) with a flow rate, water mass (0.02 kg/s), and air mass (0.07 kg/s).

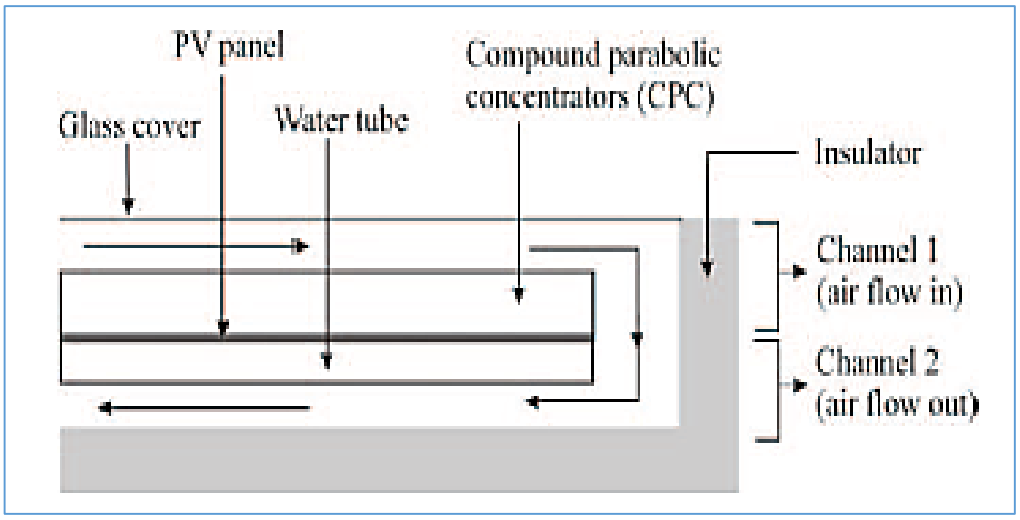

Figure (2.22) Sectional side view of double pass PV/T Combi collector, [55].

S. S. S Baljit et al. (2017) [56], they studied to improve a (PV/T) collector with tri-functions that produce water and hot air, generating electricity. Consists of a stainless steel swiveling tube for heating water, a dual-pass air duct for heating air, a Fresnel lens for primary focus, and a compound parabolic concentrator lens (CPCs) for secondary focus. The simulation results indicated that in the case of single fluid, total equivalent efficiency ranged (from 30% - 60%) and (90%) for dual fluids.

S. S. S. Baljit et al. (2019) [57], a proposal to combine condensers of two different fluids (water and air) to coolant a (PV/T) system in Figure (2.23) that would improve the electrical and thermal efficiency. When compared numerically and experimentally using the mean absolute error rate method, the efficiencies were achieved (13.02%), (and 67%), respectively, at rates of airflow (0.0103 kg/s), water (0.0164 kg/s) and solar radiation (650 W/m^2).

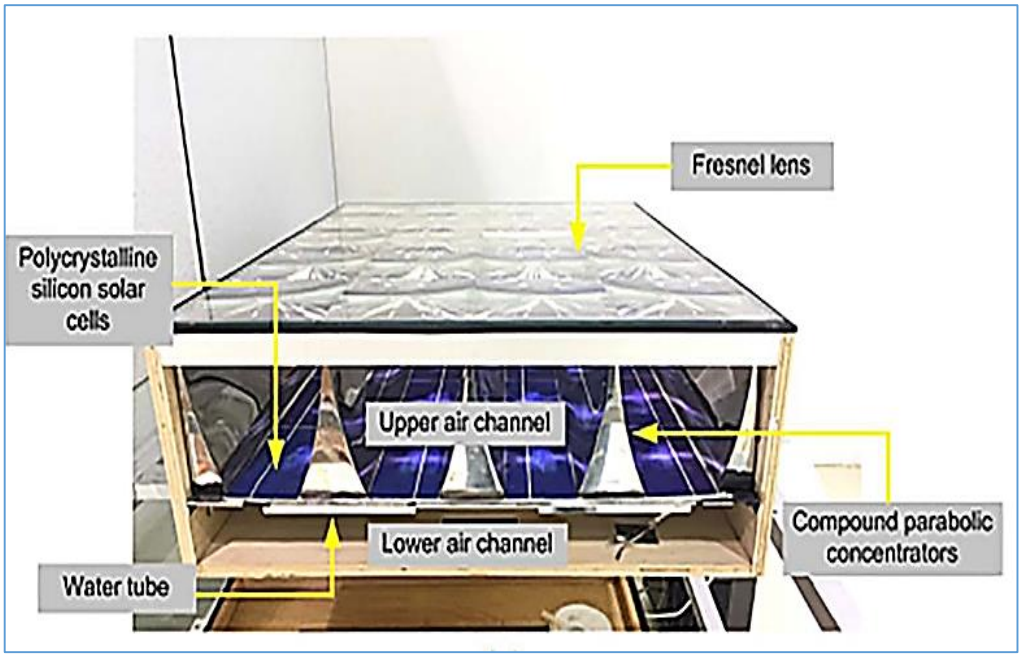

Figure (2.23) Diagram of the combined (air+ water) PV/T collector [57].

M. Imtiaz Hussain et al. (2019) [58] studied mathematical modeling and computational fluid dynamics (CFD) by (MATLAB and ANSYS FLUENT) programs, respectively. For a (PV-T) dual fluid (nanofluid + air) system. A numerical experimental investigation of samples and metal oxide nanoparticles (CuO, Al_2O_3, and SiO_2) at different concentrations was carried out with the base fluid (water). The results confirmed the largest percentage concentration, thermal conductivity of the nanofluid (CuO), compared to other types.

Muhammad Imtiaz Hussain, Jun-Tae Kim, (2020) [59] analyzed the comparison of a (PV/T) system based on (water + air) with a fluid (PV/T) model. Evaluations of the periodic experimental results of all the systems mentioned above confirmed the economic feasibility of the dual-fluid (PV/T) system in the short and long term. It has a greater energy and energy efficiency of (20% and 11%), respectively, compared to the single-fluid system. Further, it has a low energy cost.

Table 2.3 The summary of the authors studied PV-T combi (air-water), (air-nanofluid) passed

papers	Module-type	Study-type	ENHANCEMENTS		
			Electric efficiency	Thermal efficiency	Overall Efficiency
Jie Ji et al, 2014 [51]	PV/T combi collector, with air-water heating.	Experimentally	11.8%	44.3	67.9%
M.Y. Othman et al, 2015 [53]	PV/T combi collector with double flat (water-air).	Experimentally	17%	76%	93%
Kamaruzzaman Sopian et al, 2017 [55]	PV/T combi collector (air-water) with dual duct air and section square water pipe.	Experimentally	13.26%	Increase 15.3%	88.9%
S. S. S Baljit et al, 2017 [56]	PV/T combi collector (air-water) with dual-duct air, stainless steel tube, Fresnel lens, and parabolic lens.	Experimentally	12.7%	75%	90%
S. S. S. Baljit et al, 2019 [57]	PV/T combi collector (air-water) with dual channel air.	Experimentally	13.02%	67%	93%

2.3 Summary

- ✓ A comprehensive review of the existing literature was conducted, encompassing both numerical and experimental studies related to solar panel cooling techniques. The focus was on Photovoltaic/Thermal (PV/T) cooling systems, which utilize various cooling mediums, including air, water, nanofluid, and combinations such as (air + water) and (air + nanofluid).
- ✓ The results experimental for the maximum electrical, thermal, and overall efficiencies of the different cooling techniques, air are (18.7, 68, and 86.78)%, respectively. Water, nanofluid are (14.4, 79.1, and 89)%, respectively. And combind are (17, 76, and 93), respectively.
- ✓ When the mass flow rate of air is rising for various solar radiations the temperatures decreases because air flows stronger into the accumulator when the mass flow rate of air increases.
- ✓ Thermal efficiency and overall efficiency are increases at solar radiation raise. While there is a slight increase in electrical efficiency due to higher temperatures.

Chapter Three

Numerical Model

CHAPTER THREE

NUMERICAL MODEL

3.1 Introduction

This chapter provides a detailed presentation of the methodology employed to accomplish the established goals of the study. The focus here is on the theoretical aspects, particularly in the numerical domain. The primary objective is to enhance heat transfer in various types of Photovoltaic/Thermal (PV/T) systems, aiming to achieve thermal equilibrium in photovoltaic thermal collectors utilizing channels with multi-flow. The intention is to furnish readers with a comprehensive insight into the analytical procedures involved in the study.

3.2 Governing Equations

Based on the above assumptions, the temperature distribution of the three-dimensional flow inside the (PV/T) air collector was governed by the conservation equations(continuity, momentum, and energy)[60]. In addition to the (k-ε) turbulent model by reference[61], can be described as follows:

Continuity Equation

$$\frac{\partial U}{\partial x}+\frac{\partial V}{\partial y}+\frac{\partial W}{\partial z}=0.0 \qquad \text{…….. (3.1)}$$

Momentum Equations:

X-direction:

$$\frac{\partial U^2}{\partial x}+\frac{\partial UV}{\partial y}+\frac{\partial UW}{\partial z}=-\frac{1}{\rho}\frac{\partial P}{\partial x}+\frac{\partial}{\partial x}\left(\nu_e\frac{\partial U}{\partial x}\right)+\frac{\partial}{\partial y}\left(\nu_e\frac{\partial U}{\partial y}\right)+\frac{\partial}{\partial z}\left(\nu_e\frac{\partial U}{\partial z}\right)+\frac{\partial}{\partial x}\left(\nu_e\frac{\partial U}{\partial x}\right)+\frac{\partial}{\partial y}\left(\nu_e\frac{\partial V}{\partial x}\right)+\frac{\partial}{\partial z}\left(\nu_e\frac{\partial W}{\partial x}\right) \qquad \text{……(3.2)}$$

Y-direction:

$$\frac{\partial UV}{\partial x}+\frac{\partial V^2}{\partial y}+\frac{\partial VW}{\partial z}=-\frac{1}{\rho}\frac{\partial P}{\partial y}+\frac{\partial}{\partial x}\left(\nu_e\frac{\partial V}{\partial x}\right)+\frac{\partial}{\partial y}\left(\nu_e\frac{\partial V}{\partial y}\right)+\frac{\partial}{\partial z}\left(\nu_e\frac{\partial V}{\partial z}\right)+\frac{\partial}{\partial x}\left(\nu_e\frac{\partial U}{\partial y}\right)+\frac{\partial}{\partial y}\left(\nu_e\frac{\partial V}{\partial y}\right)+\frac{\partial}{\partial z}\left(\nu_e\frac{\partial W}{\partial y}\right) \qquad \text{……. (3.3)}$$

Z-direction:

$$\frac{\partial UW}{\partial x}+\frac{\partial VW}{\partial y}+\frac{\partial W^2}{\partial z}=-\frac{1}{\rho}\frac{\partial P}{\partial z}+\frac{\partial}{\partial x}\left(\nu_e\frac{\partial W}{\partial x}\right)+\frac{\partial}{\partial y}\left(\nu_e\frac{\partial W}{\partial y}\right)+\frac{\partial}{\partial z}\left(\nu_e\frac{\partial W}{\partial z}\right)+\frac{\partial}{\partial x}\left(\nu_e\frac{\partial U}{\partial z}\right)+\frac{\partial}{\partial y}\left(\nu_e\frac{\partial V}{\partial z}\right)+\frac{\partial}{\partial z}\left(\nu_e\frac{\partial W}{\partial z}\right) \quad \text{……..(3.4)}$$

Energy Equation:

$$\frac{\partial UT}{\partial x}+\frac{\partial VT}{\partial y}+\frac{\partial WT}{\partial z}=\frac{\partial}{\partial x}\left(\Gamma_e\frac{\partial T}{\partial x}\right)+\frac{\partial}{\partial y}\left(\Gamma_e\frac{\partial T}{\partial y}\right)+\frac{\partial}{\partial z}\left(\Gamma_e\frac{\partial T}{\partial z}\right) \quad \text{……..(3.5)}$$

The governing equations (3.2, and 3.3) require an expression for ν_e and Γ_e to be solved

The Standard (k-ε) Model:

Kinetic energy term (k):

$$\frac{\partial}{\partial x}(kU)+\frac{\partial}{\partial y}(kV)+\frac{\partial}{\partial z}(kW)=\frac{\partial}{\partial x}\left(\frac{\nu_t}{\sigma_k}\frac{\partial k}{\partial x}\right)+\frac{\partial}{\partial y}\left(\frac{\nu_t}{\sigma_k}\frac{\partial k}{\partial y}\right)+\frac{\partial}{\partial z}\left(\frac{\nu_t}{\sigma_k}\frac{\partial k}{\partial z}\right)+G-\varepsilon \quad \text{……..(3.6)}$$

Dissipation term (ε):

$$\frac{\partial}{\partial x}(\varepsilon U)+\frac{\partial}{\partial y}(\varepsilon V)+\frac{\partial}{\partial z}(\varepsilon W)=\frac{\partial}{\partial x}\left(\frac{\nu_t}{\sigma_\varepsilon}\frac{\partial \varepsilon}{\partial x}\right)+\frac{\partial}{\partial y}\left(\frac{\nu_t}{\sigma_\varepsilon}\frac{\partial \varepsilon}{\partial y}\right)+\frac{\partial}{\partial z}\left(\frac{\nu_t}{\sigma_\varepsilon}\frac{\partial \varepsilon}{\partial z}\right)+C_{1\varepsilon}\frac{\varepsilon}{k}G-C_{2\varepsilon}\frac{\varepsilon^2}{k} \quad \text{……..(3.7)}$$

The generation term (G):

$$G=\upsilon_t\left[2\left(\frac{\partial U}{\partial x}\right)^2+2\left(\frac{\partial V}{\partial y}\right)^2+2\left(\frac{\partial W}{\partial z}\right)^2+\left(\frac{\partial U}{\partial y}+\frac{\partial V}{\partial x}\right)^2+\left(\frac{\partial V}{\partial z}+\frac{\partial W}{\partial y}\right)^2+\left(\frac{\partial U}{\partial z}+\frac{\partial W}{\partial x}\right)^2\right] \quad \text{……(3.8)}$$

Where, $\Gamma_k=\frac{\upsilon_t}{\sigma_k}$, $\Gamma_\varepsilon=\frac{\upsilon_t}{\sigma_\varepsilon}$, $\Gamma_u=\Gamma_v=\Gamma_w=\upsilon_e$, $\upsilon_t=C_\mu\frac{k^2}{\varepsilon}$

The empirical constants for$(k-\varepsilon)$ model [62]:

$C_\mu=0.09$, $C_{1\varepsilon}=1.44$, $C_{2\varepsilon}=1.92$, $\sigma_k=1.00$, $\sigma_\varepsilon=1.30$

3.3 Geometry Description and Physical Model

Figure (3.1) shows the side view cross- section area of the channels (rectangular, triangle, and transverse fins with multi-flow channel). The PV/T

system was created with a multi-flow model for three different types using the CFD softawre COMSOL Multiphysics 5.5 as shown in figure (3.2). However, creating the model began by identifying two geometric domains related to the PV/T system, the aluminum absorption, and one fluid domain related to the air. The channels are made of aluminum with a thickness of (1 mm). Insulation materials composed of compressed foam, with a thickness of 30 mm, are strategically applied to the edges and the bottom of the system. However, the part in direct contact with the solar panel base remains uninsulated. This design choice utilizes the insulating properties of compressed foam to effectively prevent heat transfer from the surroundings to the collector. The dimensions for all three models are consistent at 860 mm in length, 610 mm in width, and 61 mm in height. The project area of the PV panel is measured at 0.524 m^2. Channels dimensions shown in the table (3.1)

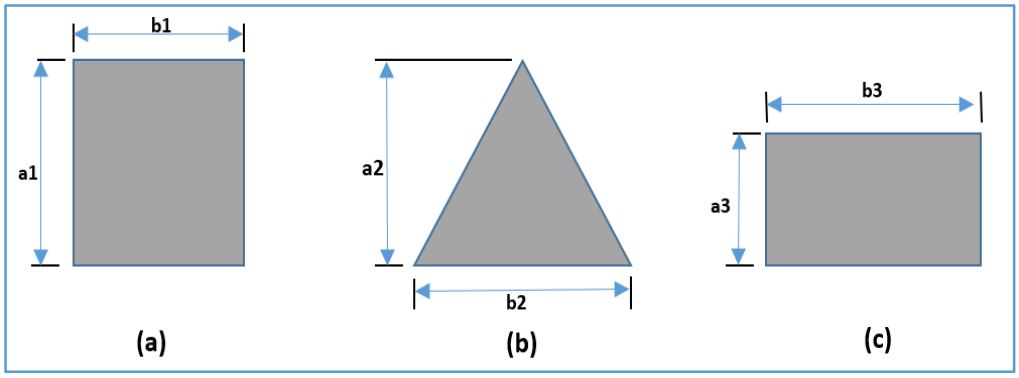

Figure (3.1) Illustrates the cross-section to all the three models.

Table (3.1) Shows the dimensions of the channels.

Part index	Model type	Dimension(mm)
a1	Rectangular (a)	61
b1		40
a2	Triangular (b)	61
b2		40
a3	Transverse fins (c)	61
b3		100

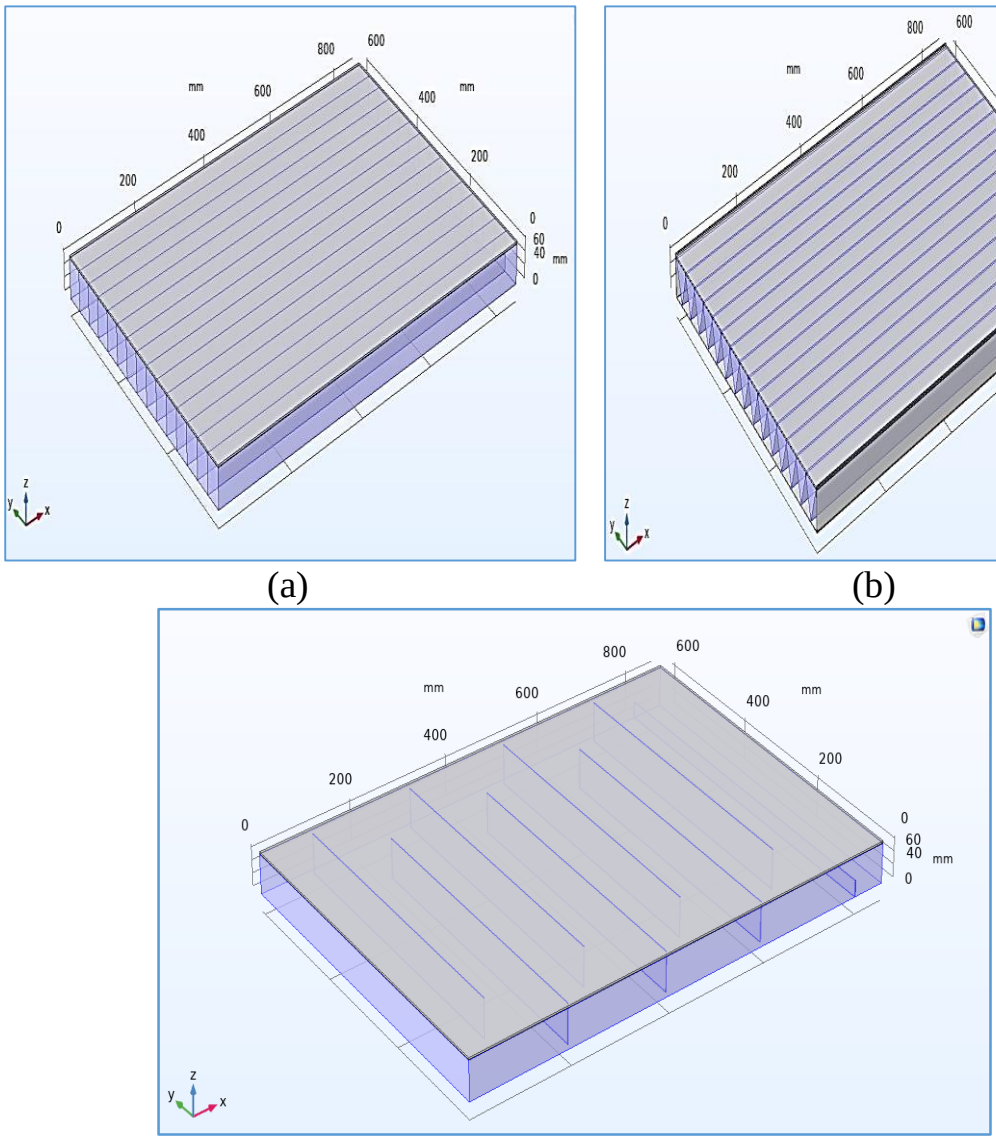

Figure (3.2) Computational domain of PV/T system: (a) Rectangular channel, (b) Triangle channel, (c) Transverse fins with multi-flow channel.

3.4 Mathematical Modeling

Numerical calculations that are carried out at using a steady-state setting with (COMSOL Multiphysics 5.5) software. The partial differential equation (PDE) governed continuity, momentum, and energy equations have been solved for the turbulent, stationary, and incompressible flow. The fluid's heat transport is connected, and the pressure governing equation algorithm virtually automatically accounts for the effects of velocity and pressure. The Reynolds Averaged Navier Stokes (RANS) model offers the flexibility of a set of equations utilized in the simulation. Under the following assumptions, it is possible to simplify the mathematical model of the governing equations of the

PV/T air collector with a mult-flow channel (model, c), as shown in Figure (3.3):

1. Steady-state conditions.
2. Incompressible and turbulent flow.
3. Regularity in heat flux.
4. Three-dimensional flow.
5. The ambient temperature has been taken at 38 °C.
6. An average wind speed of 1 m/s is through the simulations.
7. Both viscous dissipation and gravity effects are negligible.
8. The energy losses from the bottom and wall sides of the PV collector to the surrounding are neglected.

The following values for were considered the primary design parameters: L= 860 mm, W = 610 mm, H = 61mm, $\alpha g = 0.9$, $\alpha pv = 0.95$, $\tau = 0.92$, $\varepsilon g = 0.5$, T*a* = 38 °C, T*i* = 38°C, and V*w* =1 m/s, the schematic design of this study as shown in figure (3.3).

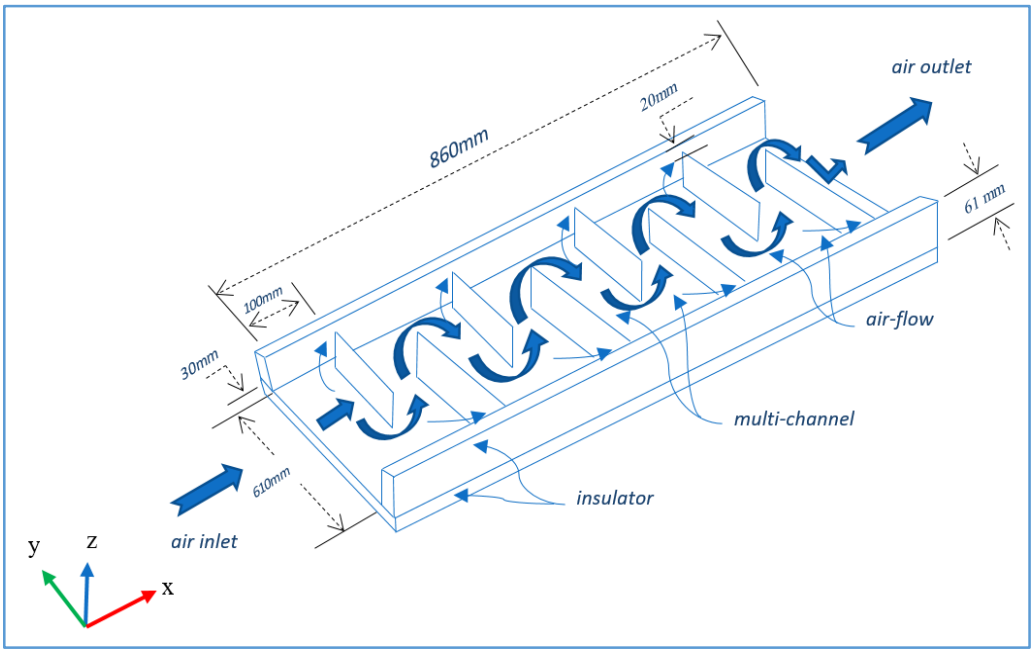

Figure (3.3) The (PV/T) collector multi-flow air duct architecture is depicted schematically (model, c).

3.4.1 Initial conditions

Initially, the (PV/T) air collector is supposed to be at ambient temperature.

$T_i = T_{am}\,, \quad at\ \tau = 0 \qquad (where\ T_i \ldots refers\ to\ \ T_{pv}\,, T_b\,, T_g, T_a\,)$

3.4.2 Boundary conditions fluid part

At the inlet flow (x=0.0):

$$\begin{cases} At\ x = 0 \\ 0 < y < w \\ 0 < z < H \end{cases} \} T = T\ in \quad \rightarrow \ u = u\ in$$

$$k = k_{in} = C_k u_{in}^2 \ ; \quad \varepsilon = \varepsilon_{in} = C_\mu k_{in}^{3/2}/(0.5 D_h C_\varepsilon)$$

Where C_k and C_ε are constants of turbulence models ($C_k = 0.003$, $C_\varepsilon = 0.03$),[61].

At the outlet flow (x=L):

In the exit unit, all gradients are assumed to be zero, and pressure is equal to atmospheric pressure.

$$\begin{cases} At\ x = L \\ 0 < y < w \\ 0 < z < H \end{cases} \} \quad \frac{\partial \emptyset}{\partial x} = 0$$

Where; *∅: is referred to the independent variables of u;w; v; T; k; and ε.*

.

At all solid walls of the solar collector (pv surface, glazing cover, and back plate): The no-slip conditions are supposed, and the side edges and bottom faces are supposed to be insulated.

3.4.3 Boundary Solid Part

The (PV) panel was treated as a rigid layer with close and stable thermal properties. Ethylene-vinyl acetate (EVA), anti-reflective coating (ARC), silicon, and (Tadler) Layers made of glass were considered to be preserved as glass units [63]. Figure (3.4) shows a cross-section of a PV/T collector with

multi-flow rectangular channels with different heat transfer coefficients, which can write mathematical equations according.

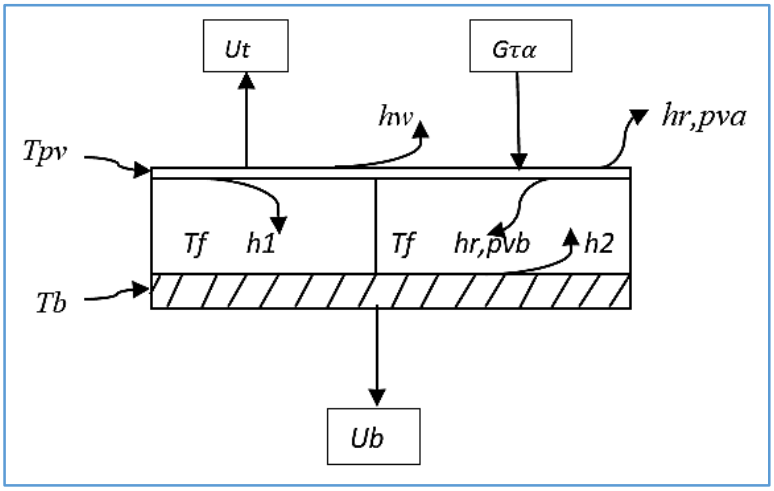

Figure (3.4) Heat transfer characteristics of Trasverse fins with multi-flow channel a PV/T air collector schematically.

Characteristics of the air used in a PV/T system, such as viscosity, density, specific heat, and thermal conductivity are constant.

Mean air temperature [64]:

$$\bar{T}f = \frac{(\mathrm{Ti+TO})}{2} \qquad \text{..... (3.9)}$$

Where:

$h1 = h2 = h$

Hydrodynamic channel diameter:

$$D_h = \frac{4wH}{2(w+H)} \qquad \text{..... (3.10)}$$

Re and *Pr* are the Reynolds and Prandtl number given as:

$$Re = \frac{\dot{m}D_h}{A_{ch}\mu} \qquad \text{..... (3.11)}$$

The useful energy rate and thermal efficiency can be calculated as follows [65]:

The useful energy rate:

$$Qu = \dot{m}Cp(To–Ti) \qquad \text{..... (3.12)}$$

The thermal efficiency system [65]:

$$\eta th = \frac{Qu}{GA} \qquad \text{..... (3.13)}$$

The electrical efficiency (*ηpv)* of the PVT air system depending on the temperature can be calculated as[66]:

$$\eta pv = \eta r[1-0.0045(Tpv-25)] \quad \text{..…….. (3.14)}$$

The overall efficiency of the PV/T air system is calculated [25][66]:

$$\eta ov = \eta th + \eta pv \quad \text{. ……. (3.15)}$$

3.4.4 Electrical Modeling of PV Cell

The PV modules are connected in parallel or in series to form the PV panel. The PV array may be single or double panels forming a solar photovoltaic system consisting of a boost converter (DC) equipped to control the output power, and inverter. Figure (3.5) shows the typical scheme of the system [14].

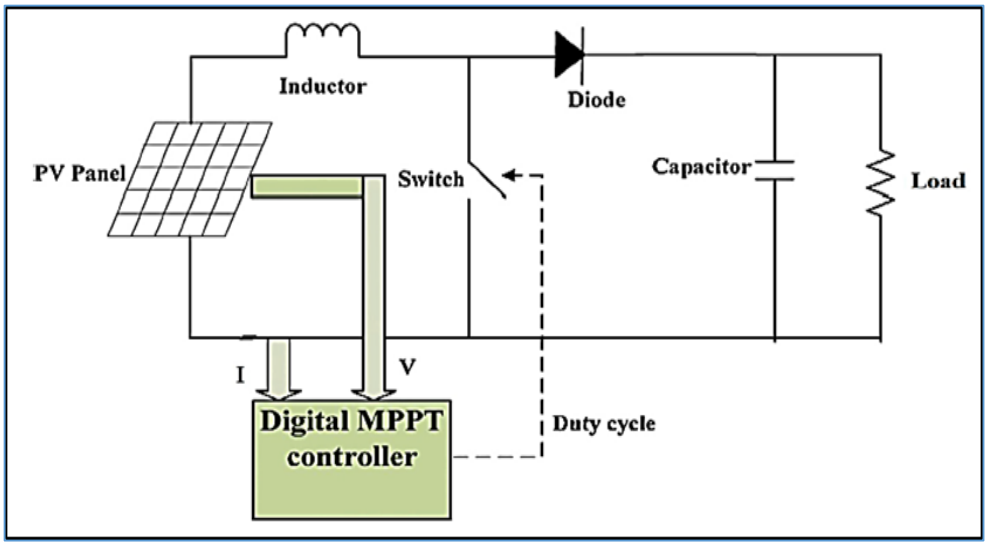

Figure (3.5) Scheme of a general PV system [14].

The representative current-voltage characteristics curve for the PV panels is shown in Figure (3.6).

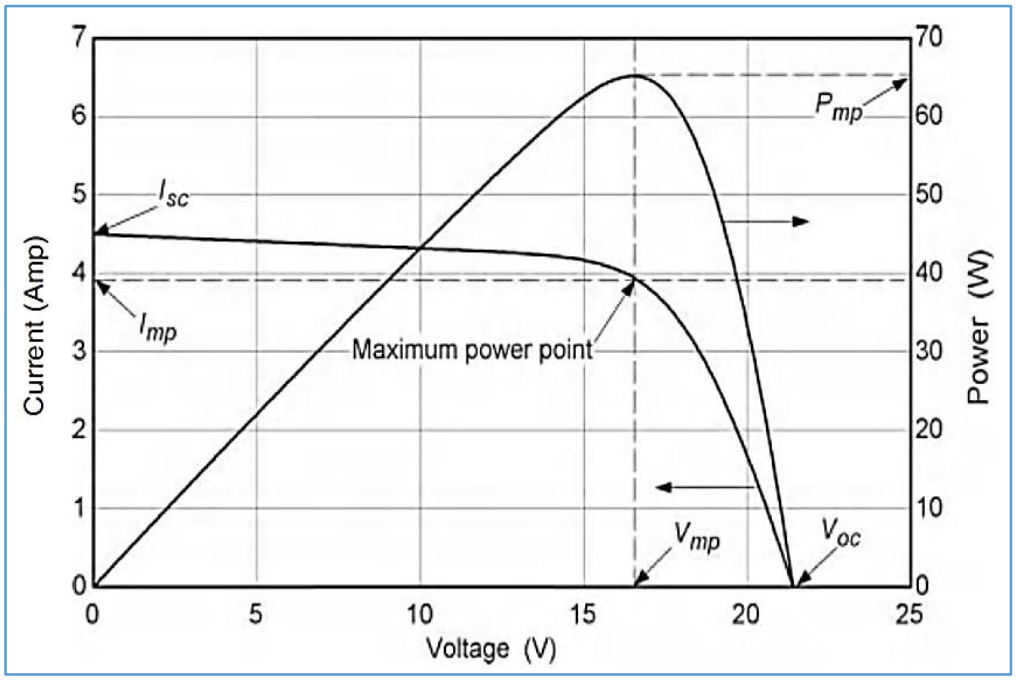

Figure (3.6) Current-voltage curve of the PV cell [7].

In a short circuit current, the voltage equals zero, and the current generated by sunlight will equal the short circuit current. The current produced by light photons is influenced by solar radiation and temperature

Cell efficiency (ηc) represents the maximum power over the solar irradiance received by the solar cell and can be expressed as follows [67]:

$$\eta c = \frac{Pmax}{G \times \mathrm{Ac}} \qquad \text{..…… (3.16)}$$

The fill factor (FF) represents the relation of maximum power divided by the open-circuit voltage and short-circuit current as follows [15]:

$$FF = \frac{Pmax}{Voc \times Isc} \qquad \text{…….. (3.17)}$$

The factors are important that influence the performance and efficiency of the (PV) cell whose packing factor (PF), which is the ratio of cell area (Ac) the number of cells (Nc) multiplied by the cell area without structure) over module area (Am). (PF) is often less than one [68]. The following equation can determine:

$$PF = \frac{Ac \times Nc}{Am} \qquad \text{……..…..(3.18)}$$

3.5 Meshing Generation and Independence Verification

The accuracy of the numerical solutions is given depending on the mesh refinement level among other factors. There are global improvements to fine-tune the adaptive network using various options available in (COMSOL multiphysics), for example (3D) test results for linear and quadratic elements. The quality of the models depends on the quality of the grid and not the number of elements, also improves significantly as long as there is a small size of the grid. Moreover, an increase in quality does not always lead to an improvement in accuracy [69]. The element is a tetrahedral shape due to the use of a 3D model, and it consists of four realities with six edges and four nodes as shown in Figure (3.7).

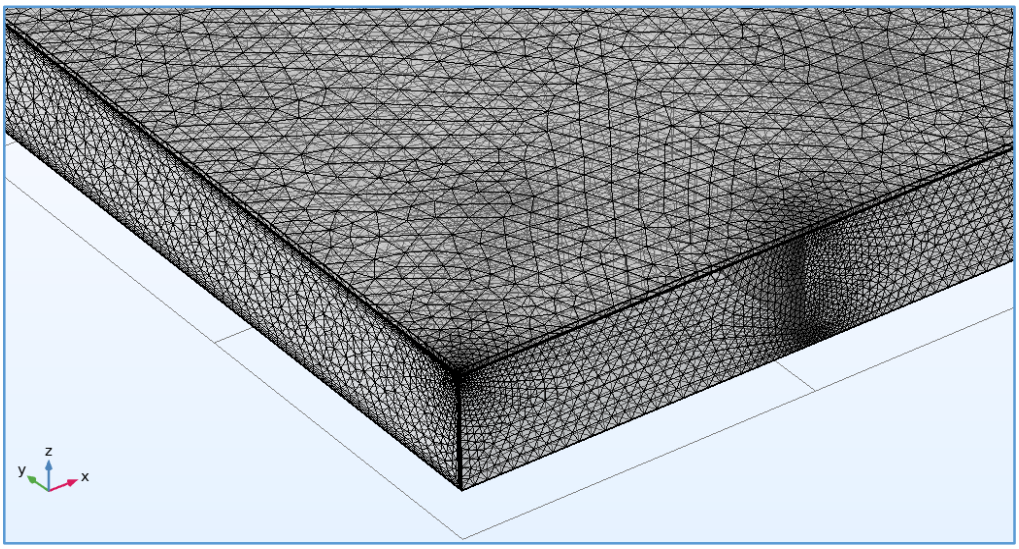

Figure (3.7). Finite element meshing of the PV/T system.

The network architecture must be taken into account while performing any simulation or analysis to choose the right type, quantity, and placement of the mesh faces. If the appropriate grid is used, partial differential equations can be solved with convergent solutions. Coarse or fine mesh faces may be utilized, depending on the intricate geometrical form of the project or the operating condition. In this simulation, the grid independence test was run to establish the mesh's ideal face size. The system (PV/T) has dimensions (860 × 610 × 61) mm, length, width, and height, respectively. The mass flow rate (0.08)kg/s and

the inlet temperature (38)° C, at solar flux 1000 W/m^2. All grid faces were used to plot the average temperature of the fluid that passed through the PV/T system. Figure (3.8) shows the grid face count regulated against outlet temperature. From the table (3.2) the best grid is concluded No. (8,623,938) elements. Indeed, better accuracy of mesh size can be obtained with more results, but increasing the number of meshes will make the computing time longer.

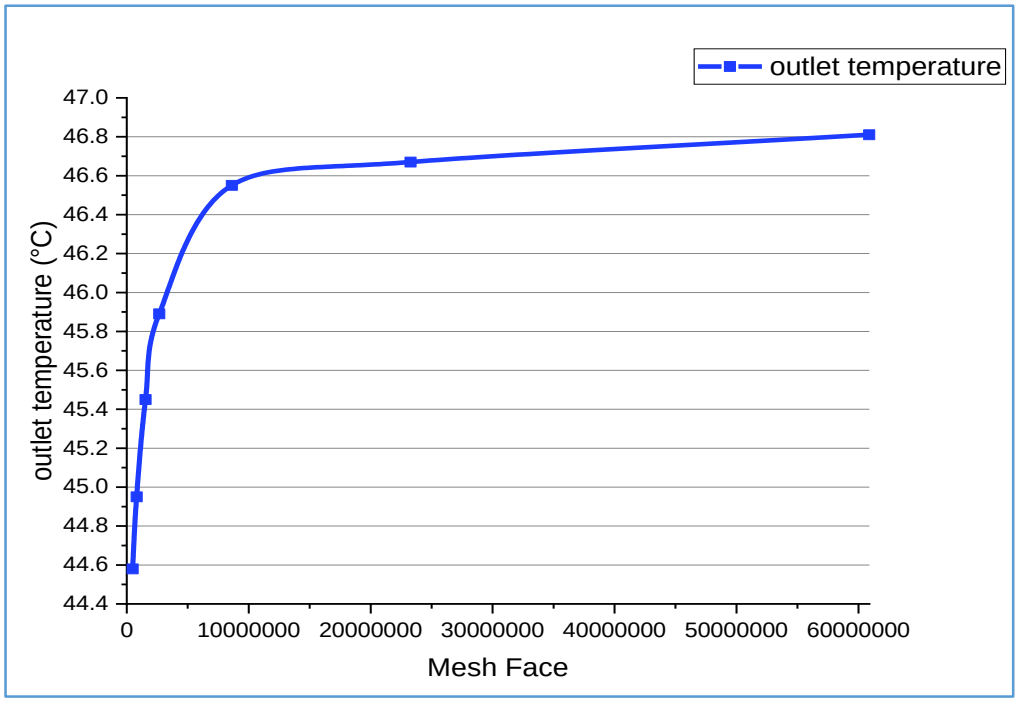

Figure (3.8). The average outlet temperature of the PV/T system versus the number of mesh faces for the grid independence test.

Table (3.2): Grid analysis.

Grid Types	Extremely Coarse	Extra Coarse	Coarser	Coarse	Normal	Fine	Finer
Mesh Element	491,338	823,101	1,541,080	2,665,479	8,623,938	23,279,095	60,882,132
Outlet Temperature (°C)	44.58	44.95	45.45	45.89	46.55	46.67	46.81

3.6 Computer Simulation

Simulations were carried out in this work according to the (COMSOL multiphysics 5.5). Software depending on the principles of computational fluid

dynamics (CFD), for a (PV/T) collector based on multiple air channels. PV was modeled as a glass module [63].

3.6.1 COMSOL Multiphysics 5.5 Software

A simulation program that accommodates all fields of engineering and scientific research to design models and devices. It is a simulation environment for external reality applications using multi-physics modeling that includes sound, electromagnetism, chemical reactions, mechanics, fluid flow, and heat transfer. (CFD) is utilized to solve equations, so you need great programs such as (COMSOL) which were used in this work as shown in Figure (3.9), to represent them graphically and numerically with an appropriate number of iterations to reach the optimal model.

The model to be tested is created using the program or another piece of software. It is made up of multiple rectangular channels, the dimensions of which match the dimensions of the solar panel, with a height that is not less than 10% of its width, measuring ($860 \times 610 \times 61$) mm in length, height, and width, respectively. They are channels with multiple flows, i.e. in the vertical and horizontal direction. It is installed below the solar panel (PV) to contribute to the heat transfer and throw it outside to benefit from it in various applications as illustrated in Figure (3.10).

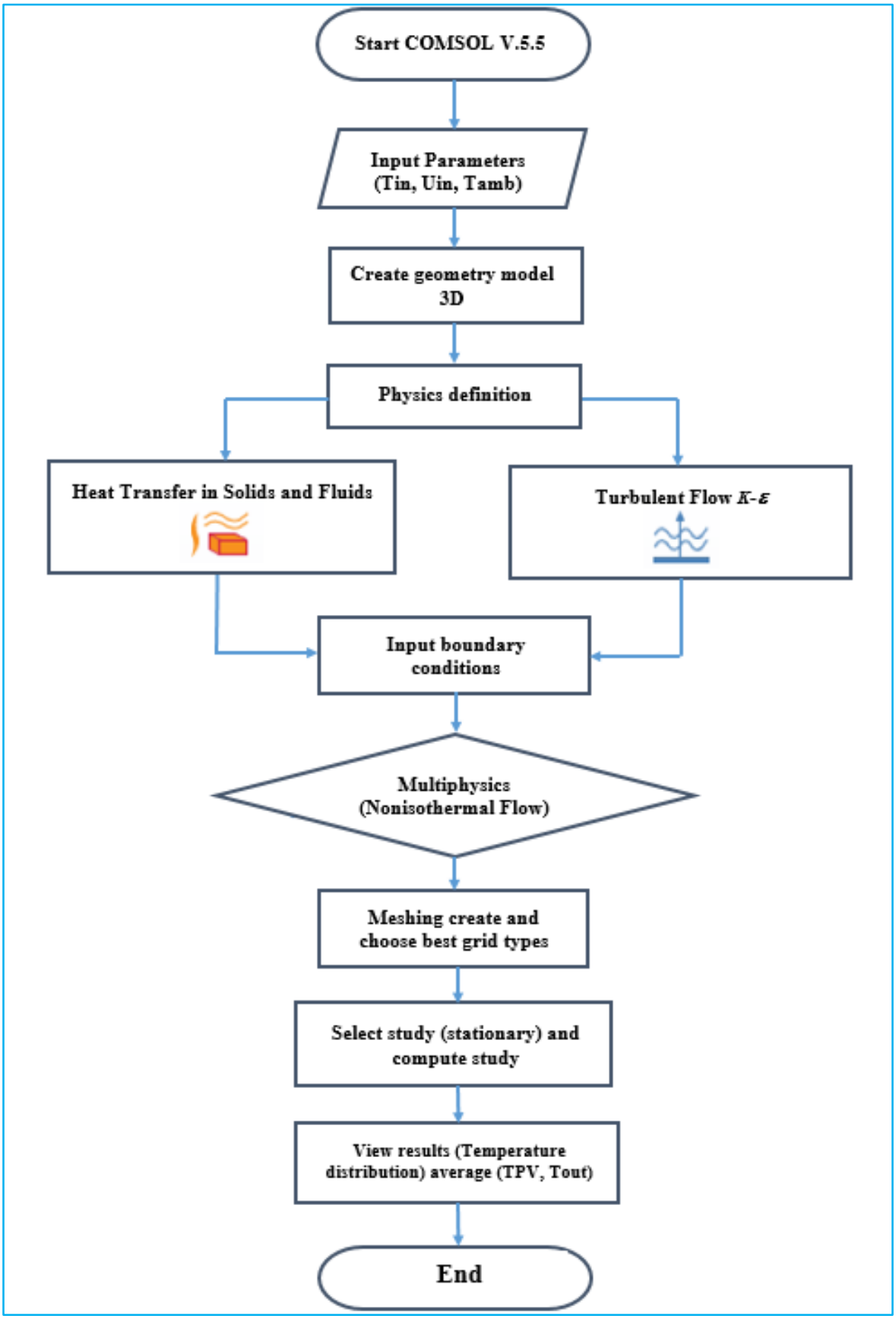

Figure (3.9). Flow chart of CFD analysis.

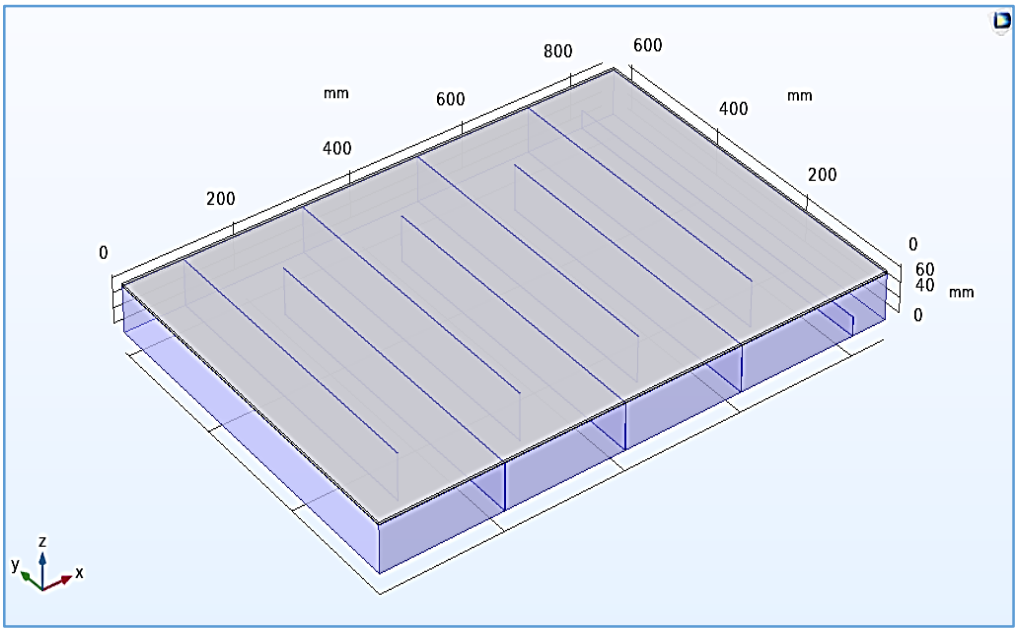

Figure (3.10). Schematic illustrating the multi-flow design of the (PV/T) collector by a program (COMSOL Multiphysics 5.5).

3.6.2 Numerical Simulation Validation

Any digital work needs to make a comparison between the current numerical results and previous studies to validate the numerical model proposed in this study, using the parameters presented in the research [25], their design was re-simulated as shown in Figure (3.11) validate the CFD results with our current work. This requires determining the average temperature of the air exiting (Tout) of the PV/T system.

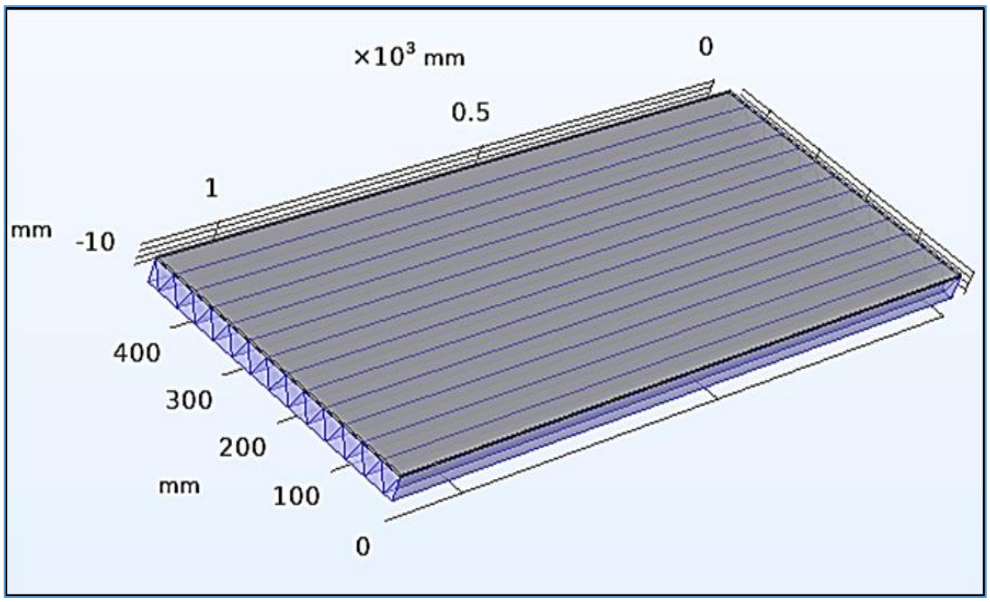

Figure (3.11) Front view of the temperature simulation validation model design [25].

The average temperature of the outlet air of the PV/T panel is shown in Figure (3.12). As can be seen, the temperature decreases with increasing mass flow rate. The error rate between validation results (4.4%) is less than 5%. It can be said that the results of the current research agree well with those of other researchers. Boundary conditions can significantly affect the accuracy of the results and can be used to predict the performance of the thermal collector (PV/T).

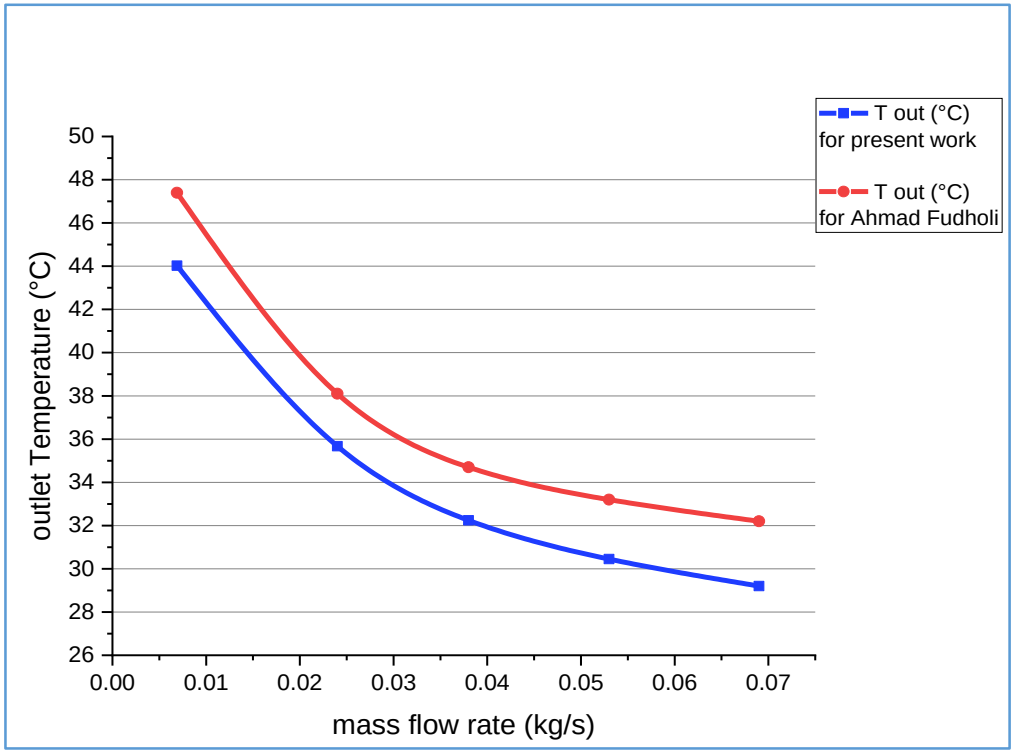

Figure (3.12) Shows theoretical CFD validation of the outlet temperature by previous studies [25].

3.7 Accuracy

The solution accuracy relies on the "Convergence Criterion" by satisfying one of the following [70]:

(i) Accepted value of the residual.

(ii) Accepted variance between values in two consequent iterations.

The mentioned approach is preferred because of includes residual source assurance after any iteration. When the maximum residual for a variable is less

than the convergence criterion the solution is announced convergent. The convergence variable (∅) on nodal (n) is as follows:

$$\frac{|\emptyset n - \emptyset n-1|}{\emptyset n} \leq \varepsilon \qquad \text{……(3.19)}$$

We choose $\emptyset = 1 \times 10^{-3}$ in this study.

Chapter Four

Experimental Work

CHAPTER FOUR

EXPERIMENTAL WORK

4.1 Introduction

The experimental work carried out for this study is according to the conditions of the indoor test, which allows the use of artificial light sources to control in a much easier way the radiation of the input energy and to achieve this at any time of the day[15]. As well as all system components of the new technique (multi-flow channel) that were built under indoor test conditions are described in detail in this chapter.

4.2 System Components

To reduce the temperature of the PV module, a PV/T air system is made up of necessary components. The PV panel that needs to be installed initially and cooled is the first component of the system. The channel which is put on the PV module base, is the second component. The third component of the system is the test section that directs air toward the base of the PV module, and the fourth component is the fan that draws air from under the base to the outside at the end of the duct. The entire system was installed and all the necessary devices for testing, which we will discuss later, were connected to a steel frame according to the indoor conditions and the simulation of solar radiation, as shown in Figures (4.1) and (4.2). However, Solar flux was determined by adjusting the height of the halogen lamp (630, 720, and 820) mm per (1000, 800, and 600)W/m^2, respectively. This is done after dividing the solar panel into (12) squares recording the solar flux readings for each square, and adopting the average of the readings. Repeat this procedure in every case of change in solar flux.

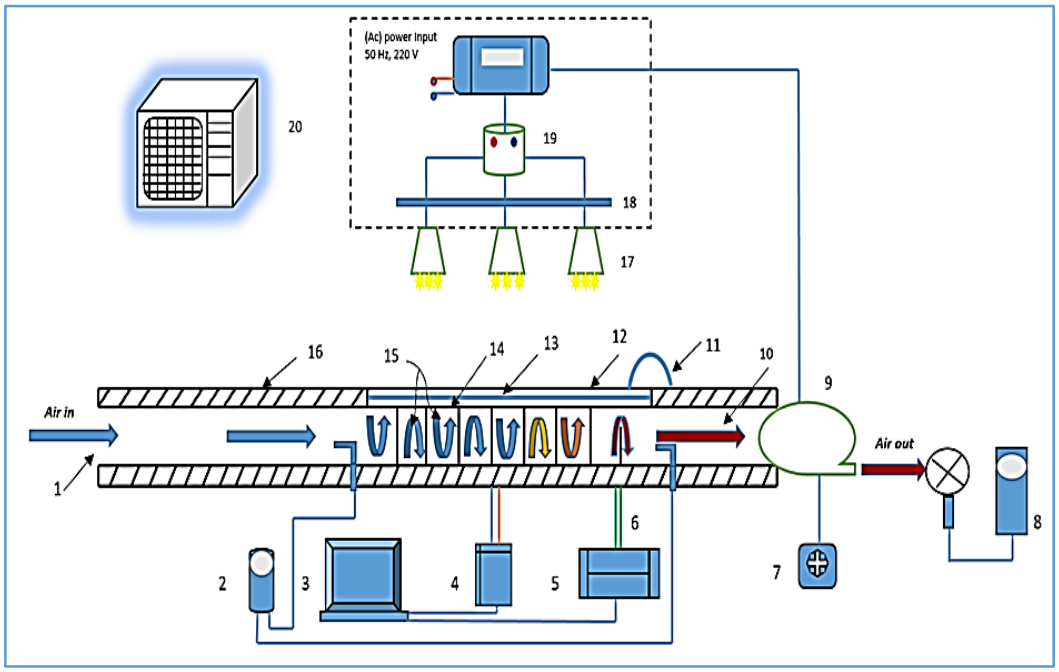

NO.	ITEM	NO.	ITEM
1	Inlet duct	11	Solar Power Meter
2	Pressure manometer	12	Glass layer
3	Laptop	13	PV layer
4	PV analyzer	14	Tadler layer
5	Data Logger	15	Multi-channel
6	Thermocouples Sensor	16	Insulation
7	Velocity regulator	17	Halogen lamps (1000)W
8	Anemometer	18	Electrical connector
9	Air fan	19	Electrical protection device
10	Outlet duct	20	Air conditioner

Figure (4.1) Schematic diagram of the experimental work setup.

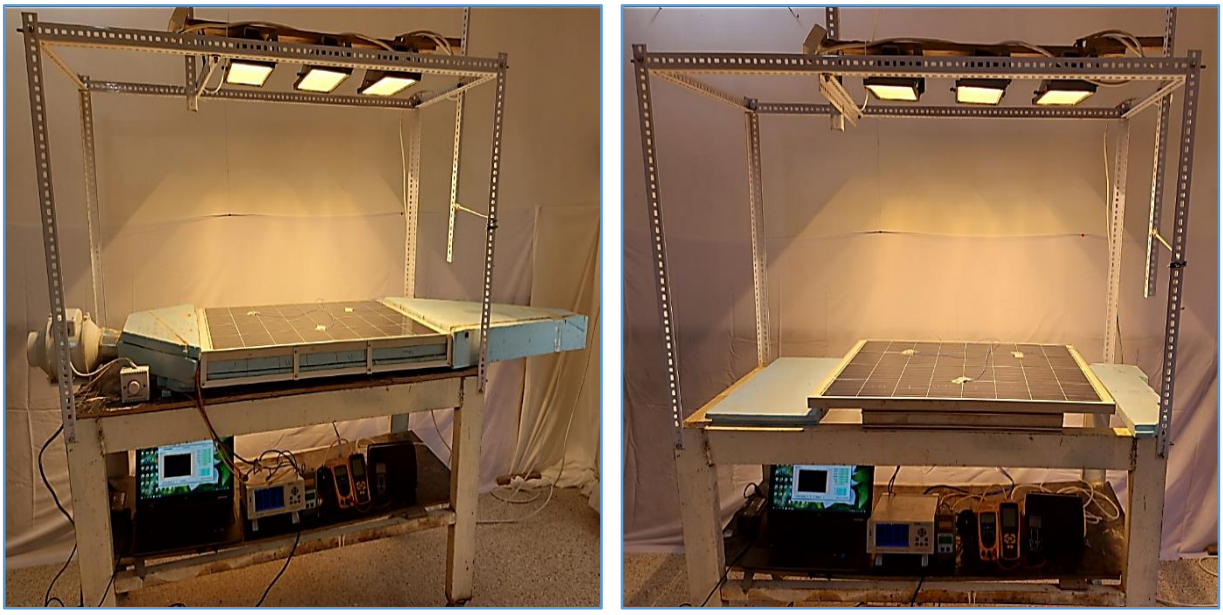

(a) (b)

Figure (4.2) Photograph of the experimental working setup, (a) PV/T system, (b) PV module.

4.2.1 Photovoltaic Panel (PV)

The PV panel is the main component of the system. It usually consists of three main components of glass (glass, silicon, and Tedler) [63], made of polycrystalline silicon whose details are listed in Table (4.1), and as shown in Figure (4.3).

Tabel (4.1) Electrical characteristics of a solar PV panel

Details	Specification
Solar cell type	Poly-crystalline silicon
Rated power (-0,+5W) (Pmpp)	100 W
Open circuit voltage (Voc)	21.5 V
Short circuit current (Isc)	6.28 A
The voltage at Pmpp (Vmpp)	17.5 V
Current at Pmpp (Impp)	5.71 A
Cell Efficiency	20.66 %
Standard Test Conditions (STC)	(G=1000 W/m^2, TC = 25 °C, AM= 1.5) ±5%

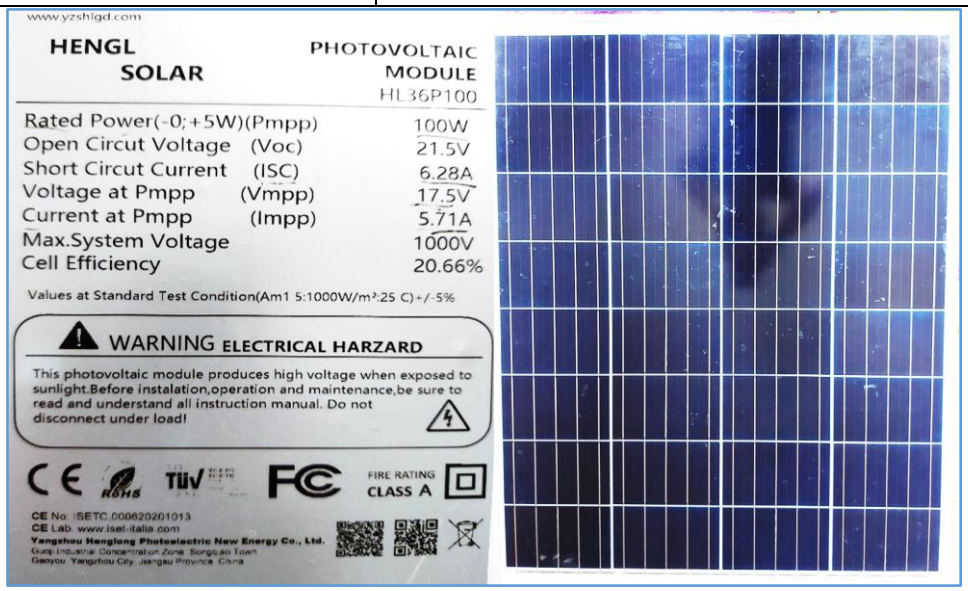

Figure (4.3) Photograph of the solar panel with specifications.

4.2.2 Multi-Flow Channels

The system's airflow duct, which is mounted to the PV module's back base, is the second important component. The channel's dimensions were carefully selected, and it is a rectangular channel based on the dimensions of the solar panel, width (W) (0.61 m), height (H) (0.061 m), the aspect ratio (W/H) is set at (10) to achieve a fully turbulent flow in the PV/T collector [71]. Using the thermal camera to acquire the most efficient heat exchange process

with the aid of air, the ideal temperature distribution for the PV panel was attained, as illustrated in Figure (4.4). It contains numerous dampers spaced apart by equal distances (100 mm) interspersed with openings equal to the distance between them, formed of channels that allow the largest heat exchange process between the air and the back of the PV module.

In addition, this design led to a longer air path in the collector [72], and it consists of channels by number (9). Furthermore, small holes (20 mm wide) were made on the other side of the partitions adjacent to the thermal insulator, their purpose is slow down the air speed. They are made of light aluminum with good heat conductivity, a thickness of (1) mm, measuring (860) mm in length, (610) mm in width, (61) mm in height, and (30) mm thermal insulator thickness to prevent heat transfer from the surrounding environment into the channel. Insulating material was placed around the air duct on all sides except the side next to the PV module back. Moreover, an air inlet duct length of (964.4)mm and an air outlet duct length is (482.2)mm, according to equations ($5\sqrt{wH}$, $2.5\sqrt{wH}$), respectively, for turbulent flow application [71]. A heat sink was used between the surface of the channels and the base of the PV module to increase the thermal conductivity as shown in Figure (4.5. a,b), to stop air leakage from the duct silicone was used to seal the gaps between the duct edge, and base before it was screwed into place as shown in Figure (4.6).

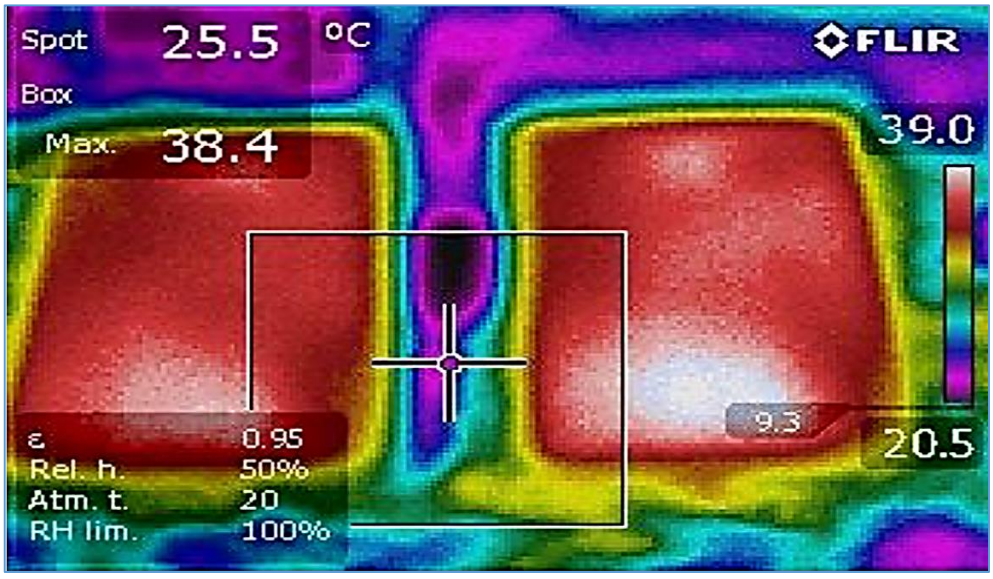

Figure (4.4) PV panel, actual thermal picture [73].

(a) (b)

Figure (4.5). (a) Thermal paste. (b) Multi-flow channel.

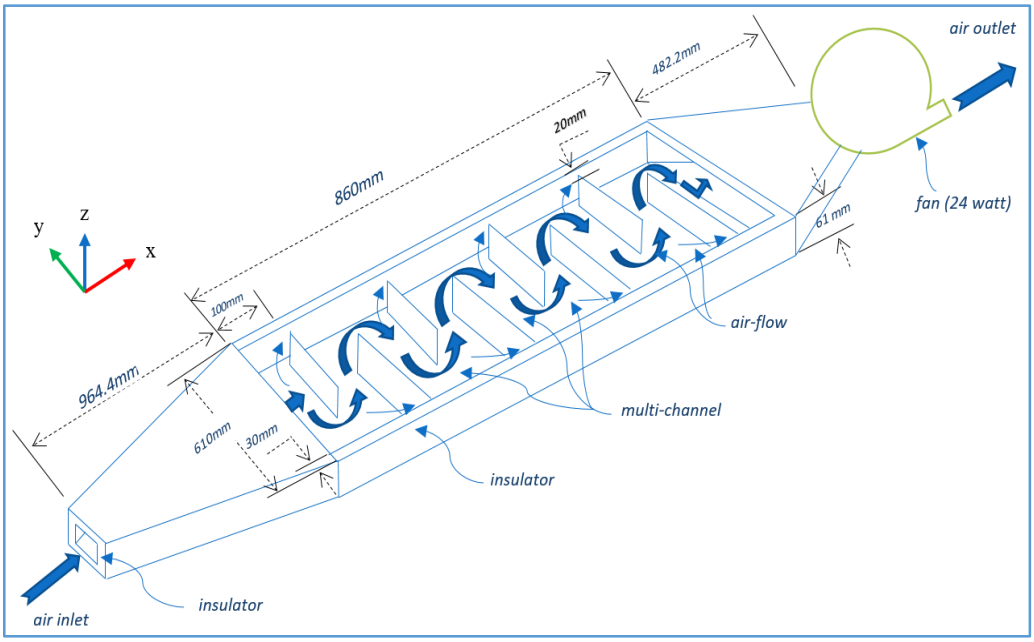

Figure (4.6). PV/T with multi-flow channel system.

4.2.3 Fan

The system's third major component is the air fan. Its purpose is to draw airflow from a multi-channel absorbent PV/T system. The fan of an AC-type variable speed that connects to a variable power supply and has a power maximum (24)W, is connected to a speed regulator to change the fan's power potential, which allows an air velocity meter to measure speed. Carefully, the fan is installed on the air duct at the end of the system, as depicted in Fig (4.7).

Figure (4.7) Photograph of the air fan.

4.2.4 Velocity Regulator

A velocity regulator (AC/220V, 50Hz) with high accuracy as shown in Figure (4.8), is used to regulate the fan and determine the speeds required for testing, which are (2, 2.5, 3, 3.5, and 4) m/s.

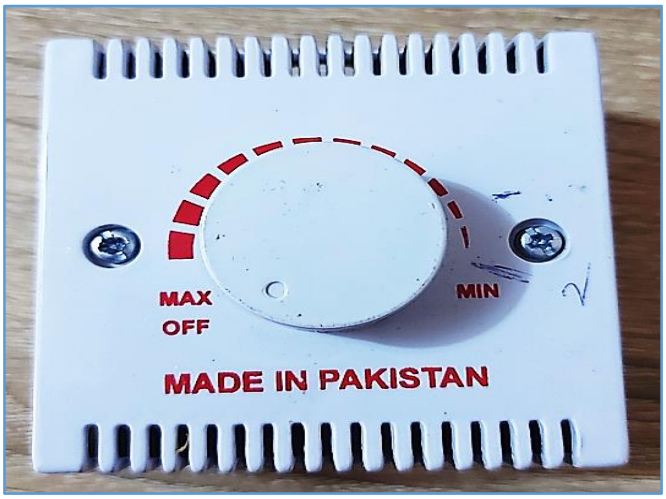

Figure (4.8) Velocity regulator type (AC/220V).

4.2.5 Halogen lamp

A simulator of solar radiation requires high-capacity lighting, and this is achieved through halogen lamps with a power of (1000W/220V). It was used in this work as shown in Figure (4.9). It is installed on an iron stand and a wooden base to prevent electrical conduction and thus reduce the risk. It is equipped with a copper electrical connection wire that allows passage of high

current, directly connected with an electrical protection device to ensure sufficient power delivery.

Figure (4.9) Halogen lamp (1000W).

4.2.6 Apparatus Structure

All components of the system are installed, on the chassis which is the last component, it can be moved to any place desired thanks to its design. The structure consists of three main parts, the upper part holds the halogen lamps, the middle part holds the PV/T collector and the last part holds the test devices. It has been painted to avoid rust and has four wheels to make it easy to move, as shown in Figure (4.10).

Figure (4.10) Install the experimental structure.

4.3 Measurement Devices

To meet the conditions for the success of these readings, different measurement systems are needed for each experimental test. The primary factors in the current work, include temperature, pressure, air mass flow rate, solar irradiation, and the panel power are specifically measured using a variety of instruments. It is explained in more detail below.

4.3.1 Solar Power Meter

This meter was used to measure the amount of solar radiation hitting the PV module and how it affected its performance and efficiency. as seen in Figure (4.11). Throughout the experiment's day, measures of sun radiation were taken every fifteen minutes, the gadget has an LCD screen and pyrometer sensor. The measuring range of the device is (1-3999W/m^2), and its details are described in Appendix (A) (Table A.1). It features a calibration button that can be used to read at night and calibrate it the reading must be (0) W/m^2 as shown in Appendix (B) (Fig. B.1).

• Resolution: (0.1) W/m^2.

• Temperature Error ±0.38W/m²/°C

• 0.25 seconds were consumed for sampling.

• Operating temperatures should be between 0 and 50 ℃, and humidity: less than 80% RH.

Figure (4.11) (Pyranometer SM206) A solar power meter.

4.3.2 Data Logger Thermometer Device

As depicted in Figure (4.12), the multi-channel temperature measuring instrument is essential for measuring the surface temperature of the PV module, the air inside the channel, and the output air temperature following the cooling process. Data logger (CKT4000) is the designated type, and it has (32) channels. Thermocouples (K/J/E/T/N/S/R/B) can be used with the gadget, and the reading accuracy is (0.2)ºC, details are explained in Appendix (A) (Table A.2).

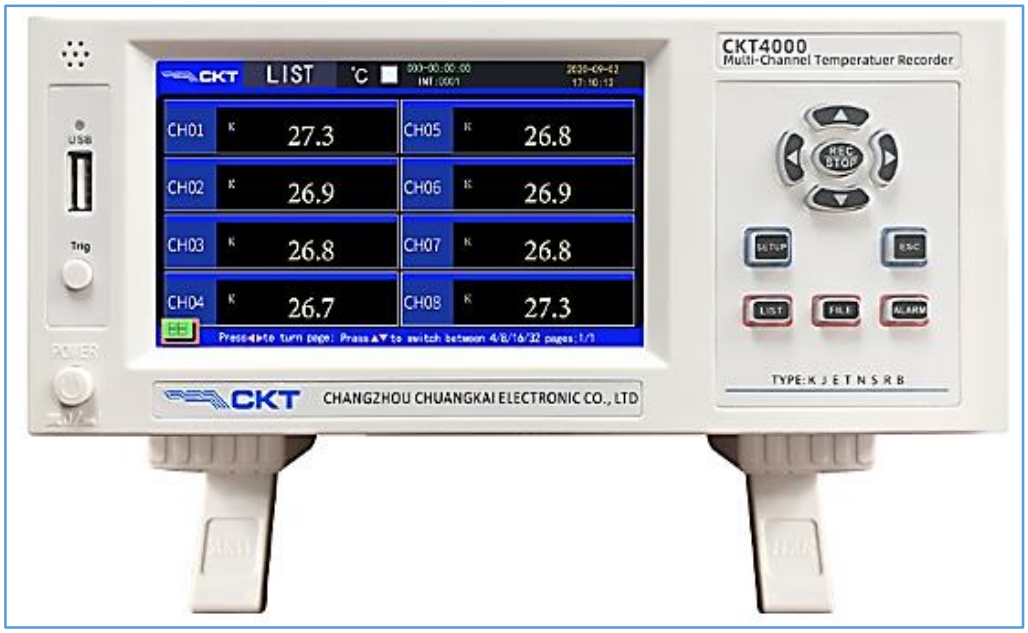

Figure (4.12) Apparatus a data logger thermometer (CKT4000).

4.3.3 Anemometer

The air velocity inside the channel was measured by using an anemometer (GM8902+), as shown in Figure (4.13). Appendix (A) (Table A.3), contains device specifications and calibration of the device by the Ministry of Science and Technology, according to the manuscript attached in Appendix (B) (Fig. (B.3).

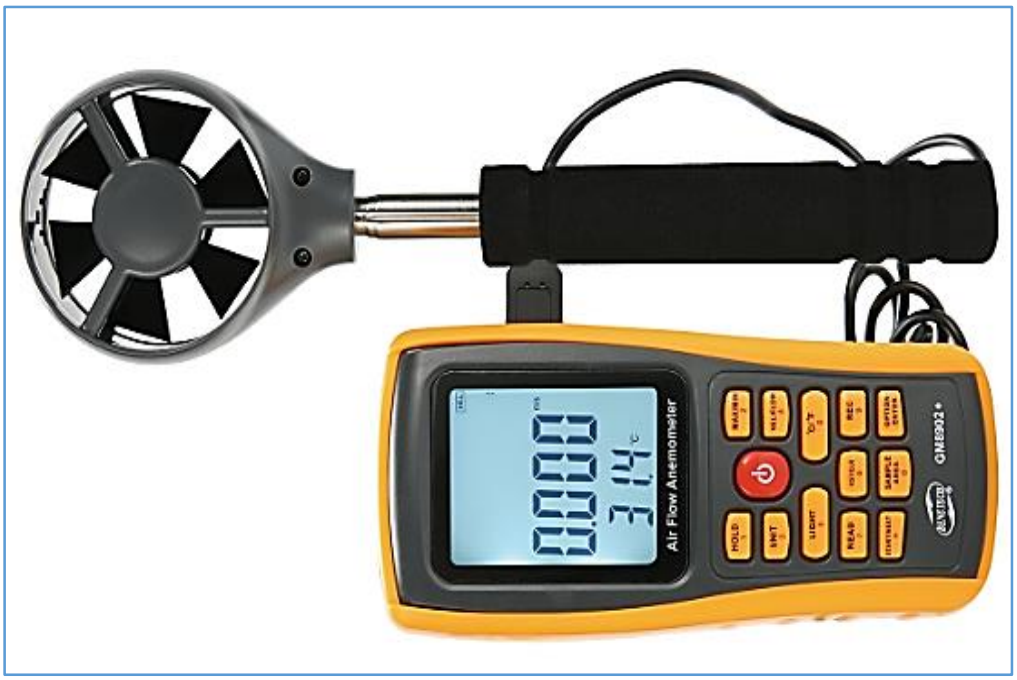

Figure (4.13) Apparatus (GM8902+) anemometer.

4.3.4 Thermocouples Sensor

The system temperature thermocouples at several points to measure temperature. Different lengths of the K-type thermocouples utilized in Fig. (4.15a) are illustrated. They had a connection to the electronic data gadget. The accuracy ratio of the readings as well as the thermocouples used to measure a temperature range. They were accurately installed in the following positions:

1. To assess the surface temperature over time, three thermocouples per one-third were placed on the surface of the PV module with and without cooling, as shown in Figure (4.14a)

2. To evaluate the PV panel temperature with or without cooling, five thermocouples have been deployed throughout the PV base at different locations, as shown in Figure (4.14b)
3. A pair of thermocouples is installed at the air inlet of the duct.
4. At the airflow from the outlet of the PV/T duct, two thermocouples are connected.

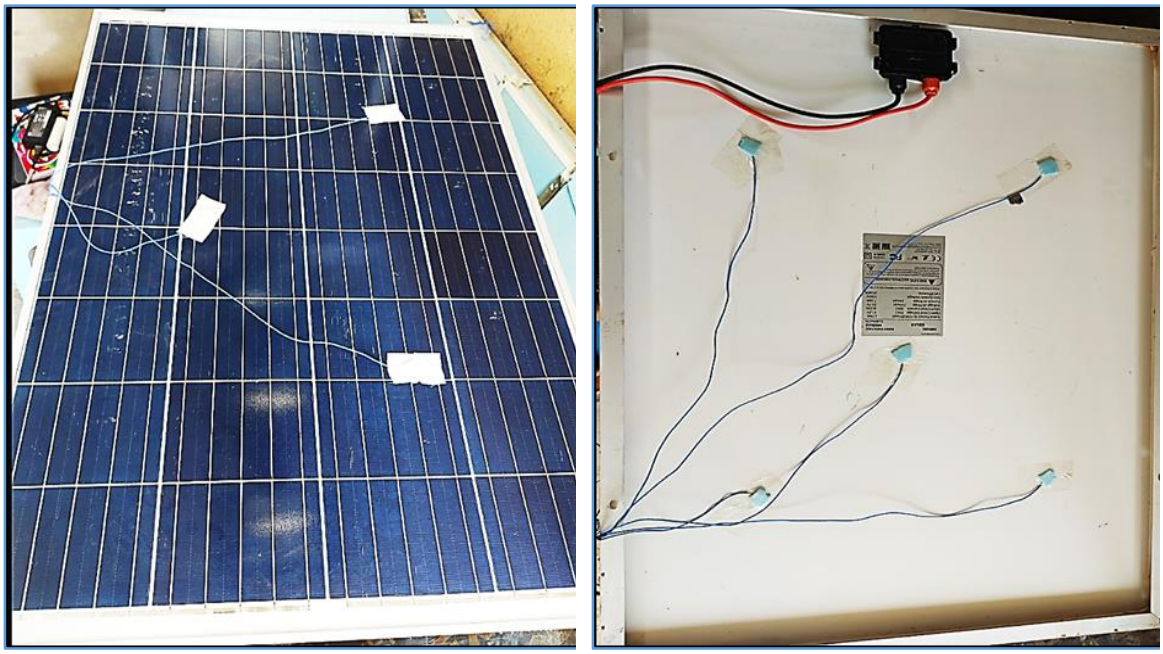

(a) (b)

Figure (4.14). The location of the thermocouple. (a) At the surface of the solar panel. (b) At the base of the solar panel.

By recording readings at three different grades and comparing them with the readings of the mercury thermometer at freezing temperature (0 °C), boiling water temperature (100 °C), and human body temperature (37 °C), calibration of the temperature sensor (thermocouples) was performed to obtain the best readings. The calibrated results are displayed in Appendix (B) (Table B.2).

The method of installing thermocouples is very important to obtain the best reading, so to ensure this, the sensor must be installed at the point to be measured carefully enough after cleaning its location, then placing a thermal insulation layer on the thermal sensor to prevent the transfer of ambient heat to it, as well as installing a conductive aluminum thermal tape to reflect the solar radiation, as shown in Figure, (4.15,b).

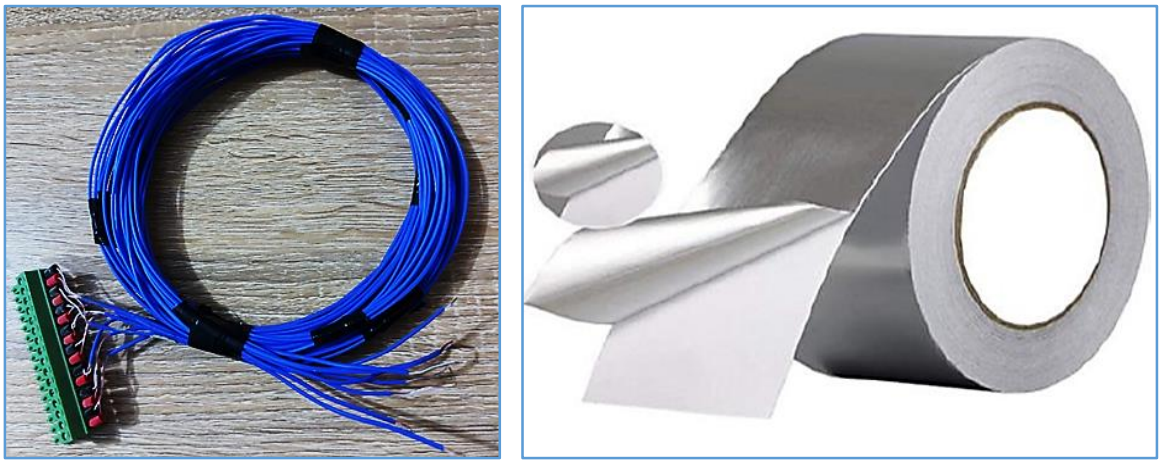

(a) (b)

Figure (4.15): (a) Thermocouples K-type. (b): Conductive aluminum heat bar.

4.3.5 PV Analyzer (PROVA 210)

It is a device used to measure the solar panel energy, voltage, and current at the power maximum (Pmax). In addition to the greatest open circuit voltage, the greatest short circuit current. It connects the computer with a connecting link (USB) and with the PV unit with cables with positive and negative poles as shown in Figure (4.16). The device records and draws diagrams on the computer immediately according to the specified time. The greatest power it can measure is (60V, 12A, and 500W), and the accuracy is about (1mV, 1mA), all specifications are shown in Appendix (A) (Table A.4).

Figure (4.16) Apparatus PV analyzer type (PROVA 210).

4.3.6 Pressure Manometer

Figure (4.17) shows a pressure drop measuring device that is used in the PV/T system. It connects flexible tubes with a diameter of (5 mm) placed at two points, the beginning and the end of the air duct, in a curved manner in the direction of the airflow, to determine the pressure difference between them. The device contains a digital screen and buttons to change the measurement unit. The measurement accuracy is (±0.3%) at (25°C), and the maximum pressure can be measured at (35kPa), the specifications are shown in Appendix (A) (Table A.5).

Figure (4.17) Apparatus pressure manometer type (520).

4.3.7 Voltmeter

Figure (4.18) shows a device that was used to measure the voltage and current of the air fan to extract electrical power under variable speeds starting from (2-4) m/s to determine the extent of electric power consumption.

Figure (4.18) The voltage meter (DT-830D).

4.4 Experimental Procedure

Before starting the experiments, all temperatures of the thermocouples that are used in the PV cooling system should indicate the same ambient temperature at (38°C) ± (1°C). Moreover, the tests are carried out in sequential steps as follows:

a) In the beginning, the solar simulator and axial fan are started in the desired range through voltage regulator control.

b) The test rig runs until the steady state is reached 40 minutes from the start of operation of the PV system without and with a multi-flow channel, respectively.

c) All temperature values along the PV/T system during this process are recorded every 15 minutes by utilizing a data logger.

d) Pressure drop across the PV collector is recorded at the selected airflow speed and solar flux.

e) Connect the PV analyzer device with the solar panel and the computer, and record the readings of the maximum voltage, current, and maximum power of the system in load and without load every 15 minutes.

f) In the experiments, change the air mass flow rate under the selected solar flux intensity and repeat the previous steps, it took about 30 minutes to reach steady condition and repeat the third step (c).

Chapter Five

Results & Discussion

CHAPTER FIVE

RESULTS AND DISCUSSION

5.1 Introduction

Numerical and experimental results of PV/T collector temperatures were obtained for the proposed PV/T system under test conditions at room temperature (38)°C±1, wind speed (1) m/s, and solar flux (600, 800, and 1000)W/m^2, and air MFR values (0.04, 0.05, 0.06, 0.07, and 0.08) kg/s which creates a turbulent flow when the Reynolds number is between (6256.49 - 12512.99).

5.2 Numerical Solution Results

The simulations were performed under conditions similar to the experimental for computational domains (rectangular, triangle, and transverse fins with multi-flow channel), the test was conducted among MFR with solar panel temperature (TPV), outlet air temperature (Tout), thermal efficiency, and electrical efficiency under MFR (0.04-0.08)kg/s, and solar flux (1000)W/m^2 . Shows the temperatures decrease at MFR increases due to flows air stronger into accumulator. Moreover, the MFR rising lead to thermal efficiency, and electrical efficiency increases. The comparison between the three models (a, b, and c), showed that dropping solar cell temperature about (88.03-79.45)℃, (86.81-77.63)℃, and (64.71-56.26), respectively. The outlet temperature about (39.35-39.12)℃, (39.77-39.44)℃, and (46.55-42.87)℃, respectively. The increasing electrical efficiency, about (14.8-15.59)%, (14.91-15.76)%, and (16.31-17.3)%, and thermal efficiency from (14.5-18.73)%, (24.17-26.95)%, and (65.84-75)%, for models (a, b, and c), respectively. As shown in Figures (5.1), (5.2), (5.3), and (5.4), respectively.

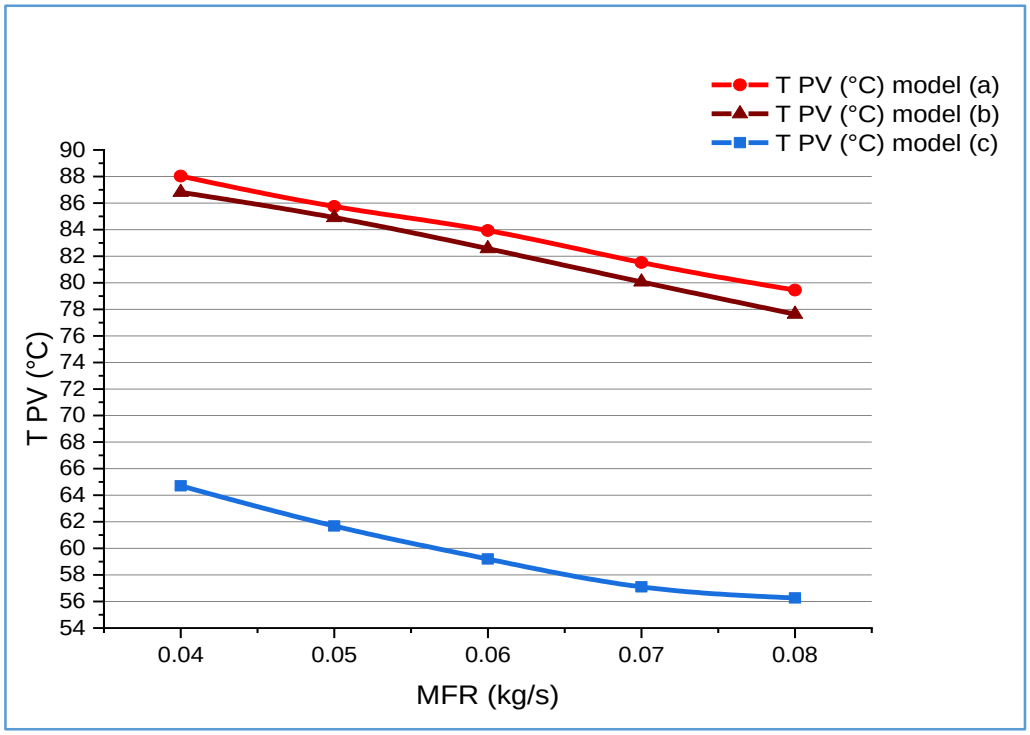

Figure (5.1) Influence of MFR variation on the PV temperature.

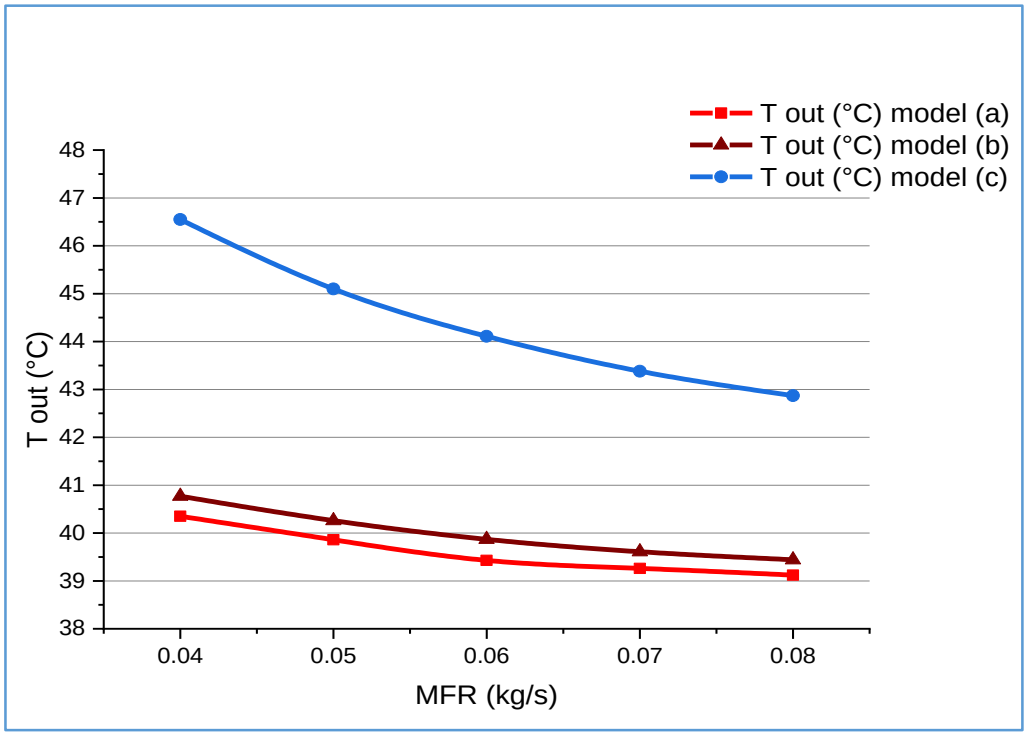

Figure (5.2) Influence of MFR variation on the Tout.

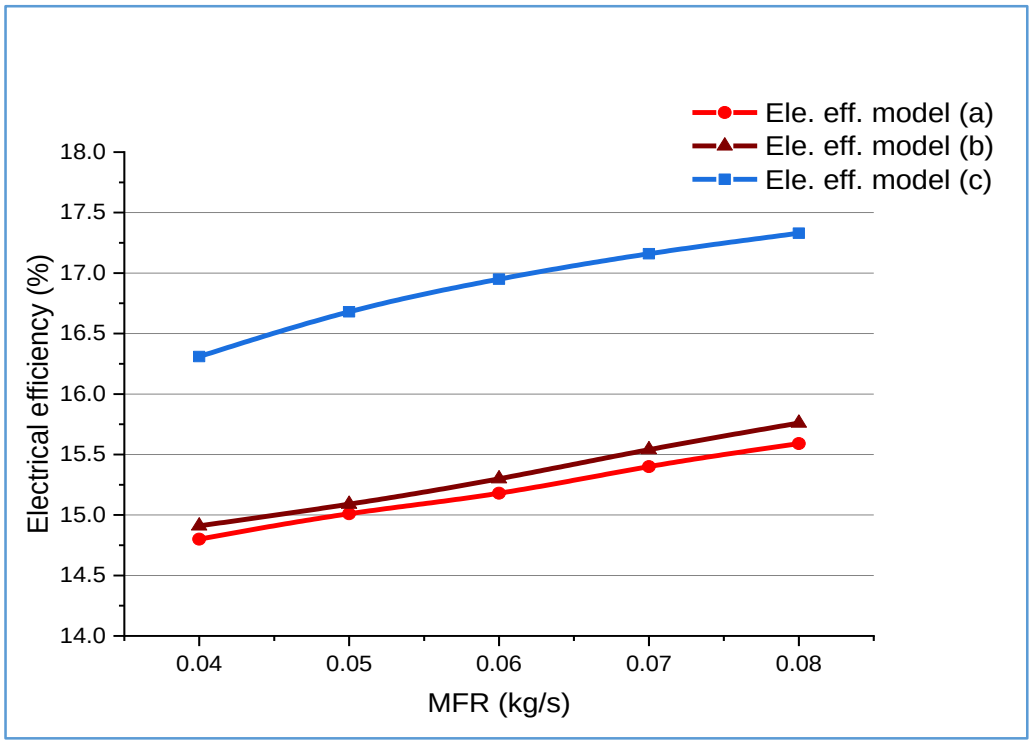

Figure (5.3) Influence of MFR variation on the electrical efficiency.

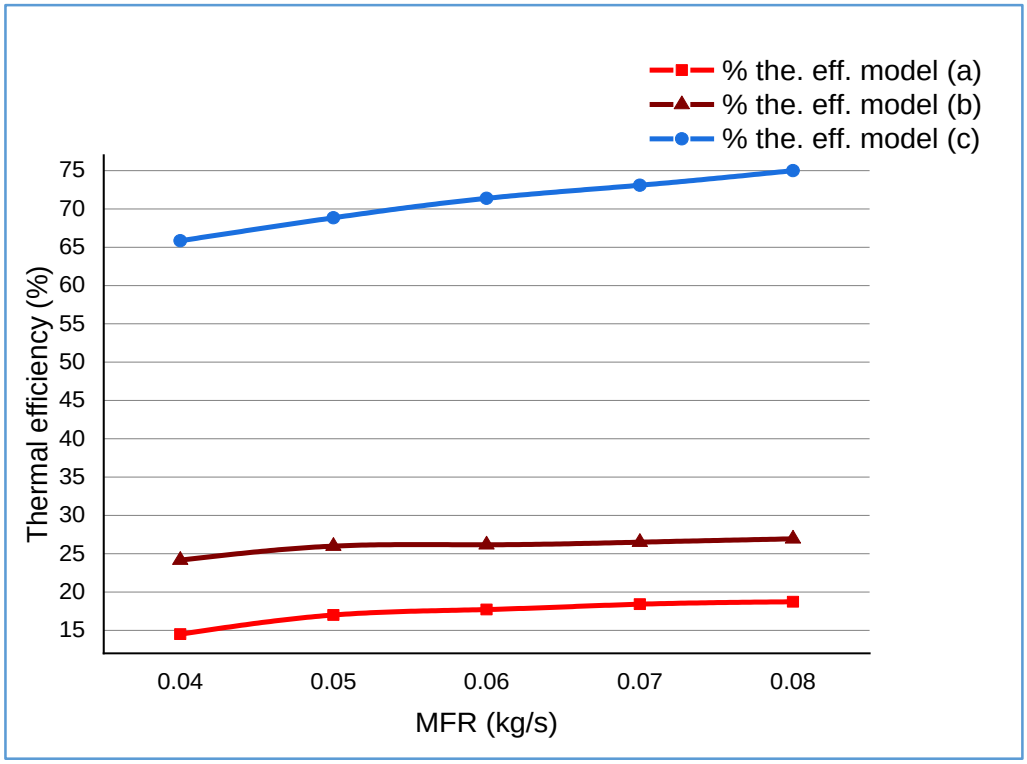

Figure (5.4) Influence of MFR variation on the thermal efficiency.

5.2.1 Numerical Results of the Proposed Model

The transverse fin with multi-flow channel model achieved the best results compared to the three models. Moreover, Figure (5.5. a, b, c) shows the temperature distribution of the PV/T system with multi-flow channel. The results found that the temperature profile of the PV surface reduced along the collector, gradually. Increasing the mass flow rate leads to a reduction in the temperature of the solar cells and thus enhances their performance and efficiency. The simulations were performed under conditions similar to the experimental method for a PV/T collector with multiple flow channels. Furthermore, the temperature distribution of the PV/T collector is affected by changes in the solar flux (600, 800, and 1000) W/m^2 at speed constant, in other words, when the radiation increases, the temperature rises, as shown in Figure (5. 6, a, b, c).

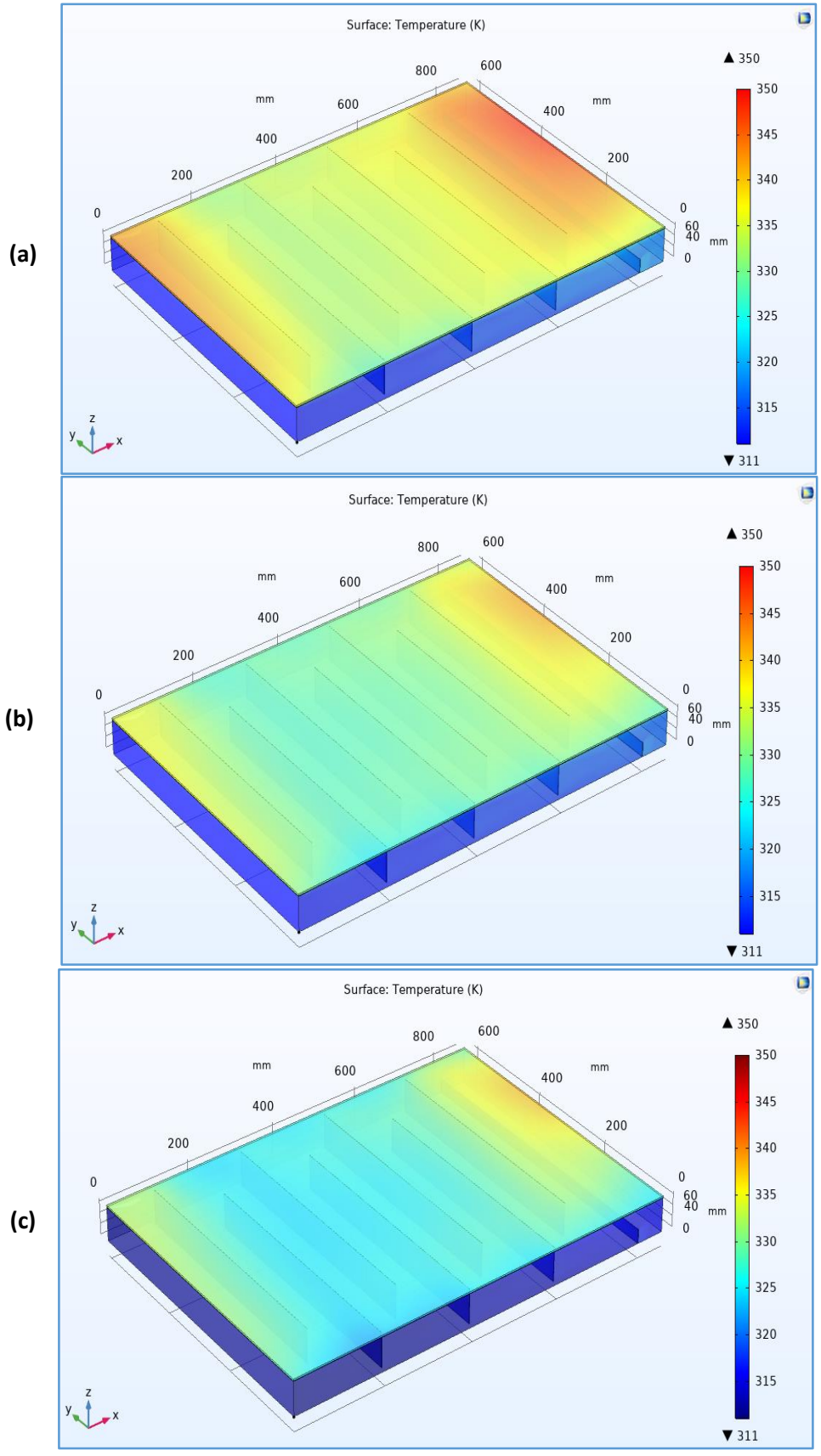

Figure (5.5) Isotherm of the PV/T system with multi-flow channel at solar flux (1000) W/m^2, with different MFR (a) 0.04 kg/s, (b) 0.06 kg/s, and (c) 0.08 kg/s.

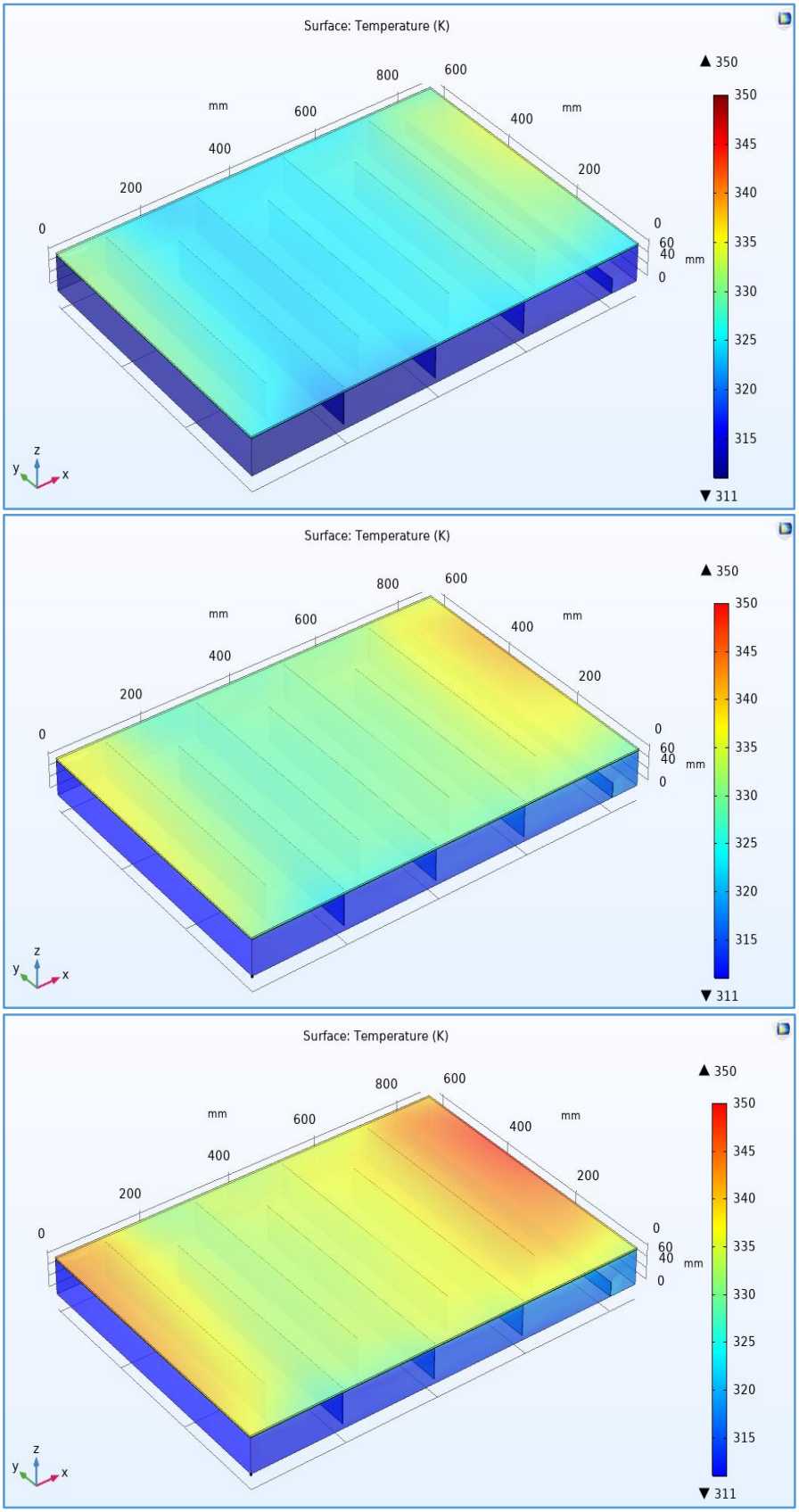

Figure (5.6) Isotherm of the PV/T collector with a multi-flow channel, at low-velocity 2m/s, under difference solar fluxes (a) 600 W/m^2, (b) 800 W/m^2, and (c) 1000 W/m^2.

5.2.2 Effect of Solar Flux on the PV Panel

The simulation was applied under the conditions of solar flux (600, 800, and 1000)W/m^2. It showed that the cell temperature (T_{PV}) increases with the increase in solar flux as shown in Figure (5.7), which leads to a decrease in electrical efficiency, and the results were (13.22%, 12.84%, and 12.53%), respectively, as shown in Figure (5.8).

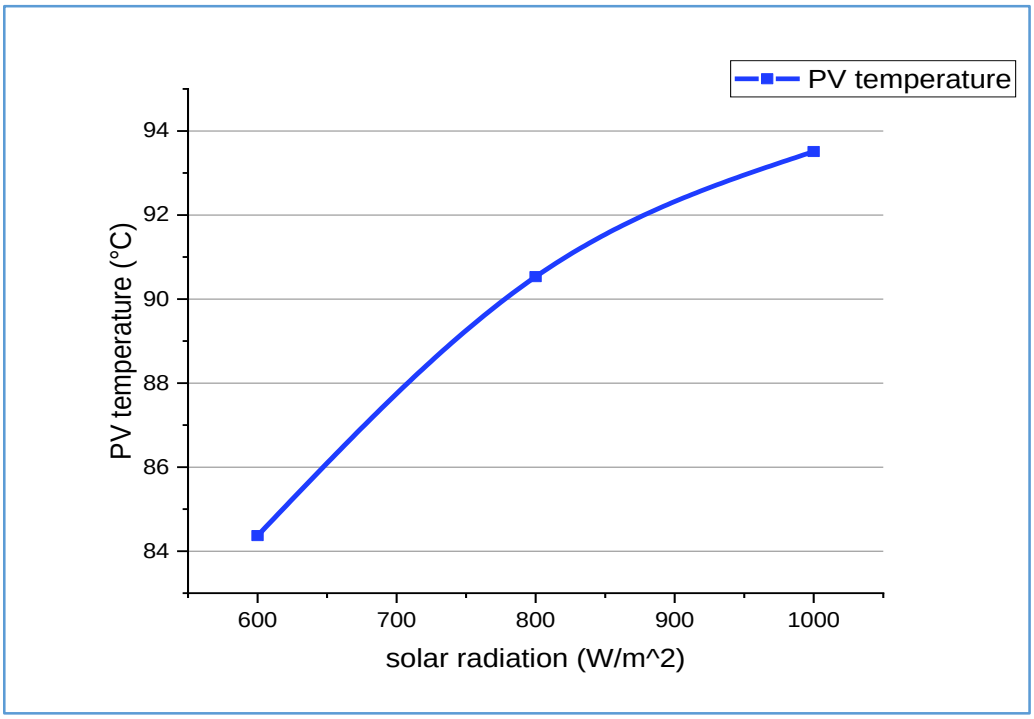

Figure (5.7) Variation of solar flux and the PV of the panel temperature.

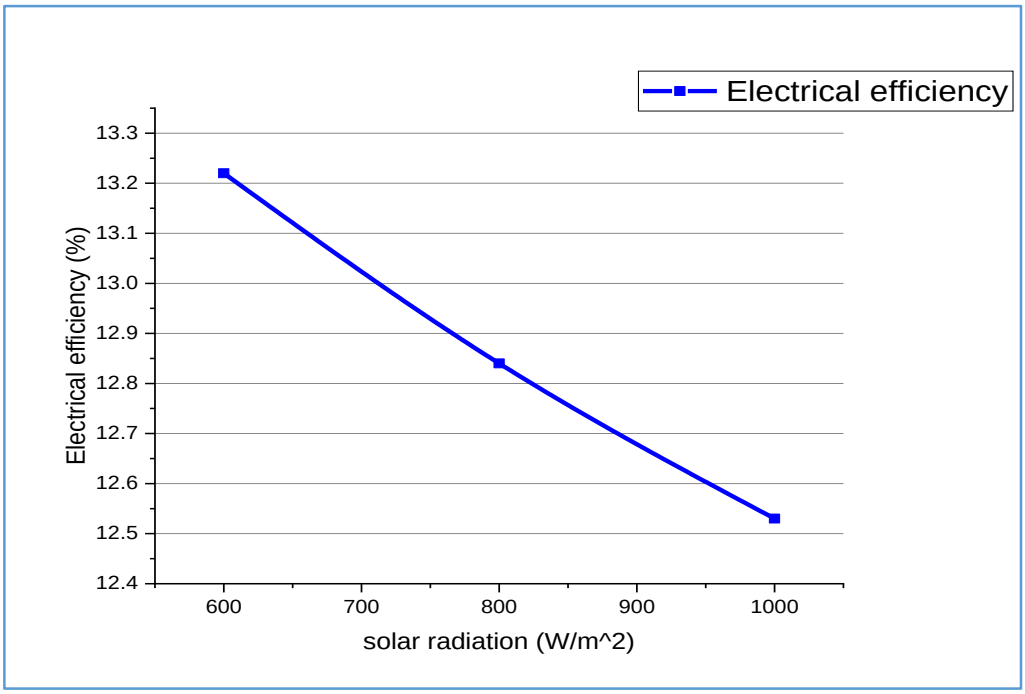

Figure (5.8) Variation of solar flux and electrical efficiency.

5.2.3 Effect of Mass Flow Rate on the PV/T System

During this numerical study of the PV/T system by flow rate inside the thermal collector variable results were obtained for the cell temperature of the PV panel, and the temperature of the outlet air, in addition to the change in electrical efficiency, and thermal efficiency, as shown in Figures(5.9), (5.10), (5.11), and (5.12), respectively. The ambient temperature at 38°C and the inlet flow air temperature was fixed at 38°C, and the data of the output air temperature and the temperature of the PV panel were recorded, thus the electrical efficiency of the PV/T system obtained with cooling at the mass flow rate (0.04, 0.05, 0.06, 0.07, and 0.08) kg/s. was applied with each of the solar flux (600, 800, and 1000) W/m^2.

Figures (5.9) and (5.10) showed a decrease in the cell temperature (T_{PV}) and outlet air temperature of the PV panel at different solar radiation rates, against the increase in the airflow rate. Figures (5-7), and (5-8) showed an increase in the electrical efficiency and thermal efficiency, under the same above conditions.

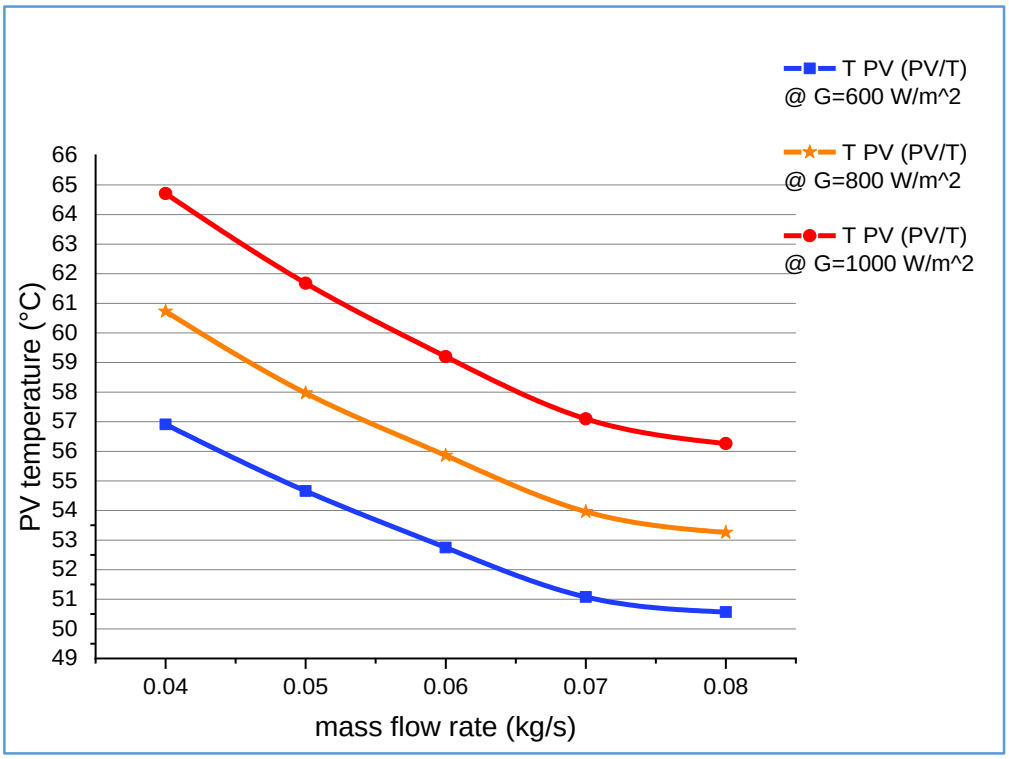

Figure (5.9) Variation of mass flow rate and the PV temperature, at different rates of solar flux.

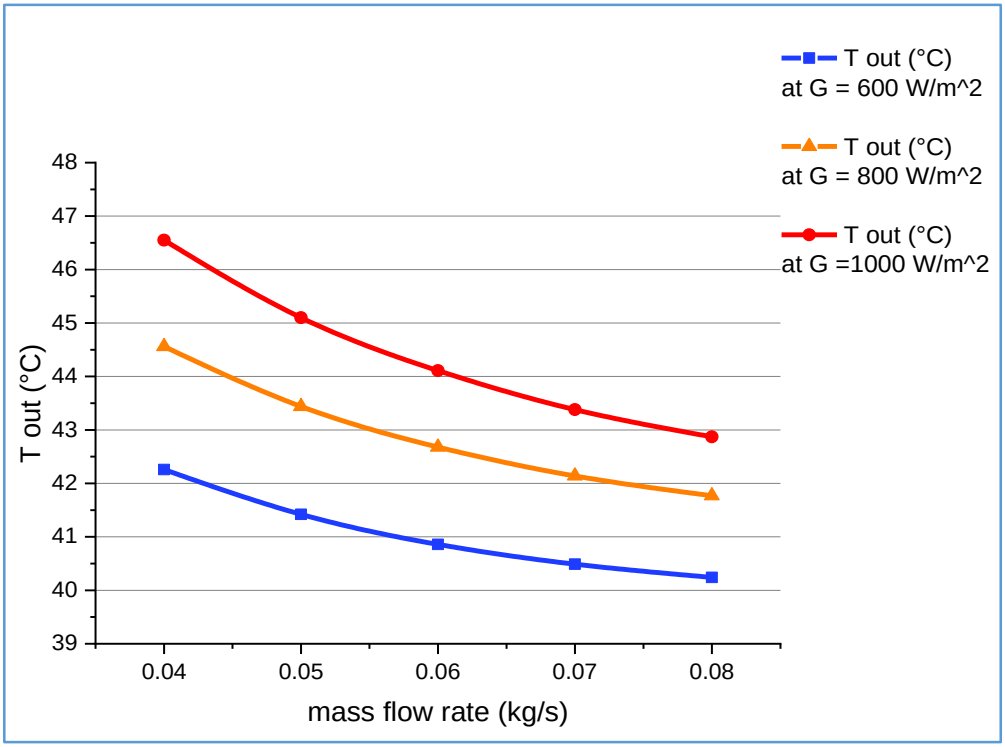

Figure (5.10) Variation of mass flow rate and the outlet air temperature(Tout) with difference solar fluxs (600, 800, and 1000) W/m^2.

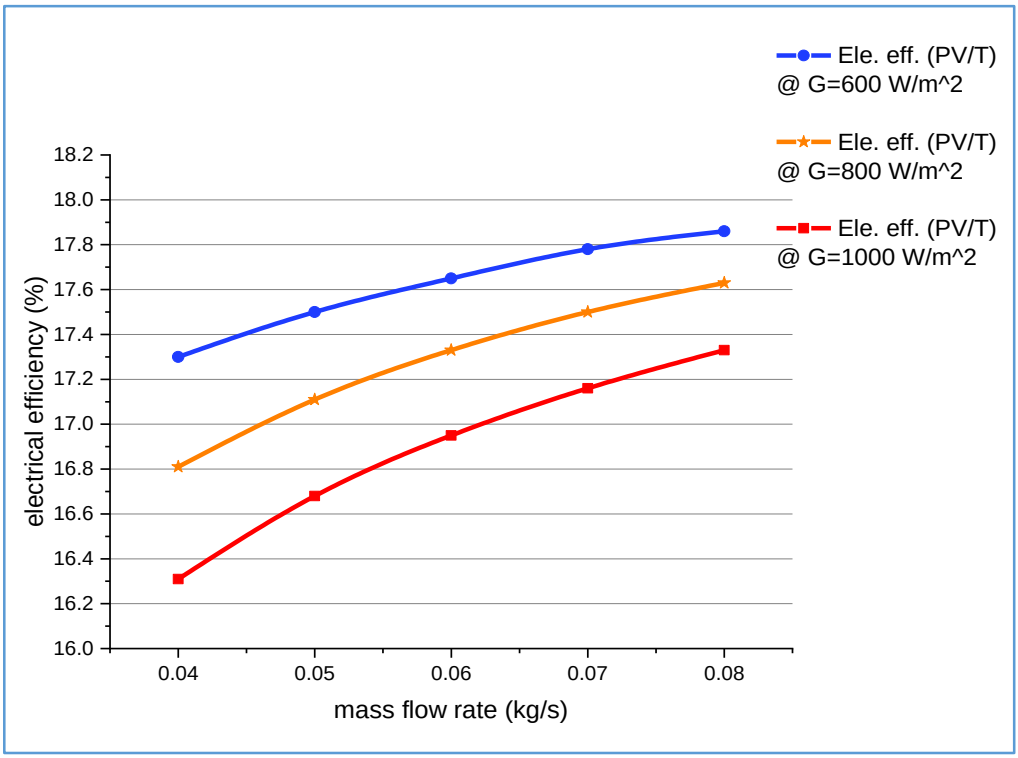

Figure (5.11) Variation of mass flow rate and electrical efficiency, at different rates of solar flux.

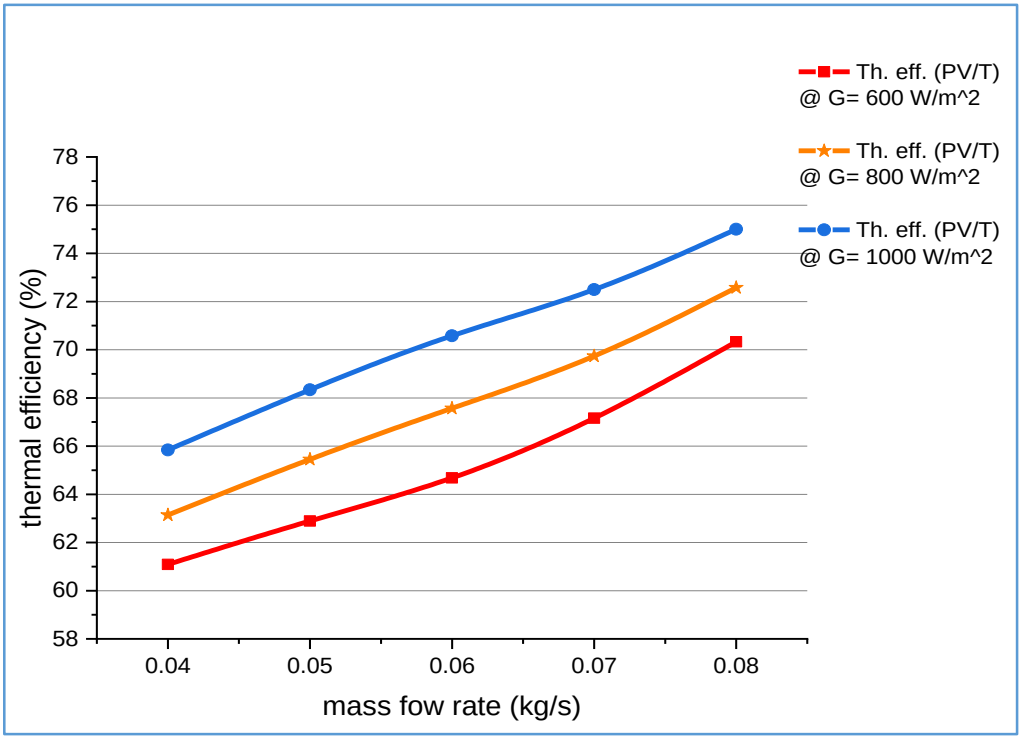

Figure (5.12) Variation of mass flow rate and thermal efficiency, at different rates of solar flux.

5.3 Experimental Results

The overall goal of this chapter is to describe the real results acquired from the experimental performance of the PV/T system, as well as the results applied to the design. To determine the possibility of combining the PV module and thermal collector, variables such as the temperature of the main PV module at different locations, inlet and outlet air temperature, ambient temperature, solar radiation, electrical and thermal efficiency, mass flow rate, and pressure drop were thoroughly investigated. These characteristics indicate whether or not the cooling mechanism can increase the PV/T system's electrical performance.

The experimental results were obtained based on five cases of mass flow rate (0.04, 0.05, 0.06, 0.07, and 0.08) kg/s, with each case three simulations of different solar flux (600, 800, and 1000) W/m^2.

5.3.1 Current-Voltage Characteristics at STC PV Panel, and Proposed PV/T System

The electrode of the PV panel must be connected in parallel with the connections of the PV analyzer device to measure the value of voltage, current, and electrical power. To know the maximum power extracted from the PV panel and through the graphical relation among (voltage - current - power). In addition, to connect it with the PV/T system at a variable air mass flow rate (0.04, 0.05, 0.06, 0.07, and 0.08) kg/s, as shown in Figures (5.13) and (5.14), respectively. This indicates that the relation between voltage and current is no-load, voltage maximum, maximum current with load, and maximum power at (maximum voltage and current) under the same conditions and compared with the standard test conditions (STC) of the PV module.

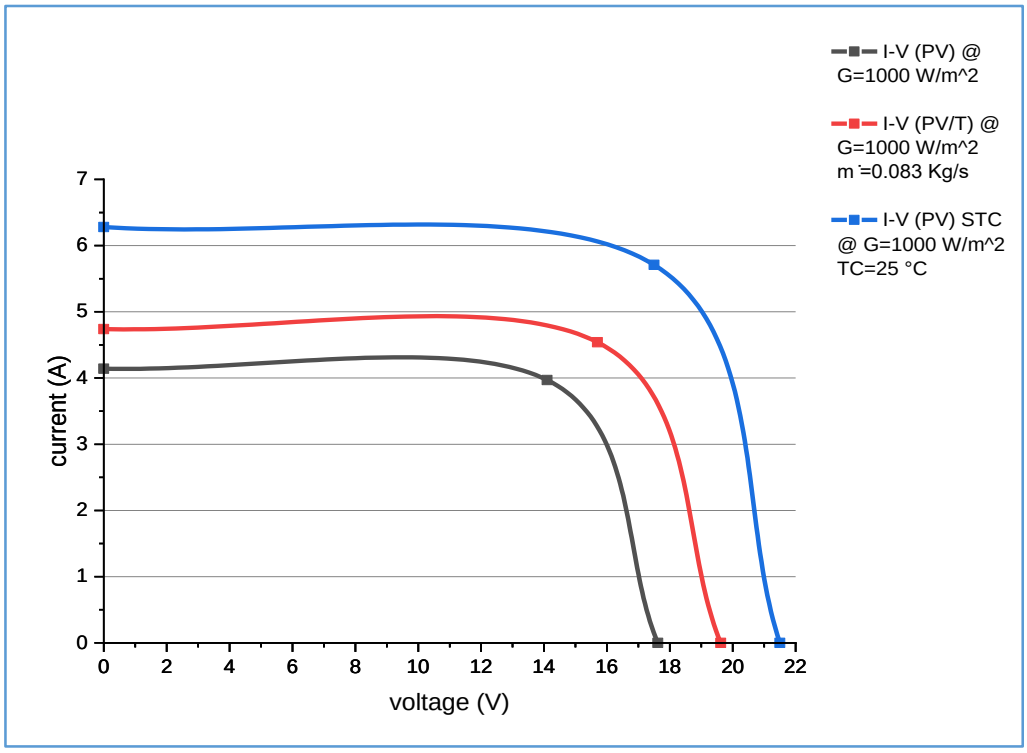

Figure (5.13) Comparison of I-V curve of the PV panel at STC, PV panel, and PV/T air system.

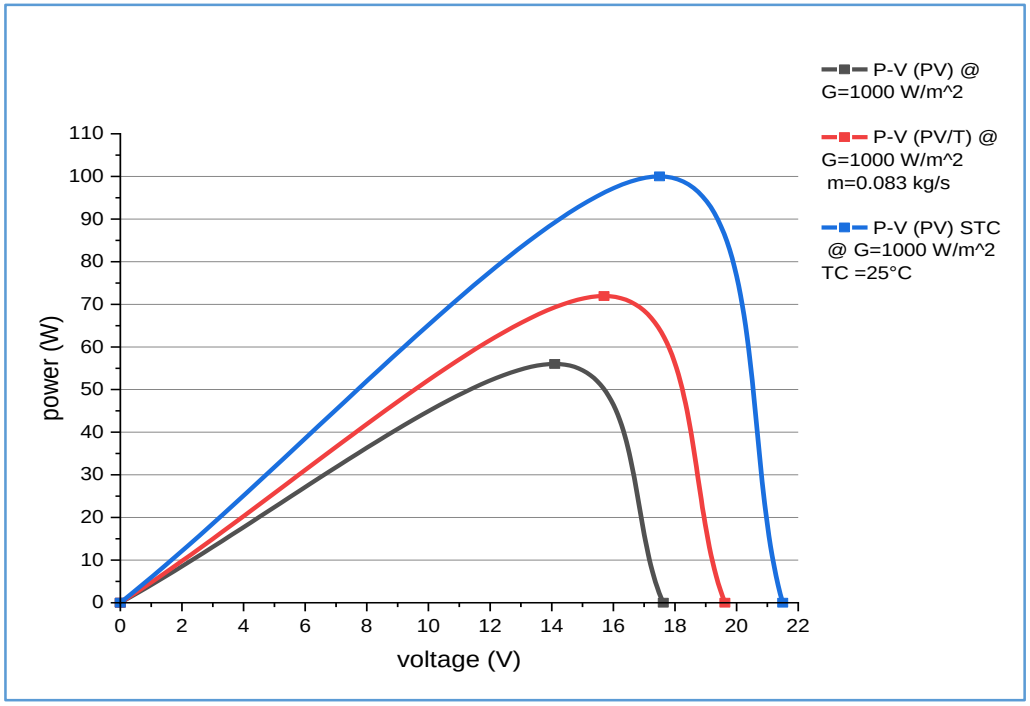

Figure (5.14) Comparison P-V curve of the PV panel at STC, PV panel, and PV/T system.

5.3.2 PV Panel Without Absorber Collector

As shown in Figure (5.15) an increase in cell temperature (T_{PV}) causes a decrease in open circuit voltage (Voc), which increases reverse saturation short circuit current (Isc), as shown in Figure (5.16), and leads to a decrease in the maximum power produced by the PV panel, as shown in Figure (5.17). Because the cell's electrical energy is determined by two factors: current and voltage.

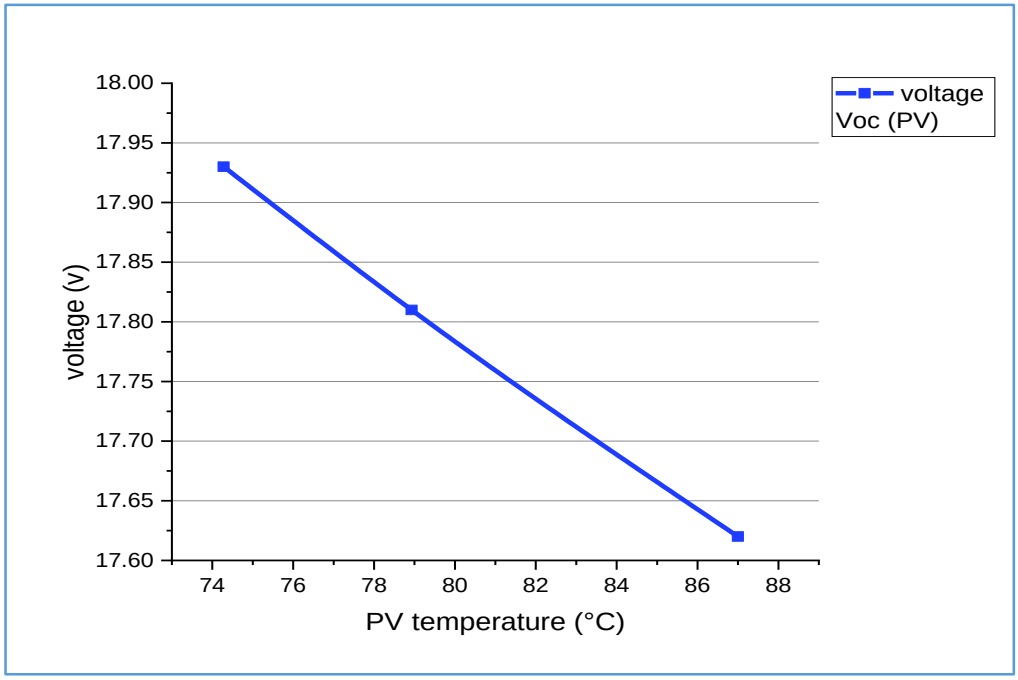

Figure (5.15) (Voc) curve with a T_{PV} change of the PV panel at a solar flux (600,800, and 1000) W/m^2.

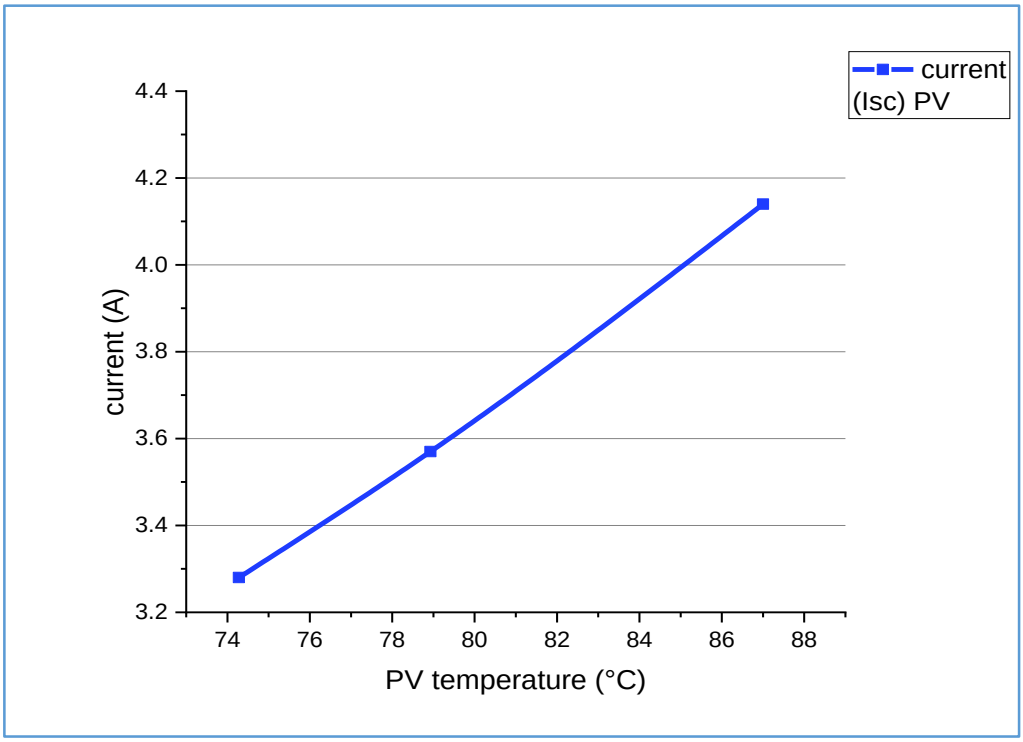

Figure (5.16) (Isc) curve with a cell temperature change of the PV panel at a solar flux (600,800, and 1000) W/m^2.

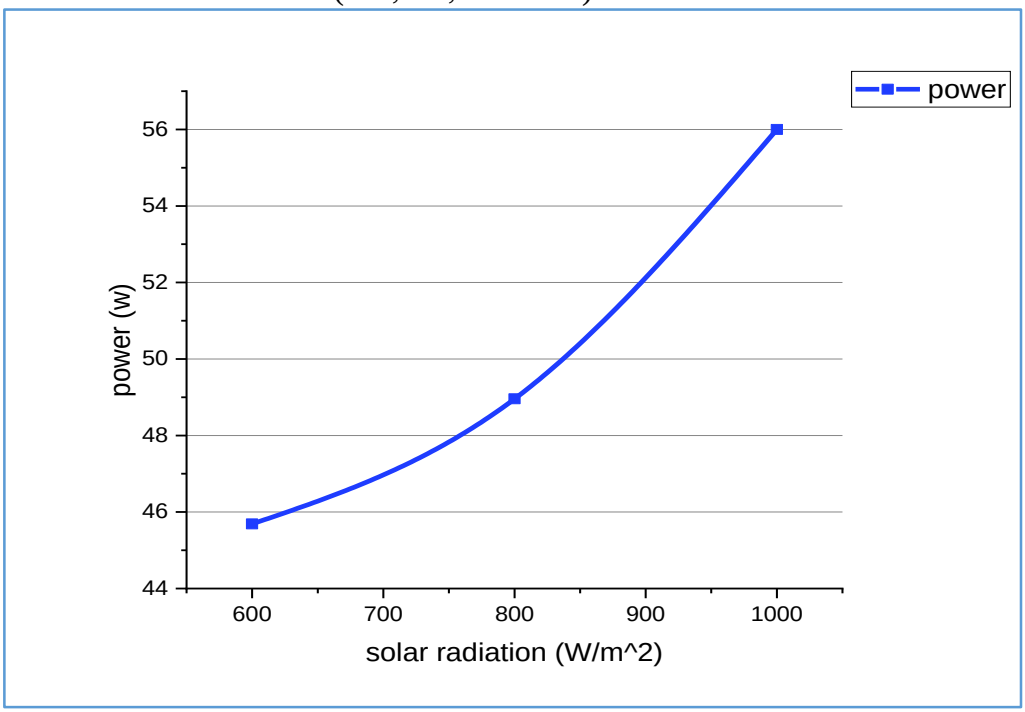

Figure (5.17) Curve of the Electrical power with difference solar flux for PV module.

Furthermore, the change in maximum power is clearly defined as shown in Figures (5.18) and (5.19) respectively. The results of the increase in electric power output started from (45.69) W to (56) W. In this test the fill factor (FF) declined from (0.80-0.769) at (600) W/m^2. At (1000) W/m^2 they are good (FF)

range limits, because they are within the (STC), fill factor limits which should be between (0.7) and (0.8). At (600) W/m^2 the PV module efficiency is (15.65)%, dropping to (14.51)% at (1000) W/m^2, due to solar flux take behavior of heat.

The efficiency of the indicated PV panel is much lower compared to the specification of the (STC), as (Isc) = (6.28)A, (Voc)=(21.5)V and electrical efficiency by the manufacturer was 20.66%. As a result the difference in the power and efficiency values under the experimental test compared to the one provided by the manufacturer decreases because the electrical efficiency of the PV module has decreased with the increase of cell temperature of the PV module during work and reached about (87)°C, and this will lead to more loss of power and efficiency.

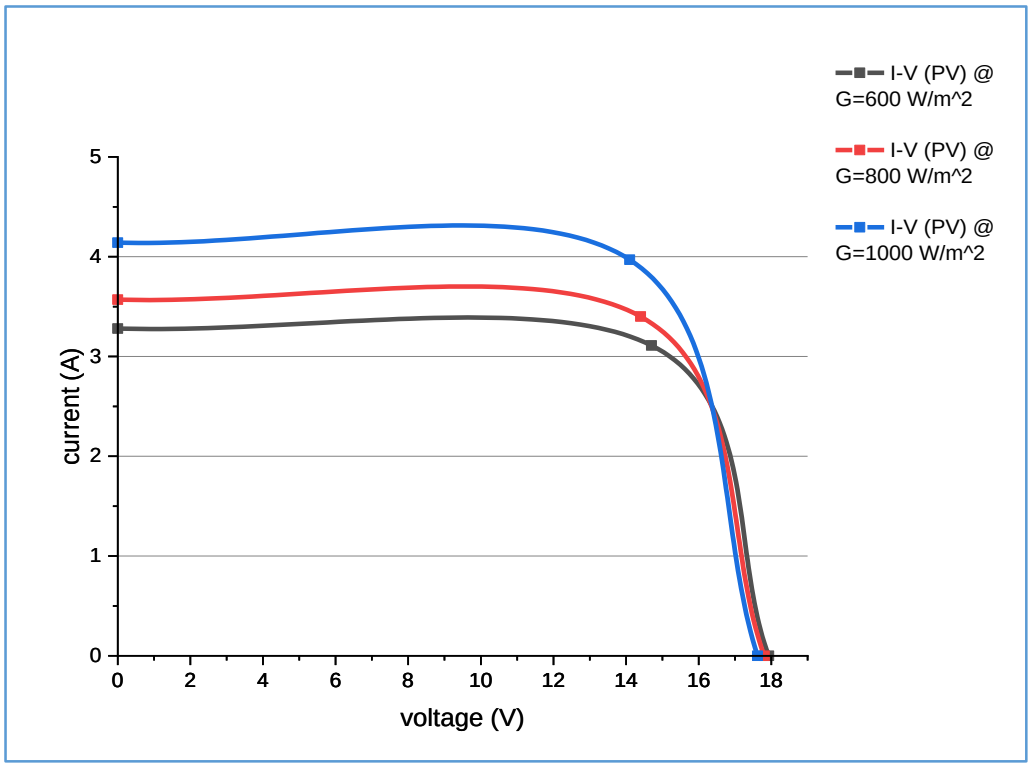

Figure (5.18) I-V curve of the PV panel with change in the solar flux.

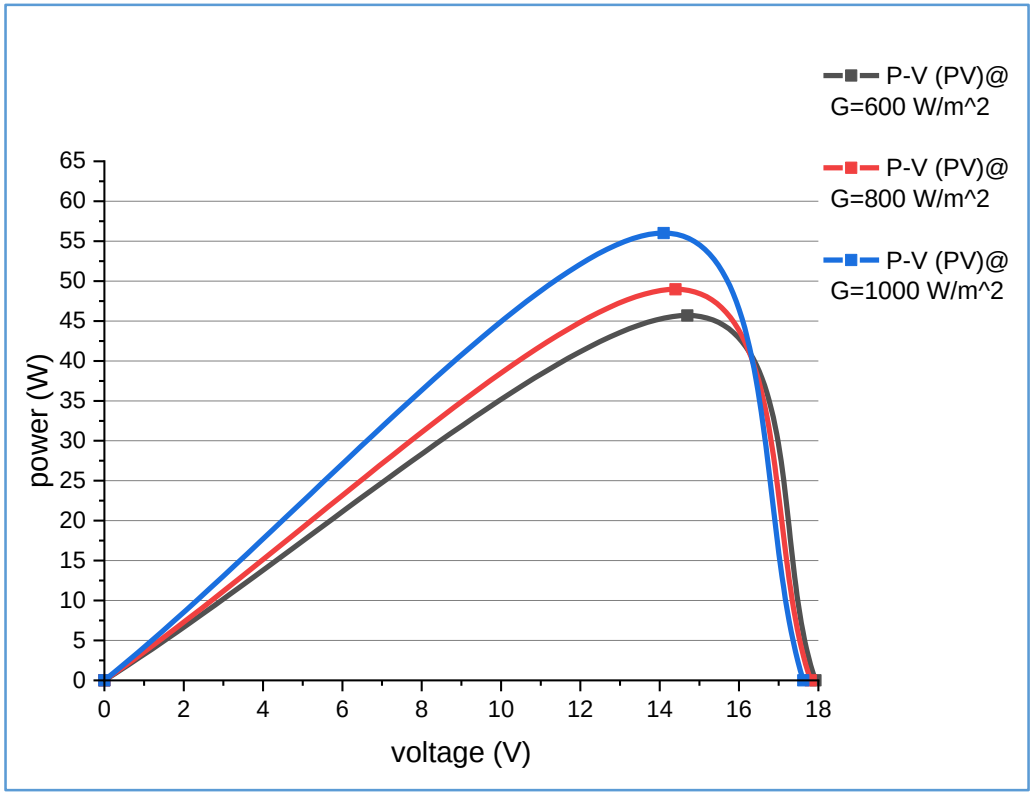

Figure (5.19) P-V curve of the PV panel with change in the solar flux.

5.3.3 Testing of the Proposed Design of a PV/T Air Collector

The indoor testing of the PV/T collector is carried out experimentally at ambient temperature and solar radiation, as well as conventional PV panels, at the same test conditions, then data are collected from the PV module and PV/T system under equal conditions. The solar flux intensity and air mass flow rate of the PV/T collector were changed variable results were obtained. The temperatures were measured for each (ambient, inlet flow, outlet flow, panel surface, and base of the PV panel). These data were recorded to determine the electrical power and electrical and thermal efficiency of the PV panel with cooling and without cooling. The PV panel and PV/T system was subjected to static simulated solar flux (600, 800, and 1000) W/m^2 for each test.

5.3.3.1 I-V and P-V Curves of the PV/T System at Different Solar Flux.

Figures (5.20) and (5.21) show the results obtained from the PV/T collector under the influence of different solar flux (600, 800, and 1000) W/m^2 and mass flow rates ranging from (0.04-0.08) kg/s, and this can be seen clearly through the higher (Voc), (Isc) with an increase of the solar radiation of the PV module.

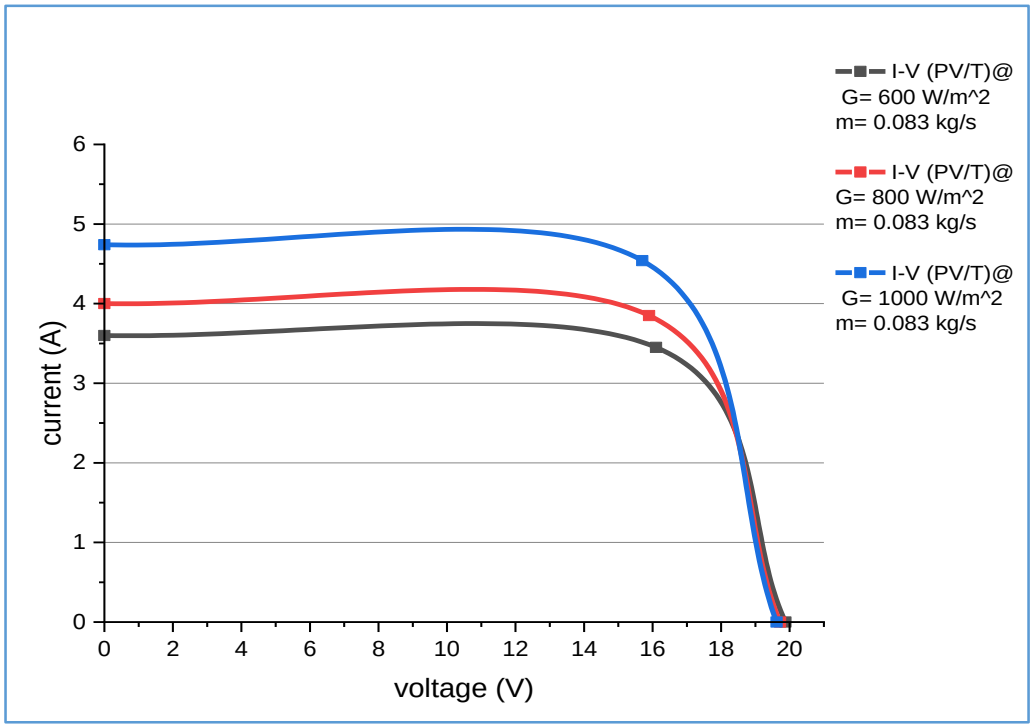

Figure (5.20) I-V curve of the PV/T system with the change in the solar flux at $\dot{m} = 0.08\ kg/s$.

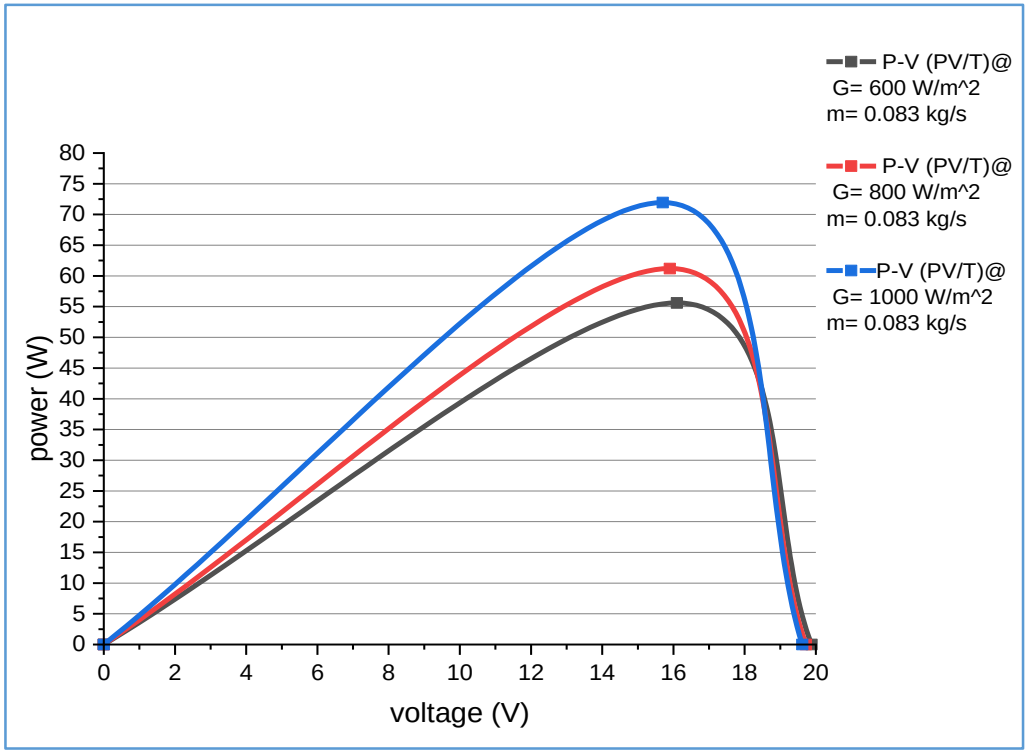

Figure (5.21) P-V curve of the PV/T system with the change in the solar flux at $\dot{m} = 0.08\ kg/s$.

5.3.3.2 I-V and P-V Curves of the PV/T Air System with Different MFR.

Thermal effects are an inherent consequence of the PV/T system, as the PV panel voltage decreases with increasing temperature. Thus, temperature will play an important role in the characteristics of the PV panel (I-V) and (P-V) curves. As the temperature of the PV panel increases due to exposure to sunlight, (Isc) will increase slightly, and at the same time (Voc) will decrease compared to the (STC) of the PV panel. The results of the electrical properties of the PV/T collector affected by temperature are clearly as in Figures (5.22), and (5.23). In this test, the ambient temperature was set continuously at (38 ±1)°C with a solar flux of (1000) W/m^2 and a mass flow rate variation of (0.04-0.08) kg/s. It can be seen that the average PV temperature decreases by (19.53)°C when the flow rate reaches (0.08 kg/s). Due to the decrease in temperature. The (Voc) and (Isc) also slightly increased by (19.62 V, and 4.74 A) respectively.

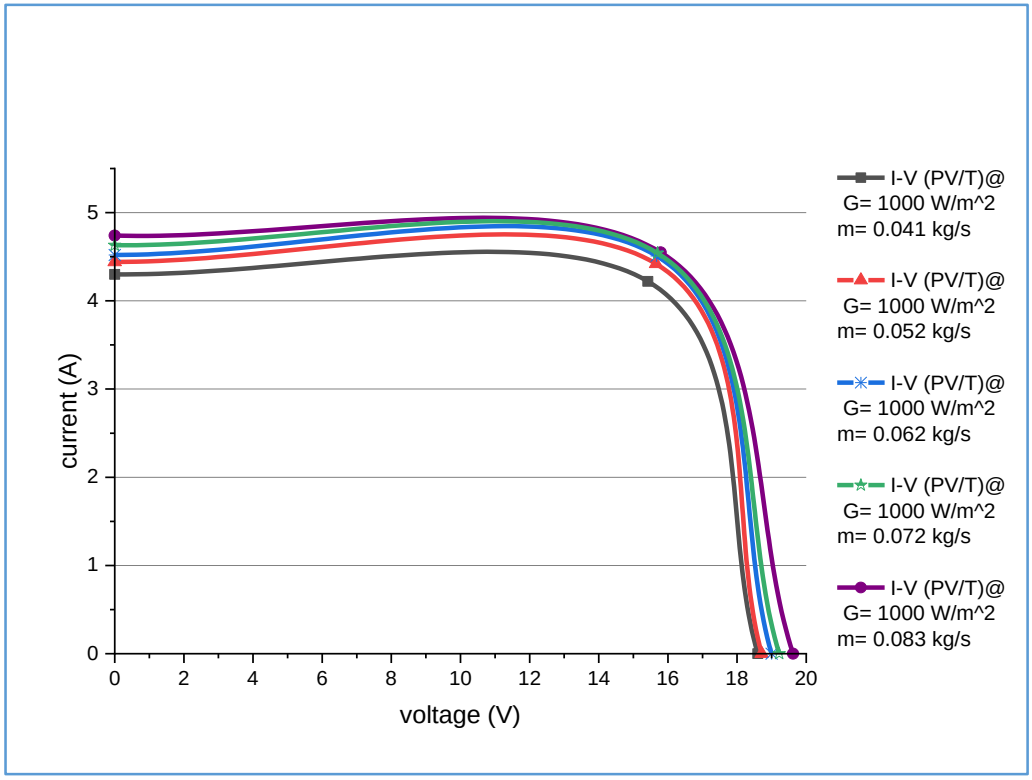

Figure (5.22) I-V curve of the PV/T system with the change in the mass flow rate at solar flux 1000 W/m^2 .

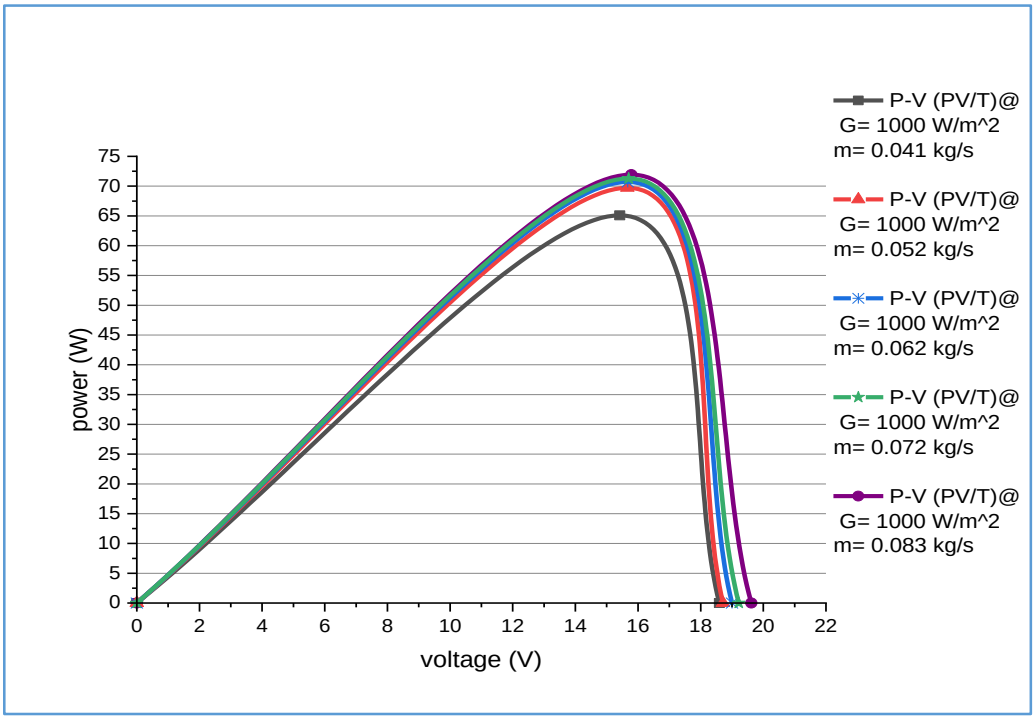

Figure (5.23) P-V curve of the PV/T system with the change in the mass flow rate at solar flux 1000 W/m^2 .

5.3.3.3 Maximum Power (P*max*) of the PV/T Air System at Different Solar Flux.

The *Pmax* of the PV/T system is clearly shown in Figure (5.24), where it can be observed that the increases with increasing solar radiation compared to the conventional PV panel.

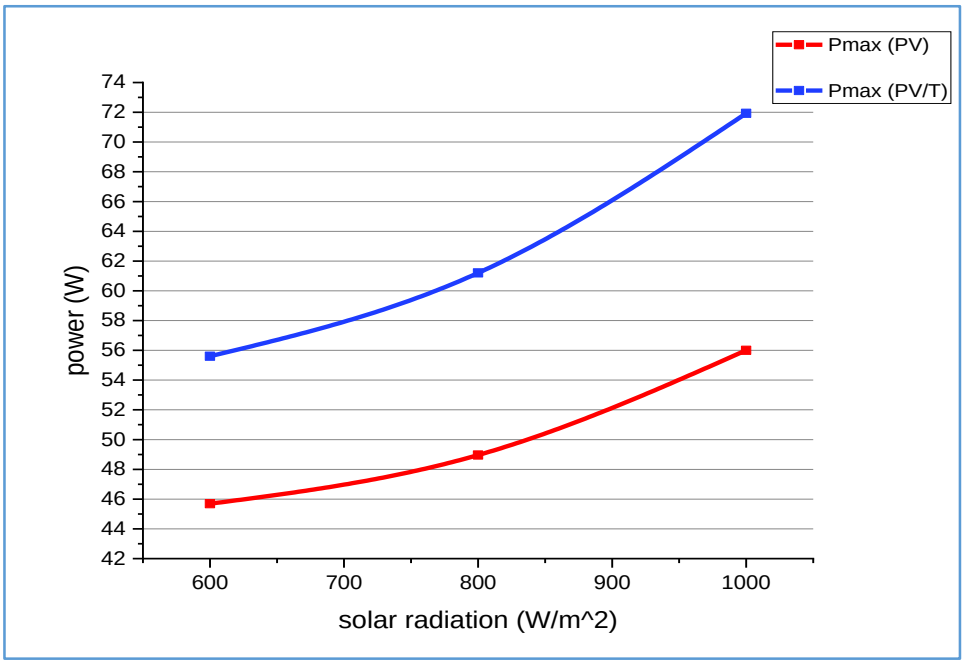

Figure (5.24) Comparison of the power PV/T system at a flow rate of (0.08) kg/s with the conventional PV panel for different solar flux.

5.3.3.4 Pmax for Different Solar Cell Temperatures (T_{PV}) of the PV/T System

The total *Pmax* is affected by the increase in the (T_{PV}), as shown in Figure (5.25). In this test, a PV/T system (Pmax) dropped from (71.93)W to (65.08)W at a mass flow rate of (0.04- 0.08)kg/s.

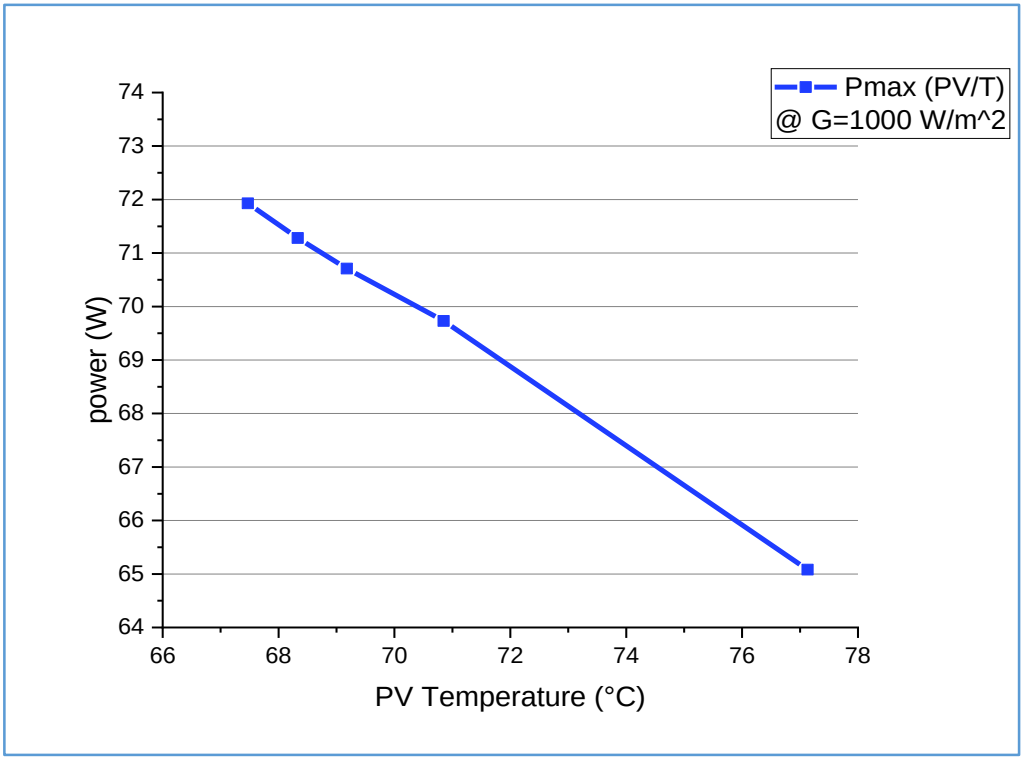

Figure (5.25) TPV-Power curve of the PV/T system with the change in the mass flow rate at solar flux 1000 W/m^2.

5.3.4 Efficiency and Performance of the PV/T Air System

Electrical and thermal parameters affect the performance and efficiency of PV/T systems. Mathematical relations were applied to the theoritical and experimental design of the PV/T system, and the traditional PV panel we obtained the electrical and thermal efficiency. The test was carried out under indoor conditions according to solar flux, the mass flow rate at different rates, and constant ambient temperature.

5.3.4.1 The Effect of Fan Speed on the Electric Power Consumption Rate

It was clearly shown through the experimental readings of the PV/T air system that the fan speed is directly proportional to the rate of energy consumption, which means that the higher the speed, the greater the rate of consumption. Its readings were recorded at a range of (2- 4) m/s opposite of (4.24 -11.31)W, respectively, as shown in Figure (5.26)

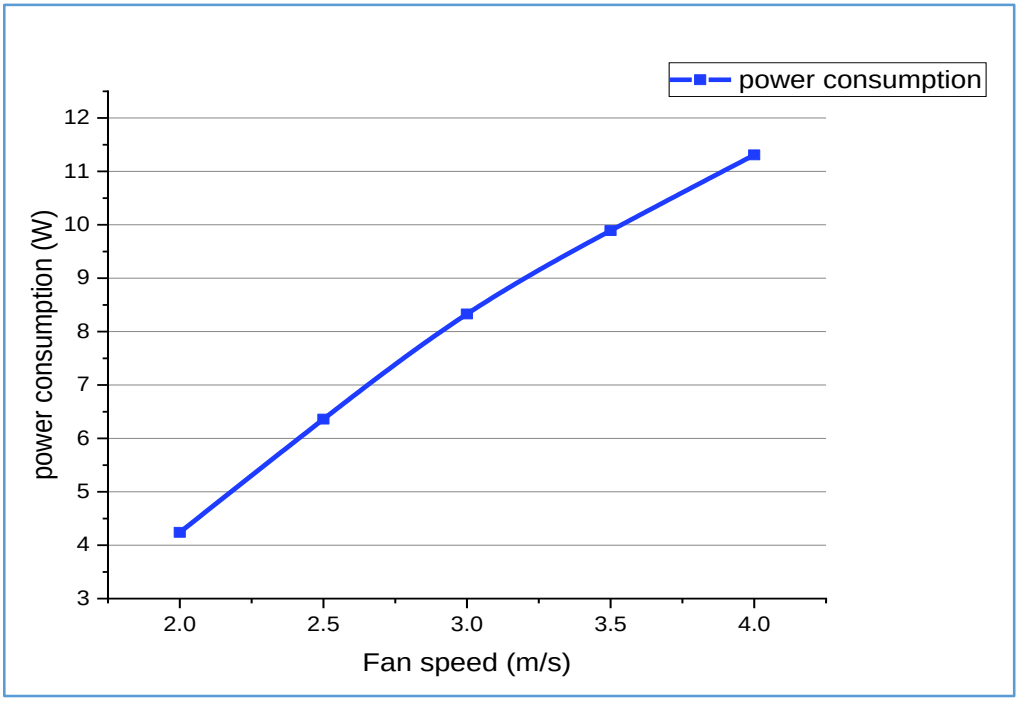

Figure (5.26) Variation of fan speed and power consumption rate.

5.3.4.2 The Effect of Pressure Drop on the Average Fan Speed

Pressure is an important factor in the performance of PV/T air systems. It has a positive effect whenever the pressure gradient between the inlet and outlet of the air is of a small value, its experimental readings are recorded at a range of (20 - 90)Pa, at varying speeds and constant solar flux (1000)W/m^2, as shown in Figure (5.27).

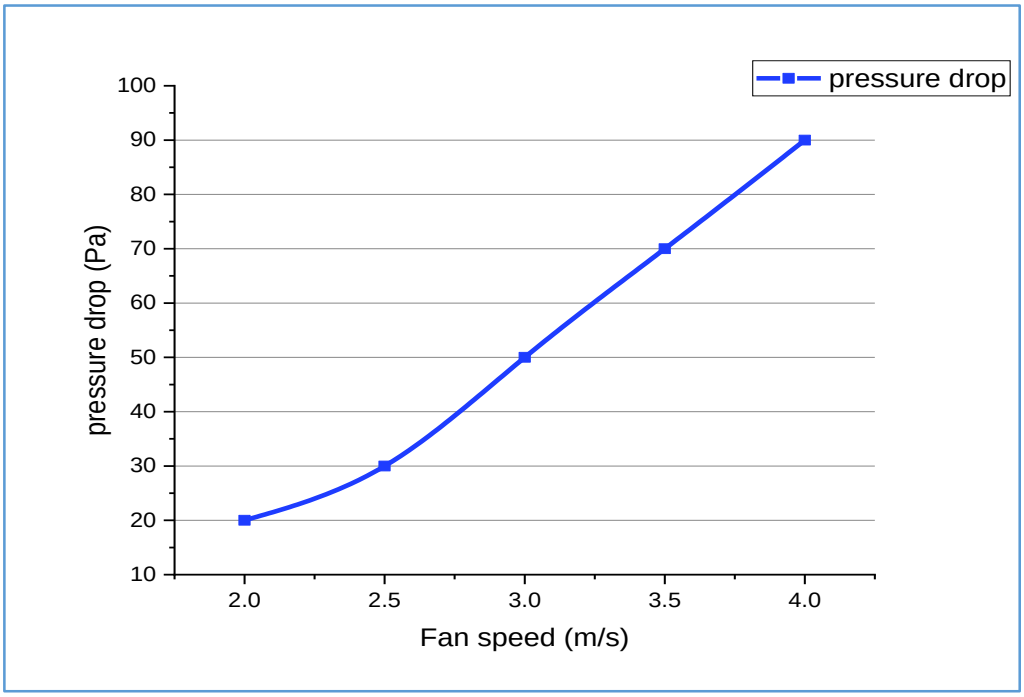

Figure (5.27) An illustration of the relation between fan speed and pressure drop.

5.3.4.3 Effect of MFR on Outlet Air Temperature (Tout) of the PV/T System

The temperature of the outlet air changes according to the flow rate in the PV/T systems so that as the flow rate increases, the temperature decreases for any level of solar flux. Figure (5.28) shows solar flux (600 W/m^2) and a mass flow rate from (0.04-0.08)kg/s The temperature decreases from (41.82-38.84)°C. Furthermore, at solar flux (1000 W/m^2) and for the same flow rates, the temperature decreases from (47.5-43.45°C). Moreover, the Figure (5.29) shows the relation of the mass flow rate with the change in temperature (Tout-Tin) under solar flux (600, 800, and 1000) W/m^2, where the results showed that when increasing (MFR), the (Tout-Tin) decreased due to the forceful flow of the fluid in the thermal accumulator.

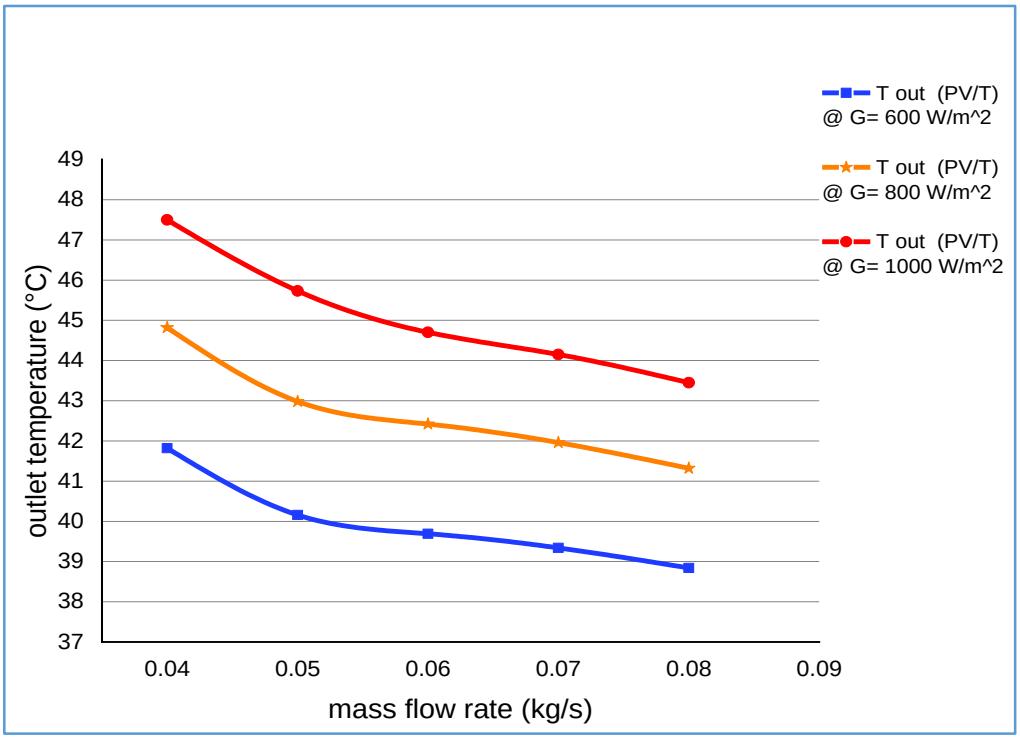

Figure (5.28) Vaiation of MFR and Tout, at different rates of solar flux.

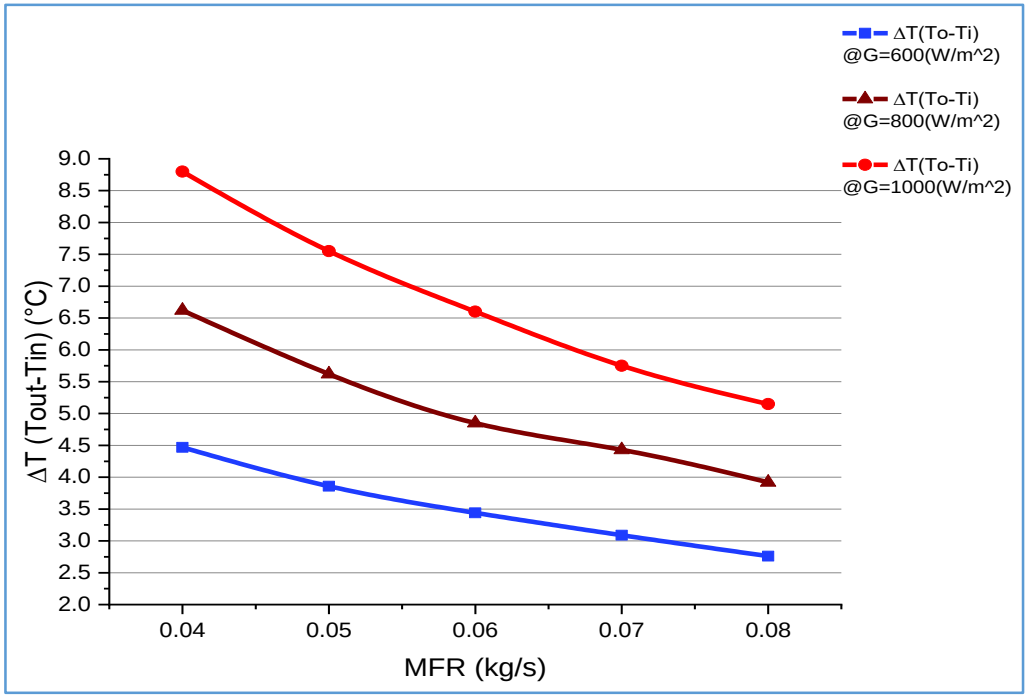

Figure (5.29) Variaton of MFR and ΔT(To-Ti), at different rates of solar flux.

5.3.4.4 Effect of MFR on PV Temperature and Efficiency.

The heat from the PV panel is absorbed by the air passing below the PV panel through the multi-flow channels in the pre-designed thermal collector and thus will affect the cooling of the PV panel unevenly due to the change in the mass flow rate inside the multi-channel collector of the PV/T system, according to a flow rate of (0.04-0.08) kg/s, which was applied with solar flux for the indoor test conditions, where (600, 800, and 1000)W/m^2 were chosen. The results showed that by increasing the flow rate at any solar flux level, the temperature of the PV panel decreases due to the increase in heat exchange between the heat transfer medium and the PV panel. Moreover, the Figure (5.30) shows the relation of the mass flow rate with the change in temperature (TPV-Tout) under a solar fluxs (600, 800, and 1000) W/m^2, where the results showed that when increasing (MFR), the (TPV-Tout) decreased due to the stronger air flow into the thermal accumulator.

For the PV/T system with a flow rate of (0.04-0.08) kg/s, with a solar flux of (600) W/m^2, the (T_{PV}) decreased from (62.95°C) to (58.9°C), as shown in Figure (5.31), and at the same time, the electrical efficiency increased from

(16.62%) to (17.03%) as shown in Figure (5.32). In addition, the thermal efficiency increased from (53.49)% to (65.57)% as shown in Figure (5.33). When the solar flux increased to (1000)W/m^2, for the same flow rate, the (T_{PV}) decreased from (76.13)°C to (67.47)°C, due to the strong fluid flow inside the thermal accumulator as shown in Figure (5.31). The electrical efficiency increased from (15.5)% to (16.26)% as shown in Figure (5.32), and the thermal efficiency increased from (63.34)% to (74.14)% as shown in Figure (5.33). Furthermore, the reported overall efficiency improved the range for solar flux (600, and 1000)W/m^2 are (70.11-82.6)%, and (78.84-90.4)%, respectively, as illustrated in Figure (5.34).

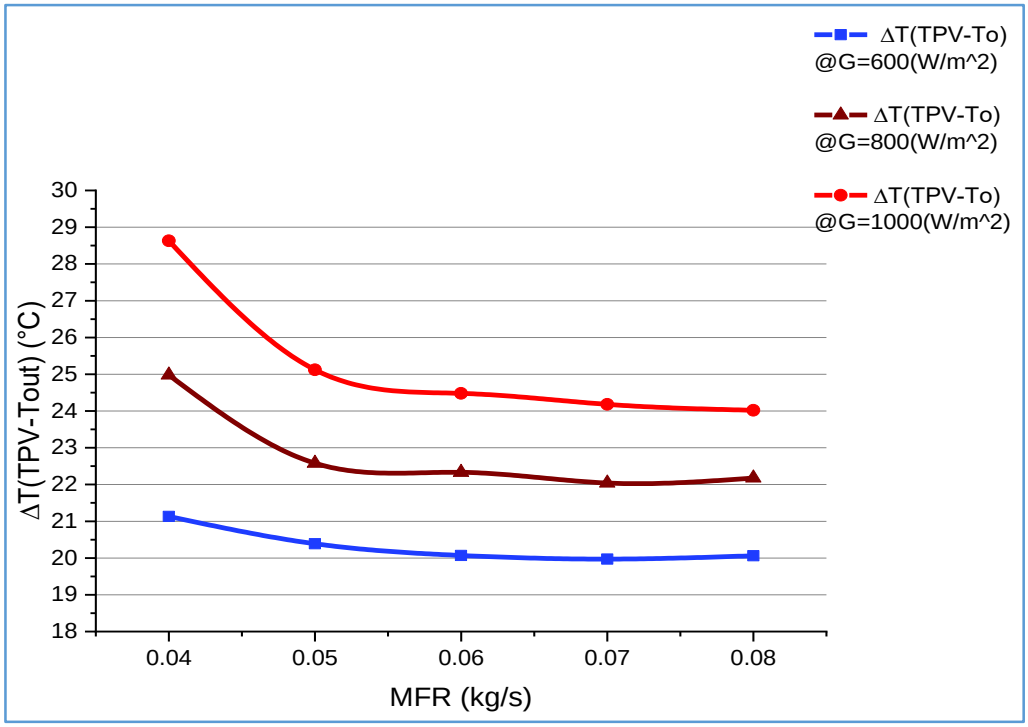

Figure (5.30) Variaton of MFR and ΔT(TPV-Tout), at different rates of solar flux.

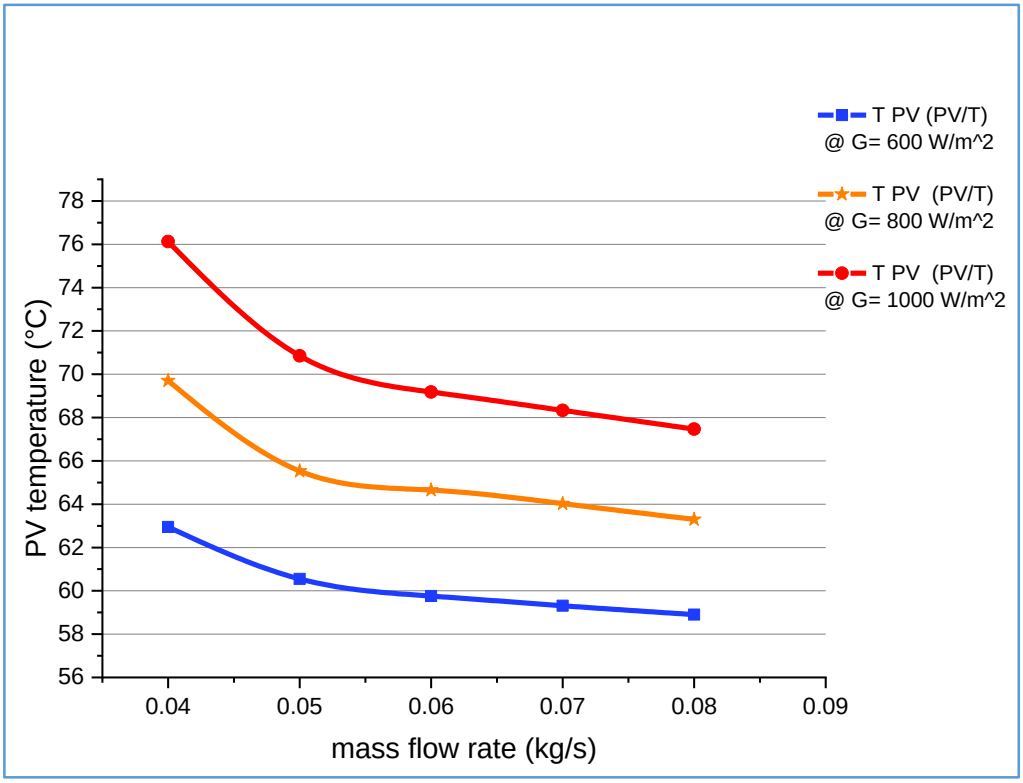

Figure (5.31) Variation of MFR and Tpv, at different rates of solar flux.

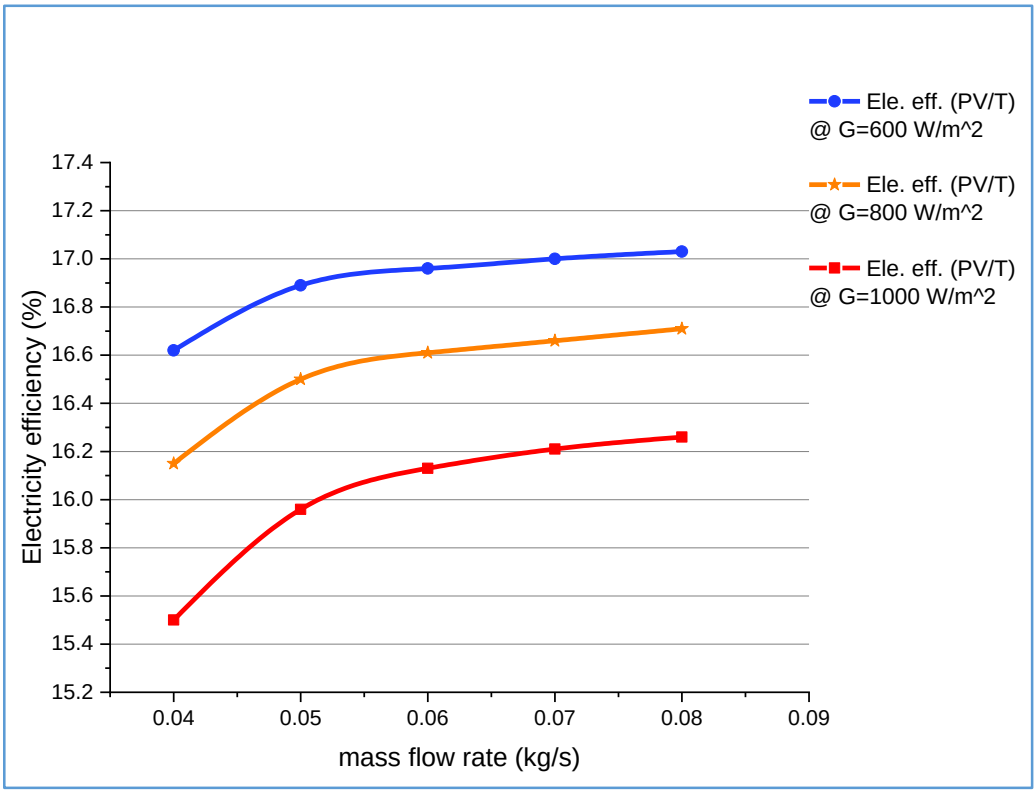

Figure (5.32) Variation of MFR and electrical efficiency, at different rates of solar flux.

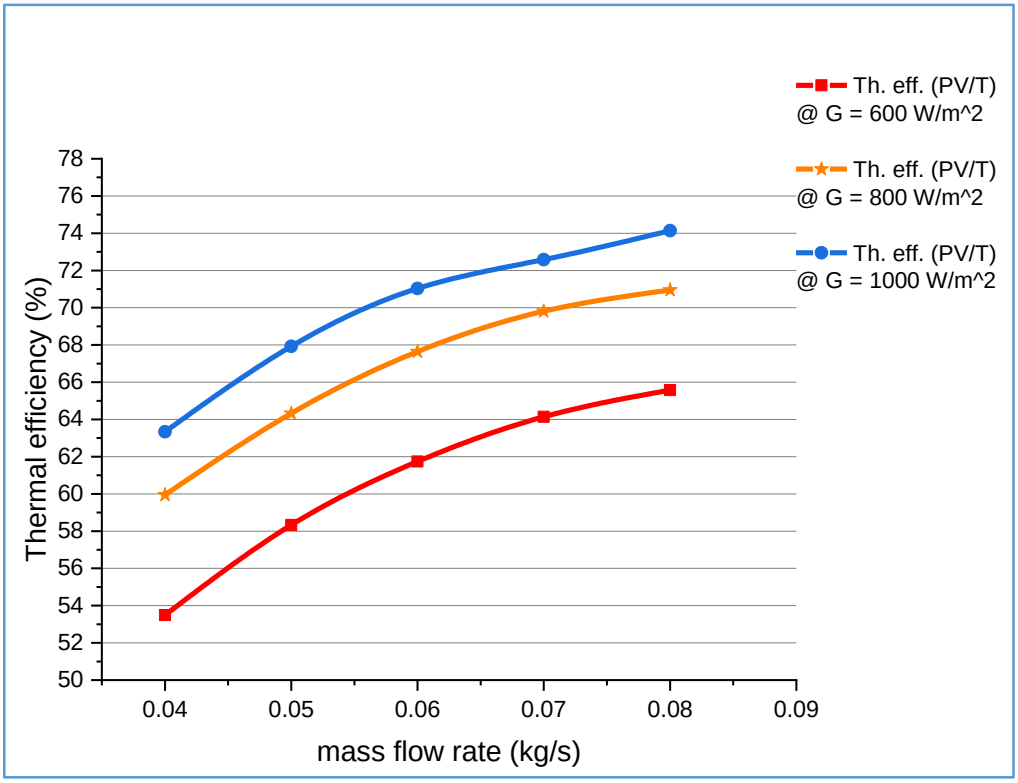

Figure (5.33) Variation of MFR and thermal efficiency, at different rates of solar flux.

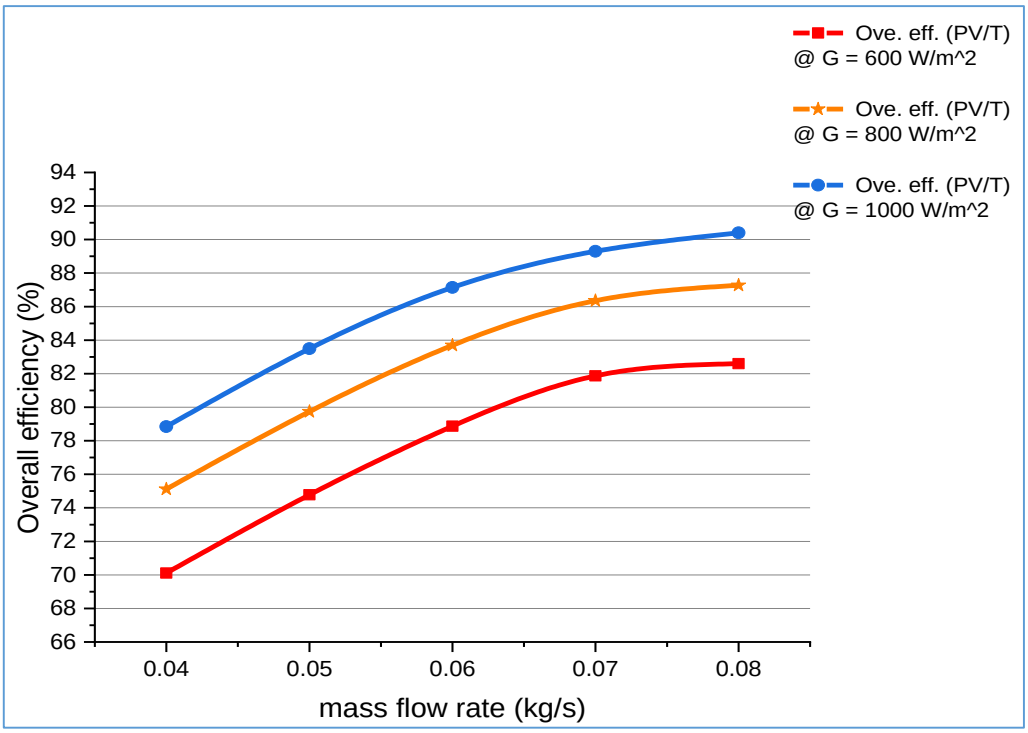

Figure (5.34) Variation of MFR and overall efficiency at various solar flux rates.

5.3.4.5 Effect of MFR on the Useful energy (Qu)

Figure (5.35) shows the relation between change of the MFR and useful heat, under solar flux (600, 800, and 1000)W/m^2, the results inducated The thermal

gain is directly proportional to the mass flow rate and solar flux, due to the strong fluid flow and the radiation behavior of the heat.

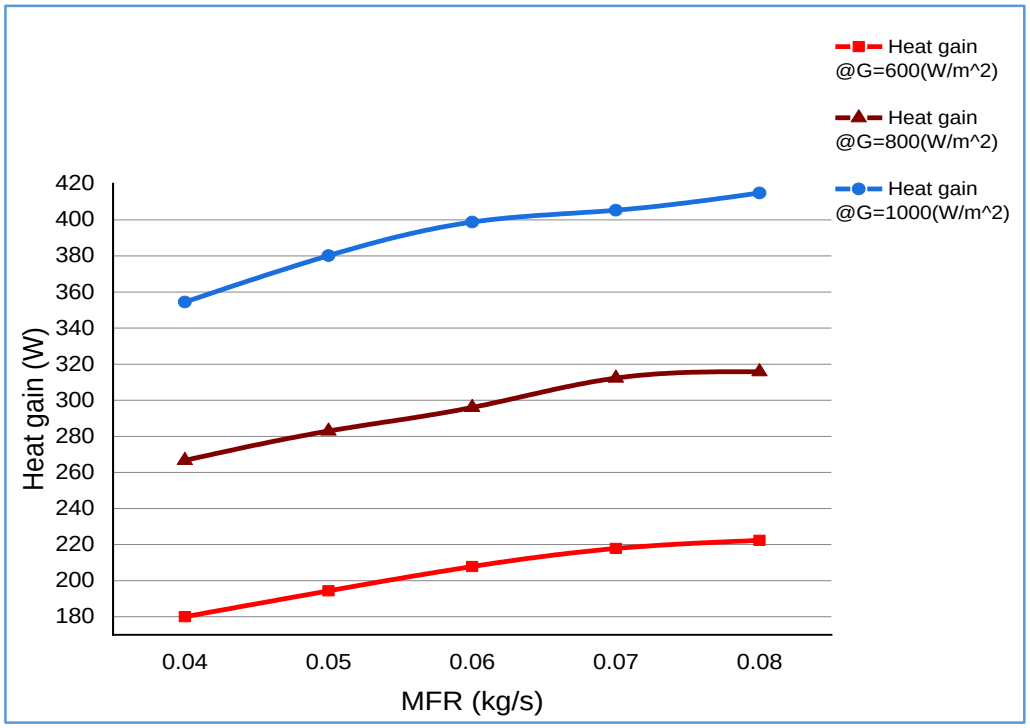

Figure (5.35) variation of MFR and heat gain, at different rates of solar flux.

5.3.4.6 Effect of (*Tout*) on the Thermal Efficiency

Increasing the MFR lowers temperatures, as more mass flow rate is available to draw heat from the channel walls thus reducing the outlet temperature. Figure (5.36) shows the thermal efficiency versus outlet temperature under the solar flux (1000)W/m^2, for a multi-flow PV/T collector, we note that there is an inverse proportion between them at constant solar flux, because temperature decrease when the mass flow rate increases under air high speed.

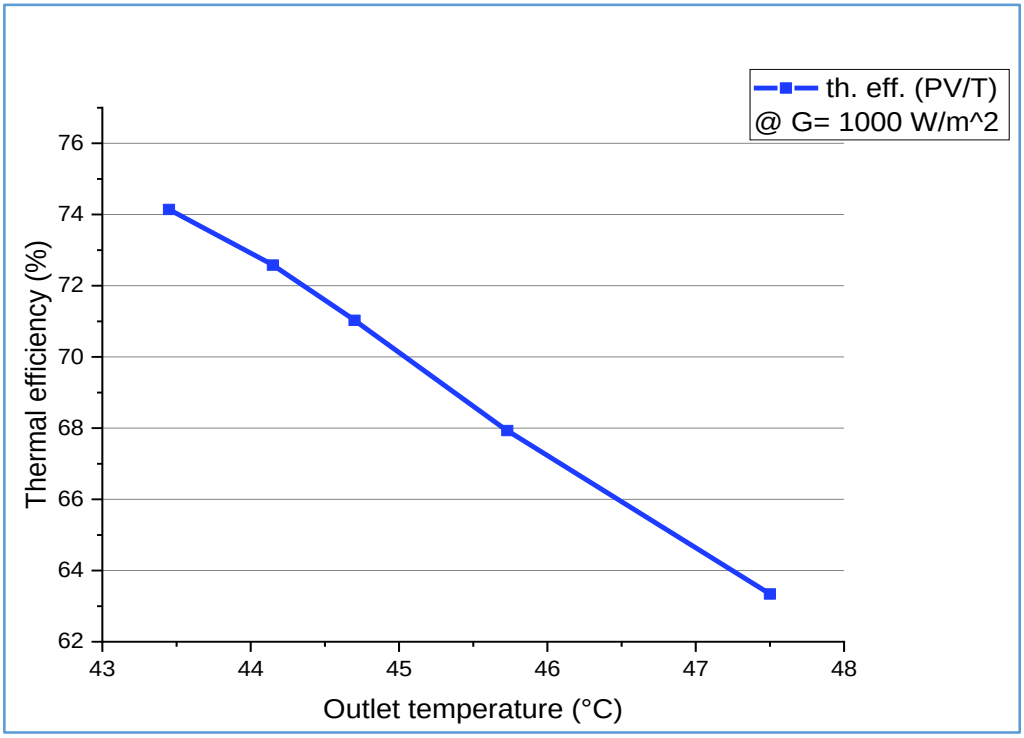

Figure (5.36) Thermal efficiency vs outlet temperature at a solar flux (1000) W/m^2.

5.3.4.7 Effect of (T_{PV}) on Electrical Efficiency

The electrical efficiency depends on the amount of solar flux falling on the surface of the PV cell. The higher the radiation intensity, the higher the efficiency. However, there is an important factor, which is the temperature, as it increases with the increase in solar flux, which negatively affects electrical efficiency. Figure (5.37) shows the relation between electrical efficiency vs. (T_{PV}), for a multi-flow channel PV/T system, with constant solar flux.

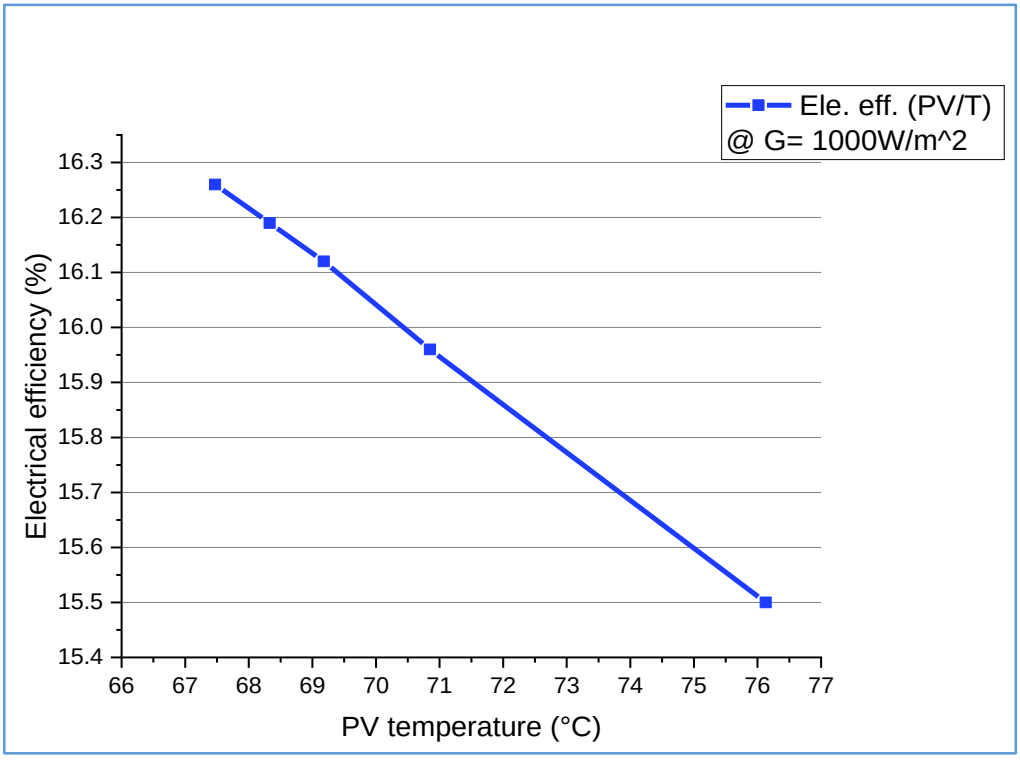

Figure (5.37) Electrical efficiency vs (TPV) at solar flux (1000)W/m^2.

5.4 The Performance of the PV/T Air System

The performance of the PV/T system can be demonstrated by the effectiveness of the multi-flow channel collector. This is known by the amount of increase in the electrical efficiency of the PV panel to evaluate the overall performance of the system. Based on the tests that have been carried out, it has been shown that electrical efficiency increases when the mass flow rate increases with the same intensity of solar flux. Figure (5.38) shows the variation of the electrical efficiency in the PV/T system when the flow rate was (0.08) kg/s and the traditional PV panel at different solar flux. The results showed that the electrical efficiency of the PV/T system ranged between (16.26-17.03)%, while the electricity efficiency of a conventional PV panel without cooling ranged between (14.51-15.65)%.

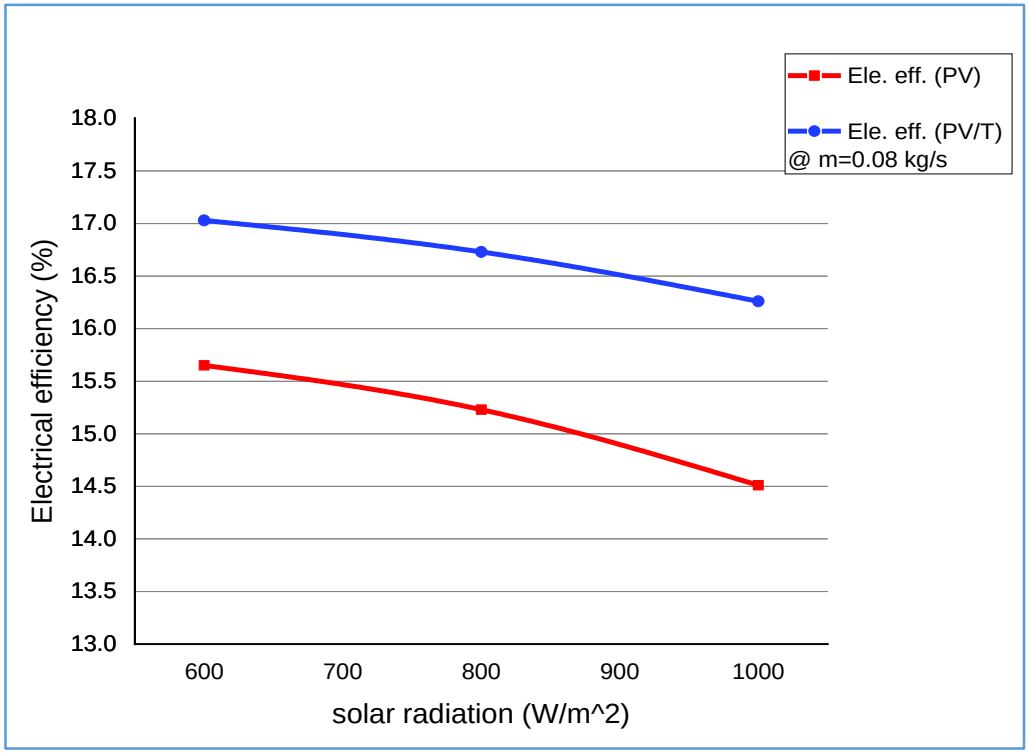

Figure (5.38) variation of solar flux and electrical efficiency, at MFR (0.08)kg/s.

5.5 Experimental and Numerical Simulations Validation, and Comparison with Previous Studies

It is very important to make a comparison between numerical and experimental results to verify the validity of the experimental work and to indicate the percentage of error between them, as well as compare with previous studies, by taking the effect of the mass flow rate on the outlet temperature of the PV/T system under solar flux constant. The temperature of the air outlet in the PV/T system cooling process is shown in Figure (5.39), at a variable air mass flow rate and constant solar flux, the temperatures decreased with increasing flow rate. The percentage error between experimental and numerical results was (1.576%).

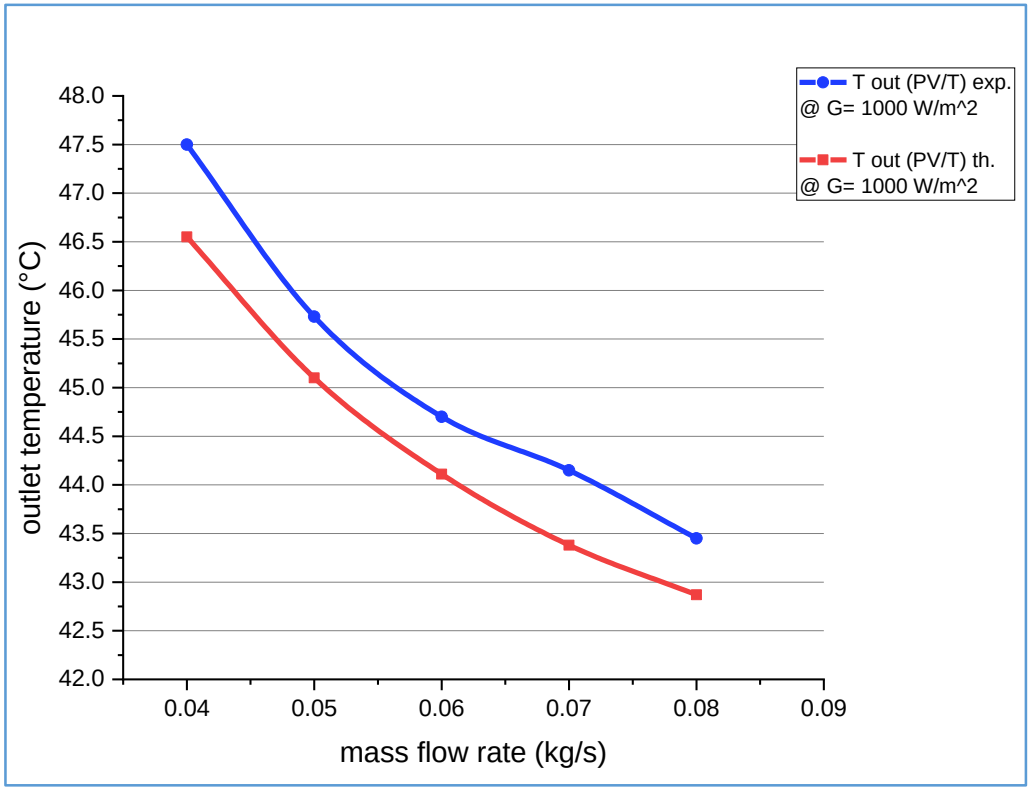

Figure (5.39) outlet air temperature versus MFR of the theoretical and experimental validation results.

Supporting the results of this study with the most important previous studies on the subject of research is necessary to compare them as shown in Table (5-2). The use of multi-flow channel technology to direct air toward the base of the PV module has a significant role in reducing the temperature of the base and thus increasing the electrical power generated by eliminating a large amount of heat that can be used in several applications.

Table (5-2) comparison of the present results with previous studies

Author	Solar thermal system	Reduction of the cell temperature (°C)	Percentage increase in cell performance (%)
Rakesh Kumar, Marc A. Rosen [2011], [74]	Solar PV/T air collector double pass with and without fins	(16)	Increase electrical efficiency (4.8)
R. Mazón-Hernández et al, [2013], [75]	Improving the electrical performance of the PV panel by induced or forced airflow	(15)	Increase in output power (15)
Hussein M. Maghrabie et al, [2017], [76]	Improvement of PV cell performance by active air cooling system	(5)	Increase in output power (4.4)
Fudholi Ahmad et al [2017], [25]	Energy and exergy analyses of the PV/T complex with ∇-groove	More than (25)	Increase electrical efficiency by more than (2.7)
Haidar Zeyad A Orfi et al, [2018], [77]	Experimental investigation of evaporative cooling to enhance the efficiency of PV panels	More than (20)	Increase in output power (10-14)
Mohsin Ahmed et al, [2019], [78]	New technology (guide air) to cool the PV module with forced air	(22.278)	Increase in output power (14.88)
Ridwone Hossain et al, [2020], [31]	New design of hybrid PV/T system to improve PV cell performance	(Tout- Tin) = more than (4)	Increase in output power (5.4)
Present study	Enhancement of performance PV/T air system by using multi-flow channels	(19.53)	Increase in output power (28.44) Increase electrical efficiency (2.52)

Chapter Six

Conclusions & Recommendations

CHAPTER SIX

CONCLUSION AND RECOMMENDATIONS

6.1 Conclusions:

The conclusions based on the theoretical and experimental results are summarized as follows:

1- The PV/T system with multi-flow transverse fins achieved the best results among other models.

2- The increased mass flow rate led to a reduction in the PV temperature, and improved electrical performance.

3- The percentage of the decrease in the PV temperature at the mass flow rate (0.08 kg/s) is (28.94%), and the maximum PV temperature reduction is about (19.53°C).

4- Maximum electrical and thermal efficiency at mass flow rate (0.08 kg/s) are (17.03%), and (74.14%), respectively.

5- Maximum overall efficiency is (90.4%). at a solar flux rate (1000W/m^2), and MFR (0.08 kg/s).

6- The maximum heat gain is (414.884W), at a solar flux rate (1000W/m^2), and MFR (0.08 kg/s).

7- The percentage increase in the maximum power of the PV module after the cooling process is (28.44%).

8- The best net electrical power added to the production of the PV module is (7.37W), recorded at (MFR) of (0.05 kg/s), and solar flux (1000 W/m^2).

9- Validation numerical model results agree with the experimental data at an approximate error (1.576%).

6.2 Recommendations for the Future Work

We can summarize the recommendations with several suggestions for future work related to the topic of this thesis:

1- Studying the geometry shape effect of airflow channels on PV/T system.
2- Investigating the different absorbent surfaces (V-grooved, corrugated, and trapezoidal) influence on the PV/T system.
3- Using the method of spraying water on the surface of the PV module in addition to the basic method (multi-flow channels) to enhance the heat exchange and clean the PV module.

References

References

[1] J. Dominguez, *Soteris_A._Kalogirou_Auth.-Solar_Energy_Engineering._Processes_and_Systems-Academic_Press_2014-with-cover-page-v2.pdf*. 2014.

[2] D. M. H. Al-Hasnawi, A. A. Abdullah, and F. Kamil, "Novel Technique for Photovoltaic Solar Cell Efficiency Enhancements by Coating with Chlorophyll," *J. Phys. Conf. Ser.*, vol. 1032, no. 1, 2018, doi: 10.1088/1742-6596/1032/1/012023.

[3] H. S. Khwayyir, A. S. Baqir, and H. Q. Mohammed, "Effect of air bubble injection on the thermal performance of a flat plate solar collector," *Therm. Sci. Eng. Prog.*, vol. 17, no. May 2021, p. 100476, 2020, doi: 10.1016/j.tsep.2019.100476.

[4] F. Kamil, "IMPROVEMENT THE PERFORMANCE OF (NITRO CELLULOSE) AND BLUE VICTORIA," no. November, 2018.

[5] H. B. Mahood, A. N. Campbell, A. S. Baqir, A. O. Sharif, and R. B. Thorpe, "Convective heat transfer measurements in a vapour-liquid-liquid three-phase direct contact heat exchanger," *Heat Mass Transf. und Stoffuebertragung*, vol. 54, no. 6, pp. 1697–1705, 2018, doi: 10.1007/s00231-017-2260-8.

[6] "picture solar energy." https://commons.wikimedia.org/wiki/Category:Insolation_maps_of_Iraq#/media/File:Iraq_DNI_Solar-resource-map_GlobalSolarAtlas_World-Bank-Esmap-Solargis.png

[7] J. A. Duffie, W. A. Beckman, and J. McGowan, *Solar Engineering of Thermal Processes* , vol. 53, no. 4. 1985. doi: 10.1119/1.14178.

[8] C. Chalkias, A. Faka, and K. Kalogeropoulos, "Assessment of the Direct Sun-Light on Rural Road Network through Solar Radiation Analysis Using GIS," *Open J. Appl. Sci.*, vol. 3, pp. 224–231, Jun. 2013, doi: 10.4236/ojapps.2013.32030.

[9] M. A. A. Mamun, M. M. Islam, M. Hasanuzzaman, and J. Selvaraj, "Effect of tilt angle on the performance and electrical parameters of a PV module: Comparative indoor and outdoor experimental investigation," *Energy Built Environ.*, vol. 3, no. 3, pp. 278–290, 2022, doi: 10.1016/j.enbenv.2021.02.001.

[10] H. Shahid, M. Kamran, Z. Mehmood, M. Y. Saleem, M. Mudassar, and K. Haider, "Implementation of the novel temperature controller and incremental conductance MPPT algorithm for indoor photovoltaic system," *Sol. Energy*, vol. 163, no. January, pp. 235–242, 2018, doi: 10.1016/j.solener.2018.02.018.

[11] S. T. Branch, "Solar Energy Application," vol. 1, pp. 2020–2021, 2021.

[12] L. Idoko, O. Anaya-Lara, and A. McDonald, "Enhancing PV modules efficiency and power output using multi-concept cooling technique," *Energy Reports*, vol. 4, pp. 357–369, 2018, doi:

10.1016/j.egyr.2018.05.004.
[13] K. I. Ishibashi, Y. Kimura, and M. Niwano, "An extensively valid and stable method for derivation of all parameters of a solar cell from a single current-voltage characteristic," *J. Appl. Phys.*, vol. 103, no. 9, pp. 1–7, 2008, doi: 10.1063/1.2895396.
[14] A. R. Jordehi, "Parameter estimation of solar photovoltaic (PV) cells: A review," *Renew. Sustain. Energy Rev.*, vol. 61, pp. 354–371, 2016, doi: 10.1016/j.rser.2016.03.049.
[15] M. Sucurovic, M. Bozic, and S. Dragicevic, "Educational set up for measurement of photovoltaic modul electrical parameters," no. January 2017, 2016.
[16] X. Zhang, X. Zhao, S. Smith, J. Xu, and X. Yu, "Review of R&D progress and practical application of the solar photovoltaic/thermal (PV/T) technologies," *Renew. Sustain. Energy Rev.*, vol. 16, no. 1, pp. 599–617, 2012.
[17] A. Palumbo, "Design and analysis of cooling methods for solar panels." 2013.
[18] S. M. Salih, J. M. Jalil, and S. E. Najim, "Experimental and numerical analysis of double-pass solar air heater utilizing multiple capsules PCM," *Renew. Energy*, vol. 143, pp. 1053–1066, 2019, doi: 10.1016/j.renene.2019.05.050.
[19] M. Gholampour and M. Ameri, "Energy and exergy analyses of Photovoltaic/Thermal flat transpired collectors: Experimental and theoretical study," *Appl. Energy*, vol. 164, pp. 837–856, 2016, doi: 10.1016/j.apenergy.2015.12.042.
[20] A. M. Elsafi and P. Gandhidasan, "Comparative study of double-pass flat and compound parabolic concentrated photovoltaic-thermal systems with and without fins," *Energy Convers. Manag.*, vol. 98, pp. 59–68, 2015, doi: 10.1016/j.enconman.2015.03.084.
[21] J. H. Kim, J. G. Ahn, and J. T. Kim, "Demonstration of the performance of an air-type photovoltaic thermal (PVT) system coupled with a heat-recovery ventilator," *Energies*, vol. 9, no. 9, 2016, doi: 10.3390/en9090728.
[22] S. Singh, S. Agrawal, and D. V. Avasthi, "Design, modeling and performance analysis of dual channel semitransparent photovoltaic thermal hybrid module in the cold environment," *Energy Convers. Manag.*, vol. 114, pp. 241–250, 2016, doi: 10.1016/j.enconman.2016.02.023.
[23] M. E. A. Slimani, M. Amirat, I. Kurucz, S. Bahria, A. Hamidat, and W. B. Chaouch, "A detailed thermal-electrical model of three photovoltaic/thermal (PV/T) hybrid air collectors and photovoltaic (PV) module: Comparative study under Algiers climatic conditions," *Energy Convers. Manag.*, vol. 133, pp. 458–476, 2017, doi: 10.1016/j.enconman.2016.10.066.

[24] Shyam and G. N. Tiwari, "Analysis of series connected photovoltaic thermal air collectors partially covered by semitransparent photovoltaic module," *Sol. Energy*, vol. 137, pp. 452–462, 2016, doi: 10.1016/j.solener.2016.08.052.

[25] A. Fudholi *et al.*, "Energy and exergy analyses of photovoltaic thermal collector with∇-groove," *Sol. Energy*, vol. 159, no. November 2016, pp. 742–750, 2018, doi: 10.1016/j.solener.2017.11.056.

[26] A. Fudholi *et al.*, "Exergy and sustainability index of photovoltaic thermal (PVT) air collector: A theoretical and experimental study," *Renew. Sustain. Energy Rev.*, vol. 100, no. July 2018, pp. 44–51, 2019, doi: 10.1016/j.rser.2018.10.019.

[27] A. M. Alsayah, M. H. K. Aboaltabooq, M. H. Majeed, and B. A. S. Bassam Abed, "CFD study to improve PV cell performance by forced air: Modern design," *Period. Eng. Nat. Sci.*, vol. 7, no. 3, pp. 1468–1477, 2019, doi: 10.21533/pen.v7i3.794.

[28] S. Y. Wu, T. Wang, L. Xiao, and Z. G. Shen, "Effect of cooling channel position on heat transfer characteristics and thermoelectric performance of air-cooled PV/T system," *Sol. Energy*, vol. 180, no. December 2018, pp. 489–500, 2019, doi: 10.1016/j.solener.2019.01.043.

[29] A. Hosseini Rad, H. Ghadamian, H. R. Haghgou, and F. Sarhaddi, "Energy and Exergy Evaluation of Multi-channel Photovoltaic/Thermal Hybrid System: Simulation and experiment," *Int. J. Eng. Trans. B Appl.*, vol. 32, no. 11, pp. 1665–1680, 2019, doi: 10.5829/ije.2019.32.11a.18.

[30] J. Hu and G. Zhang, "Performance improvement of solar air collector based on airflow reorganization: A review," *Appl. Therm. Eng.*, vol. 155, pp. 592–611, 2019, doi: 10.1016/j.applthermaleng.2019.04.021.

[31] R. Hossain *et al.*, "New Design of Solar Photovoltaic and Thermal Hybrid System for Performance Improvement of Solar Photovoltaic," *Int. J. Photoenergy*, vol. 2020, no. 1, 2020, doi: 10.1155/2020/8825489.

[32] Y. Zhao, T. Meng, C. Jing, J. Hu, and S. Qian, "Experimental and numerical investigation on thermal performance of PV-driven aluminium honeycomb solar air collector," *Sol. Energy*, vol. 204, no. June 2019, pp. 294–306, 2020, doi: 10.1016/j.solener.2020.04.047.

[33] H. U. Choi and K. H. Choi, "Performance evaluation of PV/T air collector having a single-pass double-flow air channel and non-uniform cross-section transverse rib," *Energies*, vol. 13, no. 9, 2020, doi: 10.3390/en13092203.

[34] I. Baklouti and Z. Driss, "Numerical and Experimental Study of the Impact of Key Parameters on a PVT Air Collector: Mass Flow Rate and Duct Depth," *J. Therm. Sci.*, vol. 30, no. 5, pp. 1625–1642, 2021, doi: 10.1007/s11630-020-1345-8.

[35] A. Elnozahy, A. K. A. Rahman, A. H. H. Ali, M. Abdel-Salam, and S. Ookawara, "Performance of a PV module integrated with standalone building in hot arid areas as enhanced by surface cooling and cleaning,"

Energy Build., vol. 88, pp. 100–109, 2015, doi: 10.1016/j.enbuild.2014.12.012.

[36] K. Yang and C. Zuo, "A novel multi-layer manifold microchannel cooling system for concentrating photovoltaic cells," *Energy Convers. Manag.*, vol. 89, pp. 214–221, 2015, doi: 10.1016/j.enconman.2014.09.046.

[37] A. A. B. Baloch, H. M. S. Bahaidarah, P. Gandhidasan, and F. A. Al-Sulaiman, "Experimental and numerical performance analysis of a converging channel heat exchanger for PV cooling," *Energy Convers. Manag.*, vol. 103, pp. 14–27, 2015, doi: 10.1016/j.enconman.2015.06.018.

[38] D. Su, Y. Jia, X. Huang, G. Alva, Y. Tang, and G. Fang, "Dynamic performance analysis of photovoltaic-thermal solar collector with dual channels for different fluids," *Energy Convers. Manag.*, vol. 120, pp. 13–24, 2016, doi: 10.1016/j.enconman.2016.04.095.

[39] Y. Khanjari, F. Pourfayaz, and A. B. Kasaeian, "Numerical investigation on using of nanofluid in a water-cooled photovoltaic thermal system," *Energy Convers. Manag.*, vol. 122, pp. 263–278, 2016, doi: 10.1016/j.enconman.2016.05.083.

[40] F. Yazdanifard, E. Ebrahimnia-Bajestan, and M. Ameri, "Investigating the performance of a water-based photovoltaic/thermal (PV/T) collector in laminar and turbulent flow regime," *Renew. Energy*, vol. 99, pp. 295–306, 2016, doi: 10.1016/j.renene.2016.07.004.

[41] M. S. Y. Ebaid, A. M. Ghrair, and M. Al-Busoul, "Experimental investigation of cooling photovoltaic (PV) panels using (TiO2) nanofluid in water -polyethylene glycol mixture and (Al2O3) nanofluid in water- cetyltrimethylammonium bromide mixture," *Energy Convers. Manag.*, vol. 155, no. October 2017, pp. 324–343, 2018, doi: 10.1016/j.enconman.2017.10.074.

[42] F. Yazdanifard, M. Ameri, and E. Ebrahimnia-Bajestan, "Performance of nanofluid-based photovoltaic/thermal systems: A review," *Renew. Sustain. Energy Rev.*, vol. 76, no. May 2016, pp. 323–352, 2017, doi: 10.1016/j.rser.2017.03.025.

[43] H. Fayaz, R. Nasrin, N. A. Rahim, and M. Hasanuzzaman, "Energy and exergy analysis of the PVT system: Effect of nanofluid flow rate," *Sol. Energy*, vol. 169, no. May, pp. 217–230, 2018, doi: 10.1016/j.solener.2018.05.004.

[44] A. Fudholi *et al.*, "TiO2/water-based photovoltaic thermal (PVT) collector: Novel theoretical approach," *Energy*, vol. 183, pp. 305–314, 2019, doi: 10.1016/j.energy.2019.06.143.

[45] S. G. H. and G. H. L. Joo Hee Lee, "Efficiency Improvement of a Photovoltaic Thermal," *Energy*, 2019.

[46] A. Radwan *et al.*, "Development of a new vacuum-based photovoltaic/thermal collector, and its thermal and exergy analyses,"

Sustain. Energy Fuels, vol. 4, no. 12, pp. 6251–6273, 2020, doi: 10.1039/d0se01102a.

[47] Y. Zhang, C. Shen, C. Zhang, J. Pu, Q. Yang, and C. Sun, "A novel porous channel to optimize the cooling performance of PV modules," *Energy Built Environ.*, vol. 3, no. 2, pp. 210–225, 2022, doi: 10.1016/j.enbenv.2021.01.003.

[48] Y. Cao, E. Kamrani, S. Mirzaei, A. Khandakar, and B. Vaferi, "Electrical efficiency of the photovoltaic/thermal collectors cooled by nanofluids: Machine learning simulation and optimization by evolutionary algorithm," *Energy Reports*, vol. 8, pp. 24–36, 2022, doi: 10.1016/j.egyr.2021.11.252.

[49] E. M. Abo-Zahhad *et al.*, "A new fusion-edge sealed vacuum for concentrated photovoltaic/thermal solar collector in comparison to a conventional system," *Case Stud. Therm. Eng.*, vol. 34, no. March, p. 102003, 2022, doi: 10.1016/j.csite.2022.102003.

[50] M. N. Abu Bakar, M. Othman, M. Hj Din, N. A. Manaf, and H. Jarimi, "Design concept and mathematical model of a bi-fluid photovoltaic/thermal (PV/T) solar collector," *Renew. Energy*, vol. 67, pp. 153–164, 2014, doi: 10.1016/j.renene.2013.11.052.

[51] J. Ji, C. Guo, W. Sun, W. He, Y. Wang, and G. Li, "Experimental investigation of tri-functional photovoltaic/thermal solar collector," *Energy Convers. Manag.*, vol. 88, pp. 650–656, 2014, doi: 10.1016/j.enconman.2014.09.030.

[52] H. Jarimi, M. N. Abu Bakar, M. Othman, and M. H. Din, "Bi-fluid photovoltaic/thermal (PV/T) solar collector: Experimental validation of a 2-D theoretical model," *Renew. Energy*, vol. 85, pp. 1052–1067, 2016, doi: 10.1016/j.renene.2015.07.014.

[53] M. Y. Othman, S. A. Hamid, M. A. S. Tabook, K. Sopian, M. H. Roslan, and Z. Ibarahim, "Performance analysis of PV/T Combi with water and air heating system: An experimental study," *Renew. Energy*, vol. 86, no. March, pp. 716–722, 2016, doi: 10.1016/j.renene.2015.08.061.

[54] C. Guo, J. Ji, W. Sun, J. Ma, W. He, and Y. Wang, "Numerical simulation and experimental validation of tri-functional photovoltaic/thermal solar collector," *Energy*, vol. 87, pp. 470–480, 2015, doi: 10.1016/j.energy.2015.05.017.

[55] K. Sopian *et al.*, "Performance of double pass PV/T combi solar collector with CPC: Theoretical approach," *Energy Sustain. Small Dev. Econ. ES2DE 2017 - Proc.*, 2017, doi: 10.1109/ES2DE.2017.8015345.

[56] S. S. S. Baljit *et al.*, "Mathematical modelling of a dual-fluid concentrating photovoltaic-thermal (PV-T) solar collector," *Renew. Energy*, vol. 114, pp. 1258–1271, 2017, doi: 10.1016/j.renene.2017.08.001.

[57] S. S. S. Baljit, H. Y. Chan, S. H. Zaidi, and K. Sopian, "Performance

study of a dual-fluid photovoltaic thermal collector with reflection and refraction solar concentrators," *Int. J. Low-Carbon Technol.*, vol. 15, no. 1, pp. 25–39, 2019, doi: 10.1093/ijlct/ctz054.

[58] M. Imtiaz Hussain, J. H. Kim, and J. T. Kim, "Nanofluid-powered dual-fluid photovoltaic/thermal (PV/T) system: Comparative numerical study," *Energies*, vol. 12, no. 5, 2019, doi: 10.3390/en12050775.

[59] M. I. Hussain and J. T. Kim, "Outdoor testing to compare the technical and economic aspects of single-and dual-fluid photovoltaic/thermal (PV/T) systems," *Appl. Sci.*, vol. 10, no. 16, 2020, doi: 10.3390/app10165641.

[60] T. L. Bergman, *Fundamentals of heat and mass transfer*. John Wiley & Sons, 2011.

[61] B. E. Launder and D. B. Spalding, "The numerical computation of turbulent flows," in *Numerical prediction of flow, heat transfer, turbulence and combustion*, Elsevier, 1983, pp. 96–116.

[62] H. K. Versteeg and W. Malalasekera, *An introduction to computational fluid dynamics: the finite volume method*. Pearson education, 2007.

[63] B. Lee, J. Z. Liu, B. Sun, C. Y. Shen, and G. C. Dai, "Thermally conductive and electrically insulating EVA composite encapsulant for solar photovoltaic (PV) cell," *Express Polym. Lett.*, vol. 2, no. 5, pp. 357–363, 2008, doi: 10.3144/expresspolymlett.2008.42.

[64] M. Zohri, S. Hadisaputra, and A. Fudholi, "Exergy and energy analysis of photovoltaic thermal (Pvt)with and without fins collector," *ARPN J. Eng. Appl. Sci.*, vol. 13, no. 3, pp. 803–808, 2018, [Online]. Available: https://scholar.google.com/scholar?q=Exergy+and+energy+analysis+of+photovoltaic+thermal+(Pvt)with+and+without+fins+collector&hl=ar&as_sdt=0&as_vis=1&oi=scholart

[65] K. E. Amori and H. M. Taqi Al-Najjar, "Analysis of thermal and electrical performance of a hybrid (PV/T) air based solar collector for Iraq," *Appl. Energy*, vol. 98, pp. 384–395, 2012, doi: 10.1016/j.apenergy.2012.03.061.

[66] A. Ibrahim, A. Fudholi, K. Sopian, M. Y. Othman, and M. H. Ruslan, "Efficiencies and improvement potential of building integrated photovoltaic thermal (BIPVT) system," *Energy Convers. Manag.*, vol. 77, pp. 527–534, 2014, doi: 10.1016/j.enconman.2013.10.033.

[67] S. R. Park, A. K. Pandey, V. V. Tyagi, and S. K. Tyagi, "Energy and exergy analysis of typical renewable energy systems," *Renew. Sustain. Energy Rev.*, vol. 30, pp. 105–123, 2014, doi: 10.1016/j.rser.2013.09.011.

[68] A. S. Joshi, A. Tiwari, G. N. Tiwari, I. Dincer, and B. V. Reddy, "Performance evaluation of a hybrid photovoltaic thermal (PV/T) (glass-to-glass) system," *Int. J. Therm. Sci.*, vol. 48, no. 1, pp. 154–164, 2009, doi: 10.1016/j.ijthermalsci.2008.05.001.

[69] E. Holzbecher and H. Si, "Accuracy Tests for COMSOL - and Delaunay

Meshes," *Proc. COMSOL Conf.*, no. 1, p. 7, 2008, [Online]. Available: https://www.comsol.nl/paper/accuracy-tests-for-comsol-and-delaunay-meshes-5436

[70] S. V Patankar, "Numerical heat transfer and fluid flow (Hemisphere Series on Computational Methods in Mechanics and Thermal Science; Hemisphere Publishing Corporation (CRC Press, Taylor & Francis Group): Boca Raton," *FL, USA*, 1980.

[71] A. Standard, "93-77. Methods of testing to determine the thermal performance of solar collectors. American Society of Heating," *Refrig. Air Cond. Eng. Inc., New York, NY*, vol. 9, 1977, [Online]. Available: https://webstore.ansi.org/preview-pages/ASHRAE/preview_ANSI+ASHRAE+93-2003.pdf

[72] B. S. Romdhane, "The air solar collectors: Comparative study, introduction of baffles to favor the heat transfer," *Sol. energy*, vol. 81, no. 1, pp. 139–149, 2007.

[73] S. Y. Hattam, "Experimental and Numerical Study to Improve the Performance of Solar Cell Using Water Cooling System," *Al-furat Al-awsat Tech. Univ. Eng. Tech. Coll. Najaf, Iraq*, 2022.

[74] R. Kumar and M. A. Rosen, "Performance evaluation of a double pass PV/T solar air heater with and without fins," *Appl. Therm. Eng.*, vol. 31, no. 8–9, pp. 1402–1410, 2011, doi: 10.1016/j.applthermaleng.2010.12.037.

[75] R. Mazón-Hernández, J. R. García-Cascales, F. Vera-García, A. S. Káiser, and B. Zamora, "Improving the electrical parameters of a photovoltaic panel by means of an induced or forced air stream," *Int. J. Photoenergy*, vol. 2013, 2013, doi: org/10.1155/2013/830968.

[76] H. M. Maghrabie, A. S. A. Mohamed, M. S. Ahmed, H. M. Maghrabie, and M. S. Ahmed, "Improving Performance of Photovoltaic Cells via Active Air Cooling System," in *Proc. 4th Int. Conf. Energy Eng*, 2017, pp. 1–5. [Online]. Available: https://scholar.google.com/citations?view_op=view_citation&hl=ar&user=IQkfp4sAAAAJ&citation_for_view=IQkfp4sAAAAJ:eQOLeE2rZwMC

[77] Z. A. Haidar, J. Orfi, and Z. Kaneesamkandi, "Experimental investigation of evaporative cooling for enhancing photovoltaic panels efficiency," *Results Phys.*, vol. 11, pp. 690–697, 2018, doi: org/10.1016/j.rinp.2018.10.016.

[78] A. M. Kudhair, "NUMERICAL AND EXPERIMENTAL INVESTIGATION ON IMPROVING PHOTOVOLTAIC MODULE EFFICIENCY USING AIR GUIDE COOLING," no. November 2019, 2012.

Appendixes

Appendixes

Appendix (A)

Table A.1: Specifications of the pyranometer (model SM206)

Property	Value
Resolution	0.1W/m², 0.1Btu/(ft²-h)
Range Error	±10W/m² (±3Btu/(ft²-h) or ±5% of measured value
Temperature Error	±0.38W/m²/°C ±0.12Btu/(ft²-h)/°C deviation at 25°
Display	3-3/4 LCD display, maximum 3999
Measurement Range	0.1-399.9W/m², 1-3999W/m², 0.1-399.9Btu/(ft²-h), 1-3999Btu/(ft²-h)
Sampling Time	0.25 seconds/time
Operating Temperature and Humidity	0~50℃, <80%RH
Storage Temperature and Humidity	-10~60℃, <70%RH
Battery	9V battery (NOT included)
Size	132*65*38mm / 5.2*2.6*1.5in
Weight	325g / 11.5oz (approx.)

Table A.2: Specifications of the data logger (model CKT4000)

Property	Value
Graduation	Thermocouple: K/J/E/T/N/S/R/B
Basic Accuracy	0.2ºC+2 words (not including thermocouple error)
Range	-200~1820ºC (Varying depending on graduation)
Channel	32 Thermocouple channels
Resolution	0.1°C

Correction	Independent error correction for each channel Y=kx+b (x=measured value)
Speed	Fast speed per channel: 0.1S, slow speed: 1S
Interface	USB interface, optional RS485 interface and RS232 interface
Cold Junction Compensation	Accuracy: 0.5ºC
Power Supply	Voltage:AC85-265V±10%, frequency 50Hz/60Hz <10W
Size and Weight	Width 220xdepth 293xheight (including feet) 106mm, about 3kg
Environmental Conditions	5~40ºC, 20%~80%RH (no condensation

Table A.3: Specifications of the Anemometer (model GM8902+)

Property	Value
Range of velocity	From 0.4 m/s to ~30 m/s
Range of temperature	From 0 ºC to 60 ºC
Accuracy	± 2 %
Display	10mm(0.4") 4-digite LCD
Operating temperature	From 0 ºC to 60 ºC
Humidity	< 85 % RH
Device screen	Large LCD for easy viewing
Dimensions W/D/H	77 * 36 * 164 mm / 3.0 * 1.4 * 6.5in
Weight	0.3 kg
Power Supply	4 x 1.5 V
Resolution	0.1 (m/s, km/h, and ft/min)

Table A.4: Specifications of the PV analyzer (PROVA 210)

Property	Value
Max. Solar panel power (Pmax) search by auto-scan	60V, 12A, and 500W
Resolution	1mV, 1mA
Manuel single point I-V test	Max. voltage (Vmaxp) at Pmax Max. current (Imaxp) at Pmax Voltage at open circuit (Vopen) current at short circuit (Ishort)
Solar panel area	0.001 m^2 - 9999 m^2
Standard light source	10 W/m^2 - 1000 W/m^2

Table A.5: Specifications of the pressure manometer (520)

Property	Value
Measuring range	±35kPa
Accuracy	±0.3%FSO(25℃)
Repeatability	±0.2%(Maximum＋/－0.5 FSO)
Linearity/hysteresis	±0.29 FSO
Response	Typical 0.5s
Low battery indication	Yes
Up overload indication	Err1
Down overload indication	Err2
Operating temperature	0~50℃
Storage temperature	-10~60℃
Power supply	1.5V AAA battery*4
USB communication	Yes

Appendix (B)
Calibration Curves and Certificates

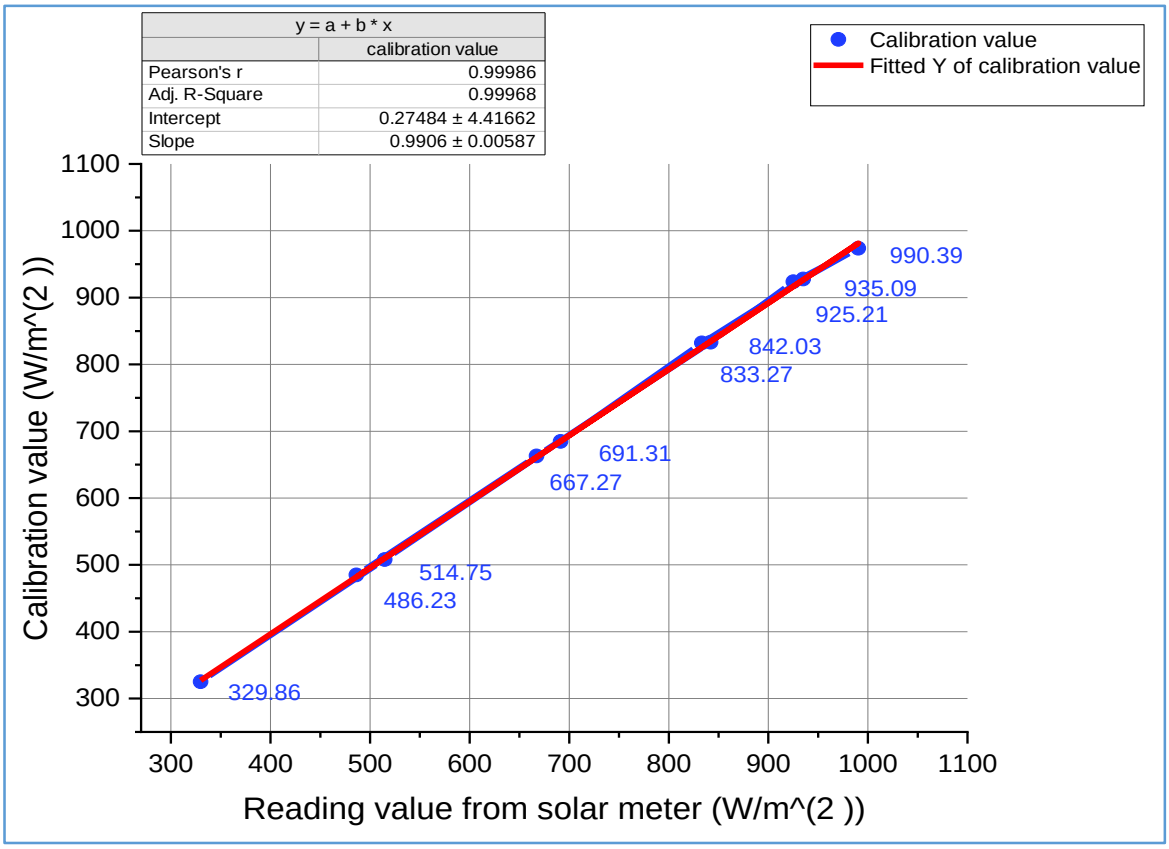

Figure (B.1) Calibration curve of the pyranometer (solar meter).

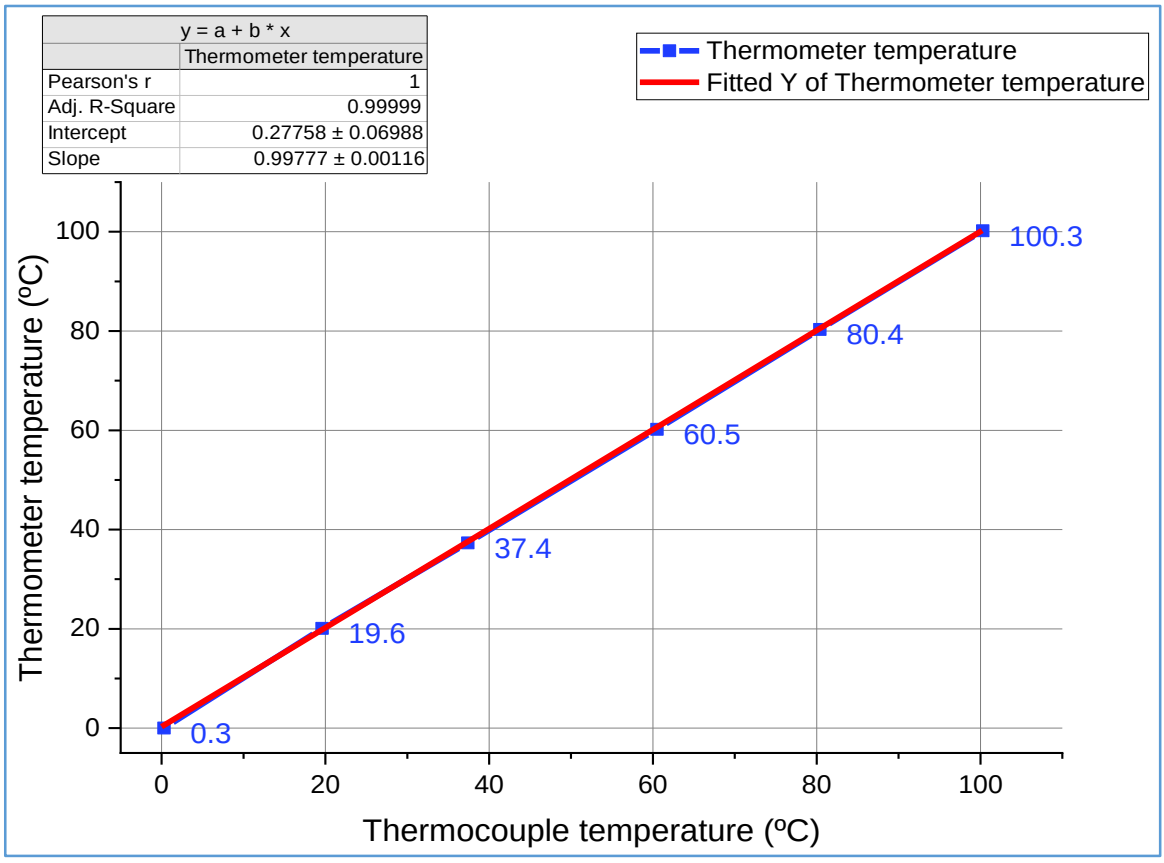

Figure (B.2) Calibration curve of the thermocouple.

Table (B.1): Temperature Sensors Calibration.

Device NO.	Freezing temperature = 0 ℃	temperature = 20 ℃	Human body temperature = 37 ℃	temperature = 60 ℃	temperature = 80 ℃	Boiling temperature = 100 ℃
Hg thermometer	0	20.1	37.3	60.2	80.3	100.2
Sensor 1	0.1	20.2	37.3	60.1	80.4	100.3
Sensor 2	0.1	20.1	36.2	60.5	80.3	100.1
Sensor 3	0.1	20.5	37.2	60.4	80.8	100.5
Sensor 4	0.2	20.3	37	60.6	80.6	100.4
Sensor 5	0.2	20.4	37.1	60.8	80.2	100.8
Sensor 6	0	20.4	36.9	60.2	80.1	100.2
Sensor 7	0.1	19.7	37	59.8	80	100.1
Sensor 8	0.5	20.1	37	60.3	80.3	99.5
Sensor 9	0.4	20.5	37.7	60.2	80.4	99.7
Sensor10	0.4	19.4	37.7	60.1	80.8	100.4
Sensor11	0.1	20.2	37.6	60.4	80.3	100.6
Sensor 12	0.4	19.3	37.5	60.1	80.3	99.8
Sensor 13	0.1	19.8	37.4	60.7	80.2	100.4
Sensor 14	0.2	20.4	37.8	60.5	80.5	100.1
Sensor 15	0.6	20.3	37.9	60.4	80.4	99.5
Sensor 16	0.3	20.5	37.2	60.1	80.1	99.8

Table (B.2) summary of the experimental results for all cases at solar flux =1000 W/m^2

Case / Result	Mean air velocity =2 m/s	Mean air velocity =2.5 m/s	Mean air velocity =3 m/s	Mean air velocity =3.5 m/s	Mean air velocity =4 m/s
Maximum output air temperature (°C)	47.5	45.73	44.7	44.15	43.45
percentage increase in ele. efficiency %	6.68	9.99	11.02	11.57	12.06
increase in output power(W)	9.08	13.73	14.71	15.28	15.93
Fan power consumption rate (W)	4.24	6.36	8.33	9.89	11.31
Maximum heat transfer amount(W)	354.464	380.142	398.772	405.317	414.884
Ambient Temp. (Tamb.) (°C)	39.55	38.05	39.1	39.41	39.5
Difference between outlet and inlet temp. (To-Ti) (°C)	8.8	7.55	6.6	5.75	5.15
Maximum inlet air temperature (°C)	38.7	38.18	38.1	38.4	38.3
Reduction in cell temperature (°C)	10.87	17.15	17.82	18.67	19.53

Table (B.3) Summary of the experimental results for all cases at solar flux =800 W/m^2

Case / Result	Mean air velocity =2 m/s	Mean air velocity =2.5 m/s	Mean air velocity =3 m/s	Mean air velocity =3.5 m/s	Mean air velocity =4 m/s
Maximum output air temperature (°C)	44.82	42.98	42.42	41.96	41.14
percentage increase in electrical efficiency %	6.04	8.53	9.06	9.38	9.84
increase in output power(W)	7.72	11	11.5	11.75	12.24
Fan power consumption rate (W)	4.24	6.36	8.33	9.89	11.31
maximum heat transfer amount(W)	266.653	282.967	296.037	312.270	315.795
Ambient Temperature (Tamb.) (°C)	41.75	40.15	40.6	41.9	40.89
Difference between outlet and inlet temp. (To-Ti) (°C)	6.62	5.62	4.85	4.43	3.92
Maximum inlet air temperature (°C)	38.2	37.36	37.45	37.53	37.4
Reduction in cell temperature (°C)	10.22	14.8	15.28	15.9	16.63

Table (B.4) summary of the experimental results for all cases at solar flux =600 W/m^2

Case / Result	Mean air velocity =2 m/s	Mean air velocity =2.5 m/s	Mean air velocity =3 m/s	Mean air velocity =3.5 m/s	Mean air velocity =4 m/s
Maximum output air temperature (°C)	41.82	40.16	39.69	39.34	38.84
percentage increase in ele. efficiency %	6.51	7.92	8.37	8.62	8.81
increase in output power(W)	5.61	8.81	9.19	9.38	9.91
Fan power consumption rate (W)	4.24	6.36	8.33	9.89	11.31
maximum heat transfer amount(W)	180.051	194.351	207.844	217.814	222.345
Ambient Temperature (Tamb.) (°C)	38.1	38	38.8	39.1	38.2
Difference between outlet and inlet temp. ΔT(To-Ti) (°C)	4.47	3.86	3.44	3.09	2.76
Maximum inlet air temperature (°C)	37.35	37.3	37.41	37.25	37.08
Reduction in cell temperature (°C)	11.67	13.73	14.52	14.97	15.38

جمهورية العراق
وزارة العلوم والتكنولوجيا
دائرة البيئة والمياه والطاقات المتجددة

العـدد: ٩٨٠ / ١٣
التاريخ: ١١/ ٥ /٢٠٢٣

الى/ جامعة الفرات الاوسط التقنية/الكلية التقنية الهندسية-النجف

م/اجابة

تحية طيبة...

أشارة الى كتابكم العدد (١٧٠٣/٢٧/٧) في ١٠ /٢٠٢٣/٥ ، نود ان نبين الاتي :

تم فحص دقة (Air Flow Anemometer GM8902) باستخدام جهاز للمقارنة حيث تم تعريض الجهازالى سرع رياح محددة في مكان محدد وتم اختبار الجهاز في استجابة التغيرات في سرعة الرياح، بالاضافة الى مقارنة القراءة التي يقيسها الجهاز بالقيمة المقاسة باستخدام مقياس معايرة بينت نتيجة الفحص ان الجهاز يستجيب بشكل فعال وان الجهاز يعطي قراءات صحيحة بدقة(90%) وكما مبين بتقرير المعايرة المرفق طيا.

كما تم تزويد الطالب ببيانات حقيقية لسرعة الرياح وشدة الاشعاع الشمسي لمحافظة الديوانية لشهر ايار.

...مع التقديـــر

المرفقات
-تقرير معايرة

د. عامر ناجي احمد
ع/ المدير العام
١١ /٥/ ٢٠٢٣

نسخة منة الى:
-قسم التخطيط والمتابعة /شعبة المعلومات والاحصاء والتوثيق.... مع الاوليات

Figure (B.3) Anemometer calibration certificate manuscript.

ANEMOMETER CALIBRATION REPORT

Equipment calibrated: Air Flow Anemometer Model: GM8902 Calibration date: May 11, 2023

CALIBRATION RESULTS:

The following results were obtained during the calibration of the Air Flow Anemometer GM8902
Measurement of air velocity:

Calibration Point: 0 m/s Reading: 0.0 m/s Error: 0.0 m/s

Calibration Point: 1 m/s Reading: 1.2 m/s Error: 0.2 m/s

Calibration Point: 2 m/s Reading: 2.3 m/s Error: 0.30 m/s

Calibration Point: 3 m/s Reading: 3.0 m/s Error: 0.0 m/s

Calibration Point: 4 m/s Reading: 3.4 m/s Error: 0.60 m/s

Calibration Point: 5 m/s Reading: 4.4 m/s Error: 0.60 m/s

Calibration Point: 6 m/s Reading: 5.4 m/s Error: 0.60 m/s

Measurement of air temperature:

Calibration Point: 20°C Reading: 20.5°C Error: 0.5°C

Calibration Point: 25°C Reading: 25.5°C Error: 0.5°C

Calibration Point: 30°C Reading: 30.5°C Error: 0.5°C

CONCLUSION:

Based on the calibration results obtained, the Air Flow Anemometer GM8902 has been found to comply with the requirements for the measurement of air velocity and temperature with 90% Accuracy.

The calibration certificate is valid until the next calibration date, which is recommended to be performed every 12 months.

Figure (B.4) Anemometer Calibration report.

ATU
Tomorrow starts today

2nd International Conference on Engineering, and Science to Achieve the Sustainable Development Goals
(9th – 10th) July 2023 in Tabriz - Iran

Final Acceptance Letter

Manuscript Number: 358

Dear: Mohammed A. Majeed

Co-Authors: Salah M. Salih

Congratulations!

It is a great pleasure to inform you that, following the peer review process, your manuscript titled

(**Cooling Performance Enhancement of PV Systems: Review**)

Had been ACCEPTED for participating in the **2nd International Conference on Engineering, and Science to Achieve the Sustainable Development Goals,** and considered for publication in **(AIP Conference proceeding).**

Thank you for your significant contribution to the ICASDG2023 conference.

Prof. Dr. Ahmed G. Wadday
ICASDG2023 Scientific Committee Chair | AIP Conference Proceeding Editor
9th – 10th July 2023 | Tabriz | Iran

ATU
Tomorrow starts today

2nd International Conference on Engineering, and Science to Achieve the Sustainable Development Goals, (ICASDG2023)

Certificate of Presentation

awarded to

Mohammed A. Majeed, Salah M. Salih

presenter of the paper ID **ICASDG22-358**, entitled

Cooling Performance Enhancement of PV Systems: Review, at the 2nd ICASDG2023 conference, 9th -10th July 2023, hosted by the University Of Tabriz, Tabriz – Iran

Prof. Dr. Mudhaffar S. Al-Zuhairy
President of Al-Furat Al-Awsat Technical University

Prof. Dr. Hasan Sh. Majdi
President of Al-Mustaqbal University

Prof. Dr. Safar Nasrollahzadeh
President of University Of Tabriz

First Conference on Renewable and Sustainable Energy 2023 (FCRSE)

Letter of Acceptance

Paper title: Theoretical Analysis of the Performance Improvement of the (PV/T) Air Collector by Multi-Flow Channel

Corresponding Author: Mohammed A. Majeed

Coauthors: Salah M. Salih

Dear Author

Your work has been thoroughly reviewed by our committee. It is with great pleasure your paper has been accepted for **presentation at** FCRSE2023.

You are kindly requested to proceed for registration.

As an initiative to support research and development in the renewable and sustainable energy field, Almaaqal University is delighted to waive the participation fees for those presenting research papers during the conference

Sincerely,

Prof. Dr Badir Albadran

Chair of organizing committee

Date:19.10.2023

Show 10 entries Search:

#	Manuscript ID	Manuscript Type	Manuscript Title	Submit Date	Current Status	Modify Date	Email	Manuscript Main File	Acceptance Certificate
1	QJES-2312-1057 (R3)	Research Paper	Experimental and Theoretical Analysis of Photovoltaic Thermal Collector Performance with Multi-Flow Channel	2023-12-06	Accepted to Online Publish	2024-02-15			

Showing 1 to 1 of 1 entries Previous 1 Next

Article Acceptance Certificate

This certificate confirms that the following paper has been accepted for publication in Al-Qadisiyah Journal for Engineering Sciences

Title: Experimental and Theoretical Analysis of Photovoltaic Thermal Collector Performance with Multi-Flow Channel
ID: QJES-2312-1057 (R3)

Authors: mohammed abd al salam Majeed

Submission Date: 06 December 2023
Acceptance Date: 15 February 2024

Khaled Al-Farhany, PhD
Editor-in-chief of Al-Qadisiyah Journal for Engineering Sciences

الخلاصة

تم دراسة تحسين أداء التبريد للمجمع الكهروضوئي / الحراري (PV/T) باستخدام الزعانف المستعرضة مع قناة متعددة التدفق عدديا وتجريبيا. تهدف الدراسة إلى تحسين الكفاءة الكهربائية للأنظمة الكهروضوئية مع قناة متعددة التدفق من خلال نقل الحرارة بين اللوحة الماصة وتدفق الهواء مع انخفاض أقل في الضغط. تم دراسة تأثير اختلاف معدل جريان الكتلة (MFR) البالغ (0.04، 0.05، 0.06، 0.07،و 0.08) كجم/ث، والتدفق الشمسي (600، 800،و 1000) وات/م^2، على درجة الحرارة اللوح الكهروضوئي وأداء المنظومة الكهروضوئية .

أجريت التجربة تحت ظروف اختبار داخلية لنظام الهواء PV/T للقناة متعددة التدفق مع مساحة مشروع (0.524) م^2، تحت ظروف اختبار داخلية. تدفق شمسي مختلف يبلغ (600، 800،و 1000) واط/م^2، ويكون MFR للهواء بين (0.04، 0.05، 0.06، 0.07،و 0.08) كجم/ث.

تم ضبط نسبة العرض إلى الارتفاع (H/W)على (10) لتحقيق تدفق مضطرب بالكامل للهواء للمظومة PV/T مع قناة متعددة التدفق. يعتمد الحد الأدنى لوحدات الدخول والخروج على معيار ASHARE لمجمعات الطاقة الشمسية الحرارية. تم إجراء تجارب النظام في المختبر باستخدام ثلاثة مصابيح هالوجين التنغستن (3000 واط) كجهاز محاكاة للطاقة الشمسية.

تم إجراء الدراسة العددية أيضًا باستخدام برنامج COMSOL Multiphysics 5.5 المتوفر تجاريًا لحل المعادلات الحاكمة ثلاثية الأبعاد للاستمرارية والزخم والطاقة لمعادلات النموذج المضطرب(κ-ε) .تم إجراء عمليات المحاكاة الحالية تحت نفس الظروف الحدودية لتأكيد دقة البيانات التجريبية مع متوسط خطأ في التحقق من درجة حرارة مخرج الزعانف المستعرضة مع نموذج قناة متعددة التدفق يقدر بـ (1.576)٪.

أشارت النتائج إلى أن درجة حرارة الهواء تتناسب عكسيا مع معدل الجريان الكتلي، علاوة على ذلك، لوحظ أن الكفاءة الإجمالية تعتمد بشكل كبير على معدل جريان الكتلة ، وكثافة التدفق الشمسي.

بالإضافة إلى ذلك، وضحت النتائج التجريبية عند معدل جريان كتلي للهواء (0.04-0.08) كجم/ث، التدفق الشمسي (600) واط/م^2، اعلى قيمة للكفاءة الكهربائية، الكفاءة الحرارية، والكفاءة الكلية (16.62-17.03)٪ ، (53.49-65.57)٪، و (70.11- 82.6)٪، على التوالي. عند نفس معدل جريان الكتلة ، والتدفق الشمسي (1000) واط/م^2، حققت النتائج (15.5 -16.26) ٪ ، (63.34-74.14) ٪ ، و (78.84-90.4) ٪ ، على التوالي. علاوة على ذلك ، النسبة المئوية للزيادة في القدرة الخارجة هي (28.44٪) بمقدار (15.93) واط.

زيادة معدل التدفق الكتلة يؤدي الى انخفاض درجة حرارة اللوح الشمسي، ويحسن الأداء الكهربائي. النسبة المئوية لإنخفاض درجة حرارة اللوح الشمسي عند معدل جريان كتلة(0.08)كجم/ث هي (28.94٪) والحد الأقصى لتخفيض درجة الحرارة (19.53) درجة مئوية. افضل صافي قدرة كهربائية مضافة الى انتاج اللوح الشمسي هي (7.37) واط عند معدل جريان كتلة الهواء (0.05) كجم/ث، و التدفق الشمسي (1000) واط/م^2.

تحسين اداء التبريد للأنظمة الكهروضوئية باستخدام قناة متعددة التدفق

رسالة مقدمة الى

قسم هندسة تقنيات ميكانيك القوى

كجزء من متطلبات نيل درجة الماجستير في

هندسة تقنيات ميكانيك القوى/ الحراريات

تقدم بها

محمد عبد السلام مجيد

بكالوريوس في هندسة تقنيات ميكانيك القوى

إشراف

الأستاذ المساعد الدكتور

صلاح مهدي صالح

شباط / 2024